NASA CR-165354
PWA-5594-157

NASA-CR-165354
19830022156

NASA

ENERGY EFFICIENT ENGINE

LOW-PRESSURE COMPRESSOR COMPONENT TEST HARDWARE

DETAILED DESIGN REPORT

Prepared by:

C.J. Michael and J.E. Halle

UNITED TECHNOLOGIES CORPORATION
Pratt & Whitney Aircraft Group
Commercial Products Division

Prepared for:

NATIONAL AERONAUTICS AND SPACE ADMINISTRATION

Lewis Research Center
Cleveland, OH 44135

Contract NAS3-20646

PRATT & WHITNEY AIRCRAFT GROUP
Commercial Products Division

East Hartford, Connecticut 06108

In reply please refer to:
WBG:WS (2999n) - E1M3
LC--81-94

13 August 1981

To: National Aeronautics and Space Administration
Lewis Research Center
21000 Brookpark Road
Cleveland, Ohio 44135

Attention: Mr. Carl C. Ciepluch, Mail Stop 301-4

Subject: Energy Efficient Engine Low-Pressure Compressor
Test Hardware Detailed Design Report PWA-5594-157

References: (a) Letter, J.W. Schaefer to W.B. Gardner, "Contract NAS3-20646 - Low-Pressure Compressor Detailed Design Report (WBS 4.2.2)," dated 20 July, 1981, serial no. 2321

(b) Contract No. NAS3-20646

Enclosures: 20 copies of the subject report

Gentlemen:

Enclosed are twenty (20) copies of the subject report, revised in accordance with the requirements of reference (a). Distribition is being made in compliance with reference (b).

Sincerely yours,

UNITED TECHNOLOGIES CORPORATION
Pratt & Whitney Aircraft Group
Commercial Products Division

W.B. Gardner
Program Manager

cc: Administrative Contracting Officer (Letter Only)
Air Force Plant Representative Office
Pratt & Whitney Aircraft Group
East Hartford, Connecticut 06108

UNITED TECHNOLOGIES

1. REPORT NO.	2. GOVERNMENT AGENCY	3. RECIPIENT'S CATALOG NO.
NASA CR-165354		

4. TITLE AND SUBTITLE	5. REPORT DATE
ENERGY EFFICIENT ENGINE -- LOW PRESSURE COMPRESSOR COMPONENT TEST HARDWARE DETAILED DESIGN REPORT	JUNE 1981
	6. PERFORMING ORG. CODE
7. AUTHOR(S)	8. PERFORMING ORG. REPT. NO.
C. J. MICHAEL, J. E. HALLE	PWA-5594-157
9. PERFORMING ORG. NAME AND ADDRESS	10. WORK UNIT NO.
UNITED TECHNOLOGIES CORPORATION Pratt & Whitney Aircraft Group Commercial Products Division	11. CONTRACT OR GRANT NO. NAS3-20646
12. SPONSORING AGENCY NAME AND ADDRESS	13. TYPE REPT./PERIOD COVERED
National Aeronautics and Space Administration Lewis Research Center 21000 Brookpark Road, Cleveland, Ohio 44135	CONTRACTOR REPORT
	14. SPONSORING AGENCY CODE

15. SUPPLEMENTARY NOTES

NASA Project Manager, Mr. C. C. Ciepluch, NASA-Lewis Research Center

16. ABSTRACT

This report presents the aerodynamic and mechanical design description of the low pressure compressor component of the Energy Efficient Engine. The component was designed to meet the requirements of the Flight Propulsion System while maintaining a low cost approach in providing a low-pressure compressor design for the Integrated Core/Low Spool test required in the Energy Efficient Engine Program.

The resulting low-pressure compressor component design meets or exceeds all design goals with the exception of surge margin. In addition, the expense of hardware fabrication for the Integrated Core/Low Spool test has been minimized through the use of existing "minor part" hardware.

17. KEY WORDS (SUGGESTED BY AUTHOR(S))	18. DISTRIBUTION STATEMENT
Low-Pressure Compressor Integrated Core/Low Spool Test Flight Propulsion System Adjustable Stator 1 Controlled Diffusion Airfoils	Subject to the Restriction of Clause 66 of NASA Contract NAS3-20646 "FEDD DATA CLAUSE"

19. SECURITY CLASS THIS (REPT)	20. SECURITY CLASS THIS (PAGE)	21. NO. PGS	22. PRICE *
UNCLASSIFIED	UNCLASSIFIED		

* For sale by the National Technical Information Service, Springfield, VA 22161

FOREWORD

The Energy Efficient Engine Component Development and Integration Program is being conducted under parallel National Aeronautics and Space Administration contracts to Pratt & Whitney Aircraft Group and General Electric Company. The overall project is under the direction of Mr. Carl C. Ciepluch. Mr. John W. Schaefer is the NASA Assistant Project Manager for the Pratt & Whitney Aircraft effort under NASA Contract NAS3-20646, and Mr. Frank Berkopec is the NASA Project Engineer responsible for the portion of the project described in this report. Mr. William B. Gardner is manager of the Energy Efficient Engine Project at Pratt & Whitney Aircraft Group.

TABLE OF CONTENTS

TABLE OF CONTENTS (Continued)

LIST OF ILLUSTRATIONS

LIST OF ILLUSTRATIONS (Continued)

LIST OF ILLUSTRATIONS (Continued)

LIST OF TABLES

LIST OF TABLES (Continued)

This Page Intentionally Left Blank

1.0 SUMMARY

In accordance with Tasks 2 and 4 of the Energy Efficient Engine Program, NASA Contract NAS3-20646, a four-stage low-pressure Compressor Component was designed for the Integrated Core/Low Spool test vehicle.

The objective of the low-pressure compresor component design effort was to design a four-stage compressor with a pressure ratio of 1.77 and a Flight Propulsion System adiabatic efficiency goal of 89.9 percent. The experimental efficiency goal for the Integrated Core/Low Spool test component is 87.5 percent. This compressor efficiency level contributes 1.6 percent to the Energy Efficient Engine Flight Propulsion System efficiency improvement. The Flight Propulsion System efficiency is indicative of the fully developed compressor component in the mature production engine. Whereas, the Integrated Core/Low Spool efficiency represents the goal for the first run of the experimental compressor.

The low-pressure compressor component meets or exceeds all design goals for this test except for surge margin which is two percent below goal. The Flight Propulsion System adiabatic efficiency goal of 89.9 percent was attained. A summary of the low-pressure compressor component design goals and predicted performance is provided below in Table 1-I.

The low-pressure compressor was designed to meet Flight Propulsion System performance goals, but was not optimized for flight weight. Substitute materials and simplified manufacturing techniques were employed to improve fabrication schedules, reduce cost, and minimize risk. Design iterations were minimized by this approach and, hence, design costs were reduced.

TABLE 1-I

COMPARISON OF PREDICTED PERFORMANCE OF LOW-PRESSURE COMPRESSOR COMPONENT DESIGN WITH DESIGN GOALS AT THE AERODYNAMIC DESIGN POINT

Parameter	Goal	Predicted
Pressure Ratio	1.77	1.77
Adiabatic Efficiency, percent		
Flight Propulsion System	89.9	90.0
Integrated Core/Low Spool	87.5	87.5
Inlet Corrected Flow, kg/sec (lb/sec)	56.97 (125.6)	56.97 (125.6)
Surge Margin, percent	20	18
Flight Propulsion System Rotor Low Cycle Fatigue Life		
Missions	20,000	20,000
Hours	30,000	30,000
Integrated Core/Low Spool Low Cycle Fatigue Life, missions	1000	8000

This Page Intentionally Left Blank

2.0 INTRODUCTION

The objective of the Energy Efficient Engine Program is to develop, evaluate, and demonstrate the technology for achieving lower installed fuel consumption and lower operating costs in future commercial turbofan engines. NASA has set minimum goals of a twelve percent reduction in thrust specific fuel consumption, a five percent reduction in direct operating cost, and a fifty percent reduction in performance degradation for the Energy Efficient Engine (Flight Propulsion System) relative to the JT9D-7A reference engine. In addition, environmental goals on emissions (meet the proposed Environmental Protection Agency 1981 regulation) and noise (meet Federal Air Regulation 36-1978 standards) have been established.

The Pratt & Whitney Aircraft program effort is based on an engine concept defined under the NASA-sponsered Energy Efficient Engine Preliminary Design and Integration Studies Program, Contract NAS3-20628. This was discussed in detail in NASA Report CR-135396. The Pratt & Whitney Aircraft engine is a twin-spool, direct drive, mixed-flow exhaust configuration, utilizing an integrated engine-nacelle structure. A short, stiff high-pressure rotor and a single-stage high-pressure turbine are among the major features in providing for both performance retention and major reductions in maintenance and direct operating costs. Improved clearance control in the high-pressure compressor and turbines and advanced single crystal materials in turbine blades and vanes are among the major features providing performance improvement.

To meet the program objectives, four technical tasks were established by the Pratt & Whitney Aircraft and were defined in the Program Work Plan. Task 2 of the program, "Component Analysis, Design and Development", consists of designing, fabricating, and testing the high risk components as well as testing supporting technology in critical areas. The task includes the designing of all components, plus a technology program to obtain design data on shroudless hollow fan blade test specimens; two builds of the high-pressure compressor; a full annular combustor and supporting programs to define diffuser parameters and combustor geometry for low emissions; a cooled high-pressure turbine rig and supporting technology programs in aerodynamics, leakage control, and blade fabrication; aerodynamic rigs supporting the design of a low-pressure turbine; and scale model mixer testing. This report documents the aerodynamic and mechanical design of the low-pressure compressor component.

The objective of the low-pressure compressor component design effort was to design a four-stage low-pressure compressor for the Integrated Core/Low Spool test with a pressure ratio of 1.77 and a Flight Propulsion System adiabatic efficiency goal of 89.9 percent. The experimental efficiency goal for the Integrated Core/Low Spool test component was 87.5 percent.

The low-pressure compressor component design effort consists of (1) a preliminary analysis and design phase that determines the feasibility of the low-pressure compressor design, and (2) a detailed analysis and design phase that completes the compressor design for use in the Integrated Core/Low Spool test (Task 4). There is no component rig program or supporting technology program. The design data and the verification of advanced concepts are obtained principally from related Pratt & Whitney Aircraft programs such as an in-house supercritical cascade program, the NAVAIR Supercritical Cascade Test (Contract N00019-77-C-0546), and the NASA Front Stage Program (Contract NAS3-20899). Hardware for the low spool phase of the low-pressure compressor Integrated Core/Low Spool test is fabricated in Task 4 following acceptance by NASA of the detailed design.

The preliminary design of the Energy Efficient Engine low-pressure compressor component included a titanium drum rotor and flight weight aluminum cases. This design approach was modified for the Integrated Core/Low Spool test experimental hardware to reduce costs and maintain schedule. Specifically, a bolted steel rotor was adopted for reduced material cost, to avoid a weld development program, and lower risk. Non-optimized aluminum cases were utilized to reduce design iteration effort and machining time. Exisiting tooling was utilized where possible and existing design minor parts were incorporated.

Flight Propulsion System aerodynamics were fully retained in this design. Titanium blading was also retained and aluminum stators were incorporated. Steel was substituded for aluminum on the inlet guide vane (stator 1) for ease of Integrated Core/Low Spool test instrumentation, but Flight Propulsion System aerodynamics were not impacted. Axial spacing between blades and stators was set based on experience with similarly designed compressors and, as a result of the final design analysis, could be reduced for Flight Propulsion System application without impacting compressor performance.

Section 3.0 of this report describes the aerodynamic and mechanical design of the low-pressure compressor component and presents the results of the analyses performed. Section 4.0 presents the final results of the design effort. Appendix A defines the aerodynamic design in detail. Appendix B defines the nomenclature used in this report.

3.0 LOW-PRESSURE COMPRESSOR COMPONENT DESIGN

3.1 GENERAL DESCRIPTION AND MAJOR FEATURES

The low-pressure compressor is composed of four stages, 820 airfoils, and features an average blade aspect ratio of 2.24 and an average gap-chord ratio of 0.9. Its rotor hub/tip ratios at the inlet and exit are 0.84 and 0.83, respectively. The component design that evolved from the detailed design activity is illustrated in Figure 3.1-1.

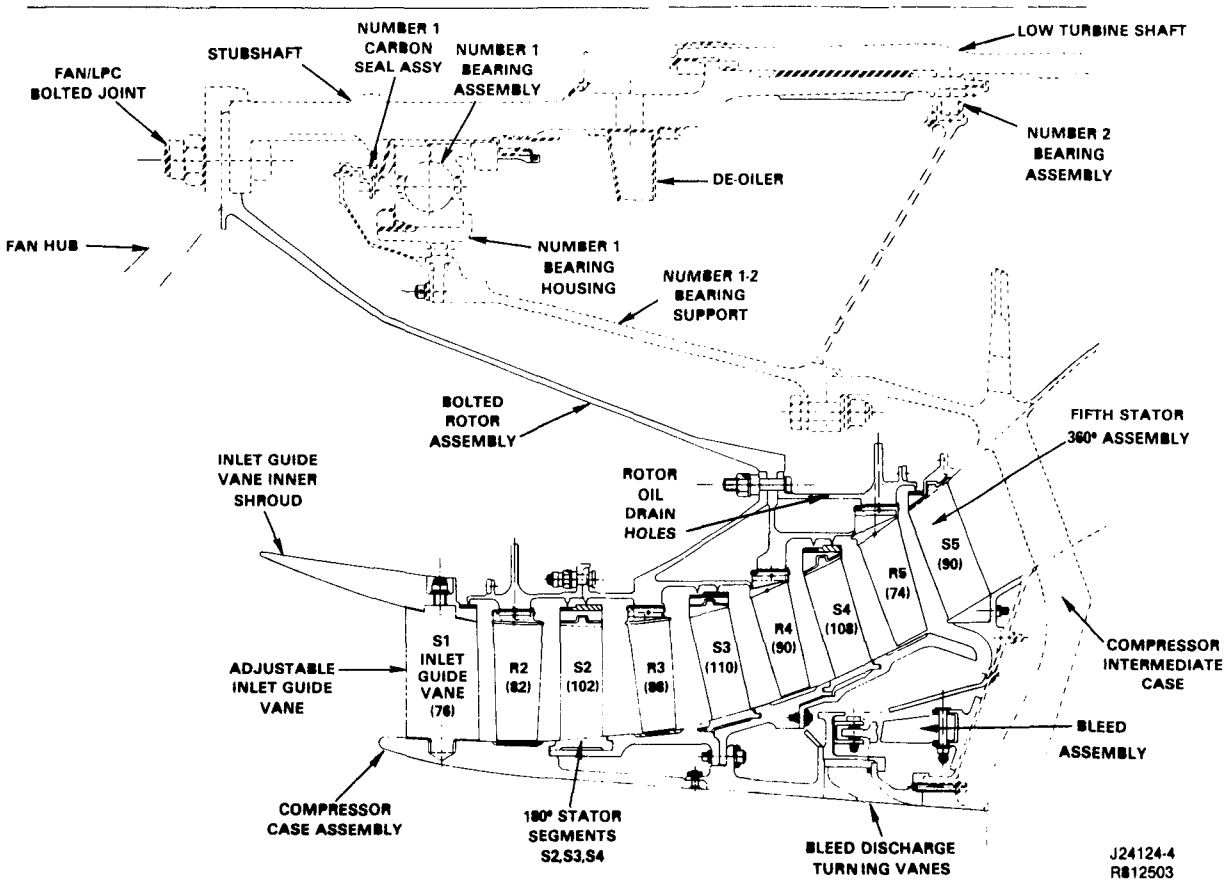

Figure 3.1-1 Low-Pressure Compressor Component Design

The Integrated Core/Low Spool low-pressure compressor rotor assembly is fabricated from steel and consists of individual disks which bolt together. This design concept was adopted for the Integrated Core/Low Spool due to its cost benefit over the flight propulsion system electron beam welded titanium design. The low-pressure compressor rotor assembly is connected to the low pressure rotor shaft through a single hub bolted to a common fan hub/low-pressure compressor hub joint forward of the number 1 bearing. The rotor features canted titanium blades with axial attachments and integral rotor knife edge seals.

The low-pressure compressor stator assembly supporting cases and inlet splitter are fabricated from aluminum for reduced weight. The low-pressure compressor cases feature circumferential, trenched, abradable rubstrips over the blade tips to provide the blade tip clearance needed to prevent rubbing under transient engine conditions, while reducing the efficiency penalty associated with tip clearance. The inner stator shrouds also feature abradable rubstrips to provide the required clearance control under the rotor knife edge seals. Rubstrip material in both inner and outer diameter locations is silicone rubber.

Low power surge protection and reverse thrust stability are provided by a fifth stage annular bleed. A circumferential gap on the outer flowpath wall ahead of the fifth stage stator provides airflow to an annular bleed ring, which translates rearward via a linkage system to allow bleed air to exit from the compressor and dump into the fan duct forward of the fan exit vanes. The bleed system is sized to provide a nominal 15 percent of flow extraction from the core flowpath.

A cross section of the low-pressure compressor design developed during the preliminary design phase is presented in Figure 3.1-2 for comparison. The features of this compressor are being retained for the Flight Propulsion System.

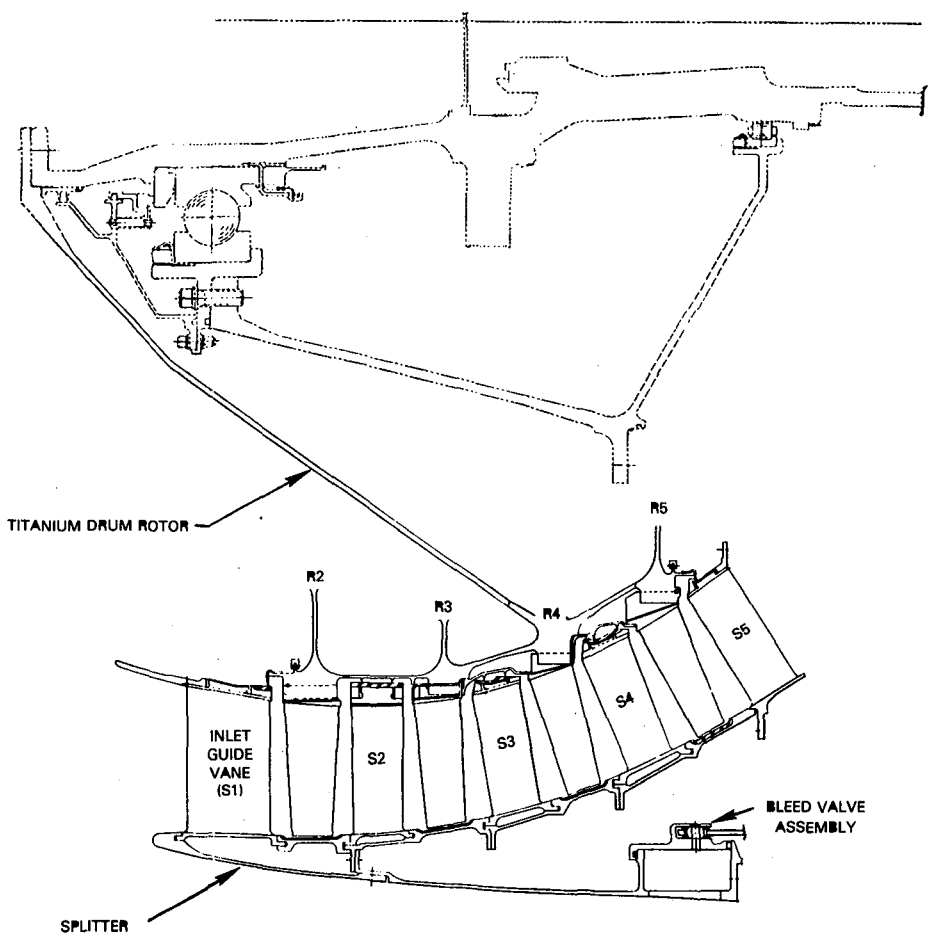

Figure 3.1-2 Low-Pressure Compressor Component Preliminary Design - Representative of Flight Propulsion System Design

3.2 LOW-PRESSURE COMPRESSOR AERODYNAMIC DESIGN

3.2.1 General Description

The low-pressure compressor aerodynamic design includes stator 1, in addition to the four stage low-pressure compressor, shown in Figure 3.2-1. Because the first test of the low-pressure compressor is in the Integrated Core/Low Spool, the low-pressure compressor design was configured with an adjustable stator 1 to provide low-pressure compressor flow capacity flexibility. The design parameters for the low-pressure compressor are listed in Table 3.2-I.

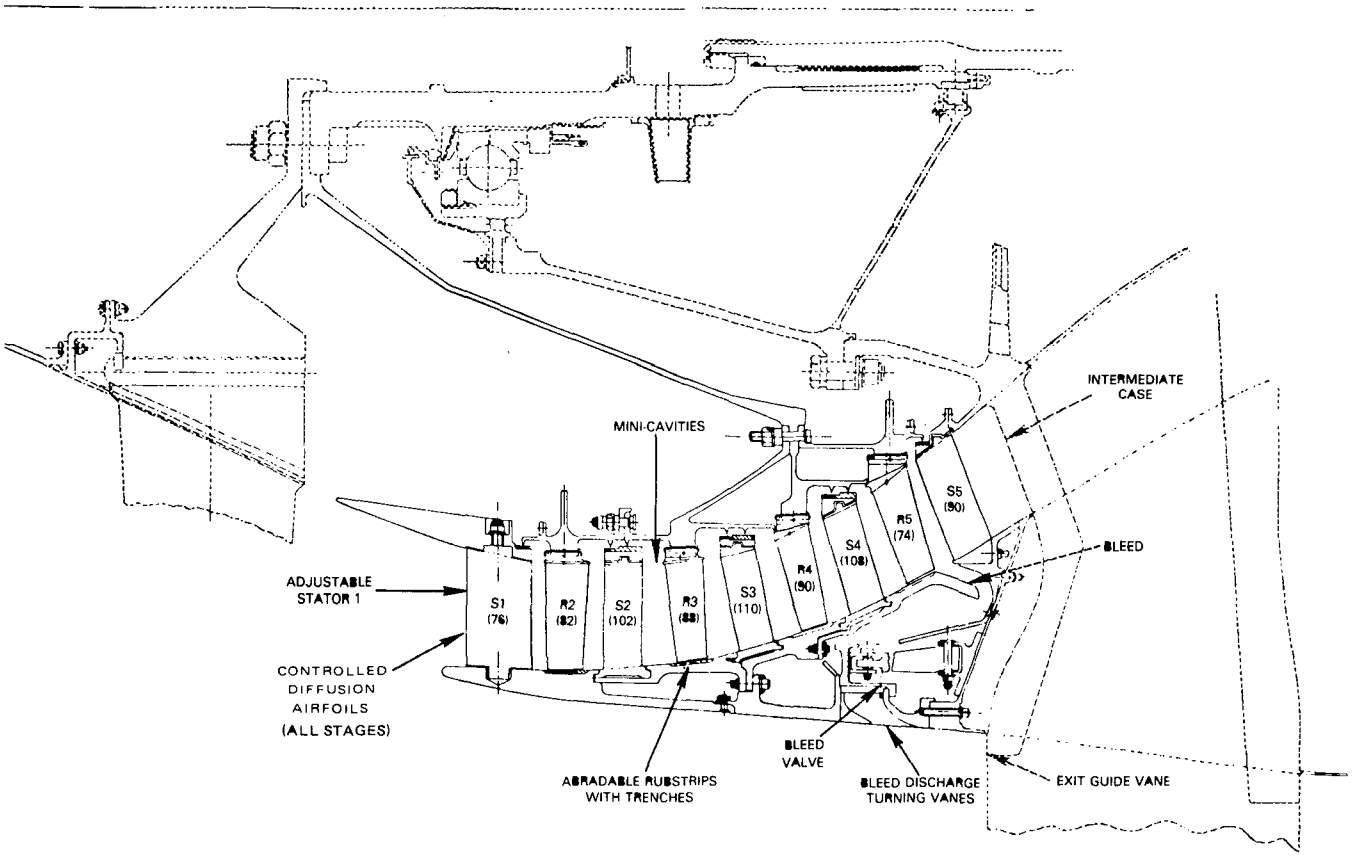

Figure 3.2-1 Stator 1 and Low-Pressure Compressor Design

Some of the major features of the low-pressure compressor aerodynamic design include the use of controlled diffusion airfoils for their increased low loss incidence range capability. Abradable rubstrips with trenches are used over the rotor tips to reduce the sensitivity of low-pressure compressor efficiency to tip clearance. Canted airfoils are used to increase root loading capability. The use of mini-cavities reduces endwall losses. Finally, a modulated

bleed with 15 percent of core mass airflow capability near the exit of the low-pressure compressor is incorporated to avoid compressor surge during starting and reverser operation.

TABLE 3.2-I

LOW-PRESSURE COMPRESSOR DESIGN PARAMETERS

	ENGINE OPERATING CONDITION			
	Aerodynamic Design Point	Max. Cruise	Max. Climb	Takeoff
Pressure Ratio	1.77	1.73	1.80	1.61
Efficiency(percent)				
Adiabatic (FPS)	89.9	90.4	89.6	92.0
Polytropic (FPS)	90.6	91.0	90.4	92.4
Adiabatic (IC/LS)	87.5	-	-	-
Inlet Corrected Airflow (lb/sec)	125.5	123.0	127.5	112.0
Inlet Specific Airflow ($lb/sec/ft^2$)	35.6	34.8	36.2	31.8
Inlet Corrected Tip Speed (ft/sec)	797	782	812	721
Exit Temperature ^oF	152	145	188	245

Low-pressure compressor rotation is counter-clockwise when viewed from the rear and the exit airflow is axial. The projected design point adiabatic efficiency, including stator 1, is 83.4 percent for the first test and 85.9 percent for the fully developed low-pressure compressor.

3.2.2 Aerodynamic Parameter Selection

3.2.2.1 General Parameters

Table 3.2-II lists the low-pressure compressor general design parameters. Figure 3.2-2 shows a portion of the low-pressure compressor predicted performance map. Figure 3.2-3 shows the predicted performance map.

TABLE 3.2-II

GENERAL DESIGN PARAMETERS
(100 Percent Speed)

Parameter	Design Point
W_ECS1, kg/sec (lb/second)	55.294 (121.9)
N_1Corrected to S1, temp.(rpm)	3921
Pressure Ratio $\frac{\text{exit pressure}}{\text{inlet pressure}}$	1.713
Stages	4
U-Tip, Corrected to S1, m/second (ft/second)- Rotor 2	242.316 (795)
Inlet Hub/Tip (Stator 1)	0.83
Exit Hub/Tip (Stator 5)	0.81
Solidity - (compressor average)	1.19
Aspect Ratio (Avg. Rotor and Stator)	2.24
W_E S1/A, kg/second/m^2 (lb/sec/ft^2)	157.200 (32.2)
Flow Coefficient, $C_{X/U}$(compressor average)	0.72
Work Coefficient, E	0.65
Reaction (compressor average)	0.60
D-Factor (compressor average)	0.38
ΔP/Po-P (compressor average)	0.33

S1 = Stator 1 Leading Edge.

Flowpath shape and the number of stages were determined from the results of preliminary studies in the optimization of low-pressure compressor/intermediate case length and loading levels. It was found that a three stage configuration required excessively high stage loadings. The addition of a fourth stage allowed a reduction in stage loadings to a level at which the design surge margin could be achieved. It also allowed a reduction in diameter and low-pressure compressor exit meridional velocity, which is diffused through the low-pressure compressor to minimize flow Mach numbers, and consequently, losses (Figure 3.2-4). This reduced the intermediate case length and loading level and resulted in a net reduction in overall length.

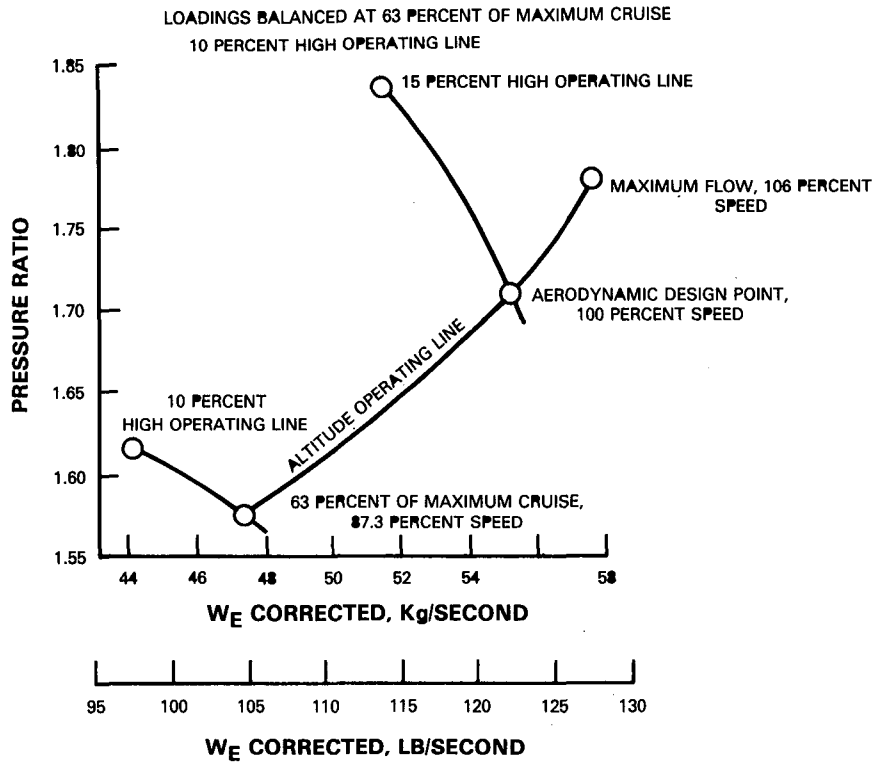

Figure 3.2-2 Low-Pressure Compressor Predicted Performance

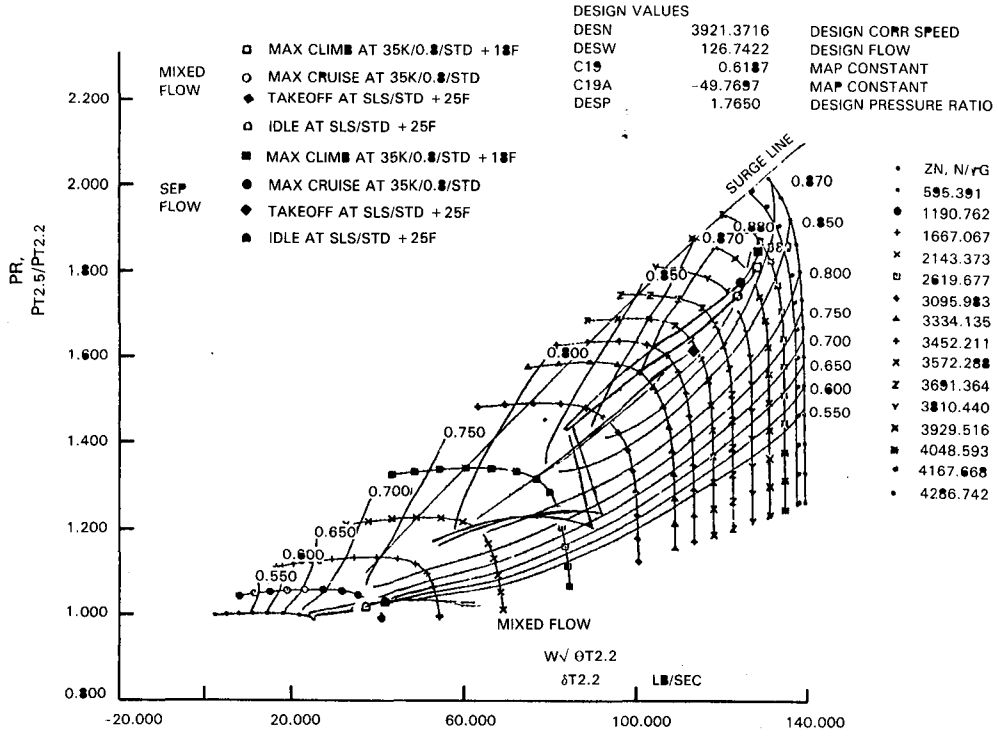

Figure 3.2-3 Low-Pressure Compressor Performance Map

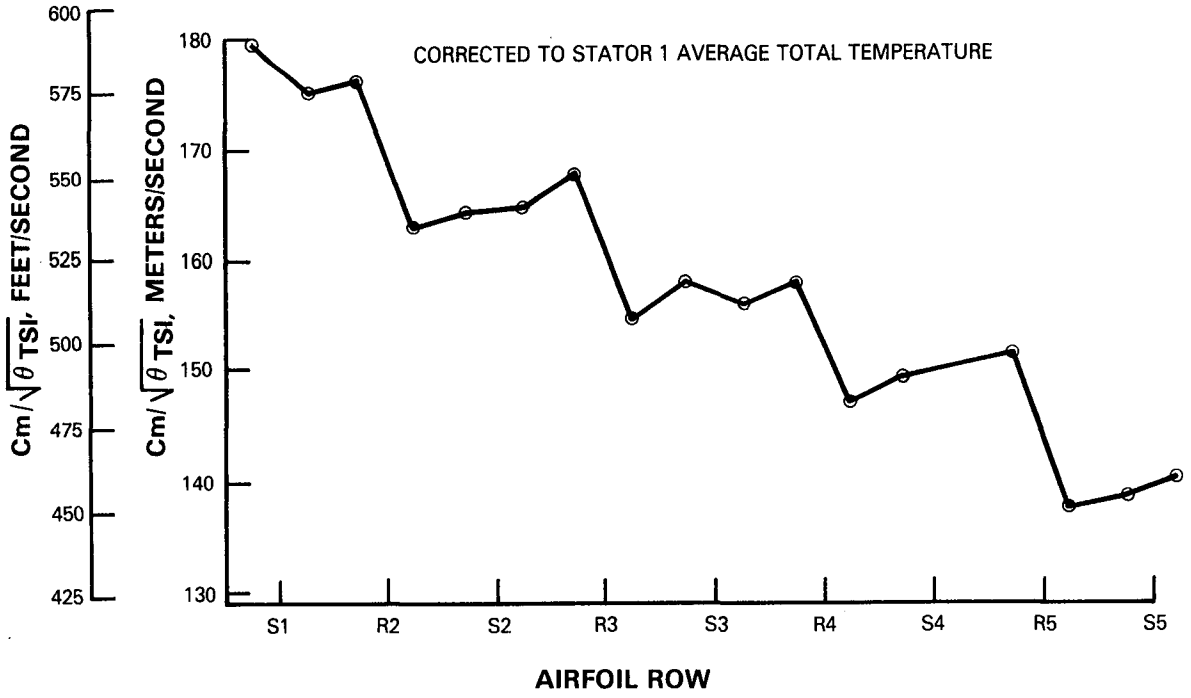

Figure 3.2-4 Low-Pressure Compressor Meridional Velocity

Area distribution was established to give a smooth axial loading distribution and flowpath. Flowpath inlet and exit dimensions were fixed prior to the final design by the fan and intermediate case designs.

Because the low-pressure compressor and high-pressure compressor counter-rotate, the low-pressure compressor discharge is axial as indicated on Figure 3.2-5 by the 0 degree exit angle of stator 5. This results in an increasing reaction through the low-pressure compressor (Figure 3.2-6). In addition, because the stage reaction is high, stators load up faster than rotors when approaching surge. As shown in Figure 3.2-7, the mean solidity of the stators was made larger (1.27) than that of the rotors (1.01) to achieve a loading balance at surge. Stator 1 has an anti-icing requirement in the Flight Propulsion System which requires hollow contstruction and, therefore, a long chord or low aspect ratio. Stator 1 also has a large solidity because it becomes more highly loaded than other vane rows at part speed.

The aspect ratio, shown in Figure 3.2-8, and solidity distribution through the low-pressure compressor were set to minimize two-dimensional loss while balancing the loading and achieving the desired surge margin.

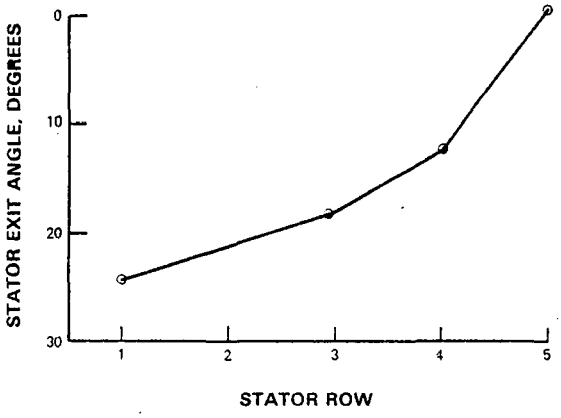

Figure 3.2-5 Low-Pressure Compressor Stator Exit Angles

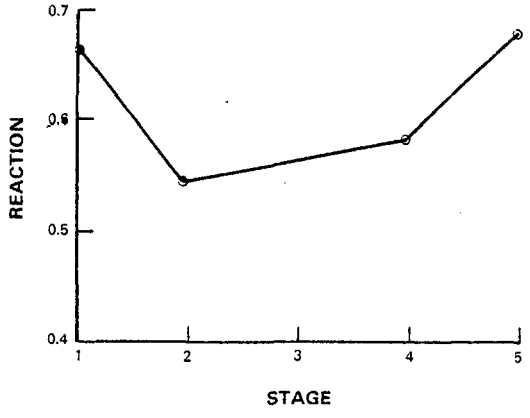

Figure 3.2-6 Low-Pressure Compressor Reaction

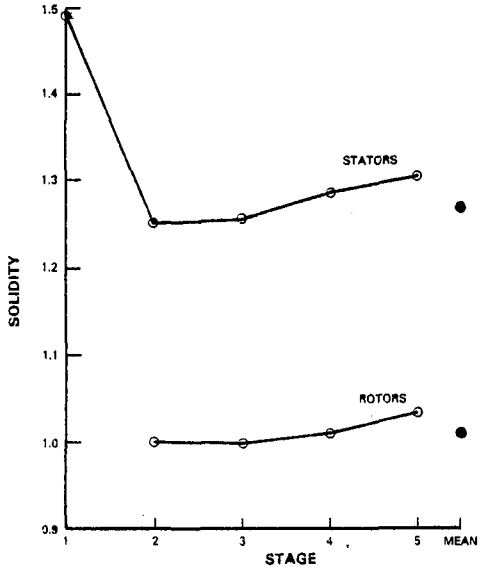

Figure 3.2-7 Low-Pressure Compressor Rotor and Stator Solidity

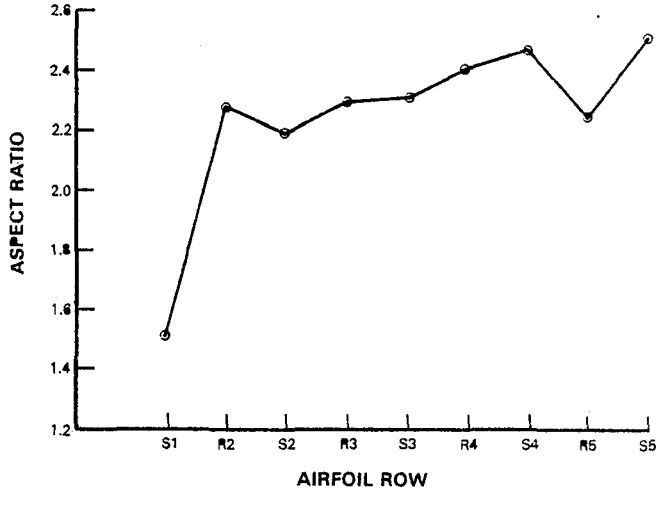

Figure 3.2-8 Low-Pressure Compressor Airfoil Aspect Ratio

3.2.2.2 Velocity Triangle Selection

Velocity triangles were selected and evaluated by utilizing an axisymmetric, streamline curvature flowfield calculation. The aerodynamic blockage factors, used in the calculation of velocity triangles, are shown in Figure 3.2-9. Blockage factors were assumed constant for off-design estimates (which is considered conservative because the resulting surge loading predictions are higher than those implied by lower blockage factors). The design point midspan loading distribution is shown in Figure 3.2-10.

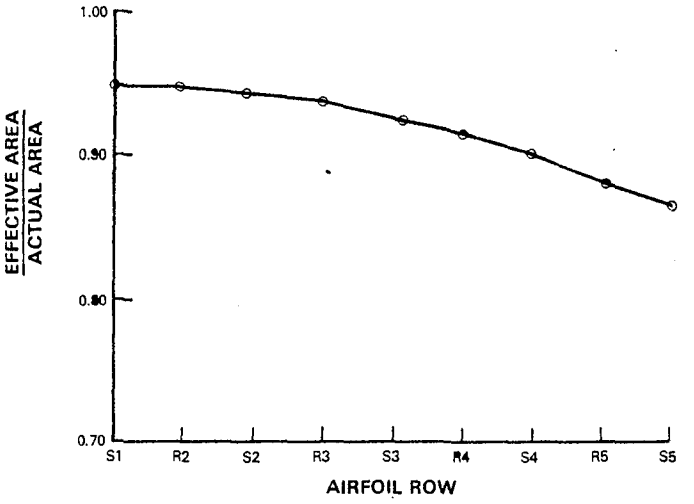

Figure 3.2-9 Blockage Factor Distribution Used in Calculating Velocity Triangles

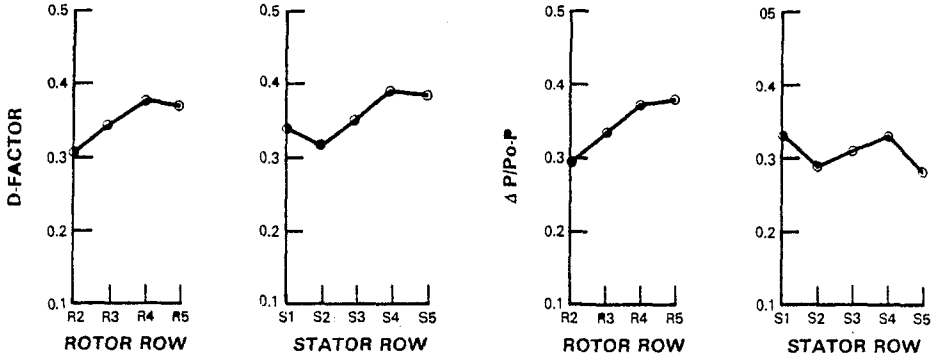

Figure 3.2-10 Low-Pressure Compressor Design Point Midspan Loading Distribution

The total pressure and angle skews shown in Figure 3.2-11 were chosen to radially balance loadings on a 10 percent high operating line at 88.7 percent speed (63 percent of maximum cruise power). This point was chosen because there is evidence that peak low-pressure compressor loadings occur near 90 percent speed. Also, it was considered desireable to operate with bleeds closed at least that far down the operating range. A negative total pressure slope and positive angle slope with radius will cause loading to shift from the hub toward the tip. In the Energy Efficient Engine low-pressure compressor, the tight flowpath curvature accomplishes most of the desired loading shift and the total pressure and angle skews are relatively flat. Predicted loading on the part speed, high operating line is shown in Figure 3.2-12.

A complete aerodynamic summary for the aerodynamic design point is included as Appendix A.

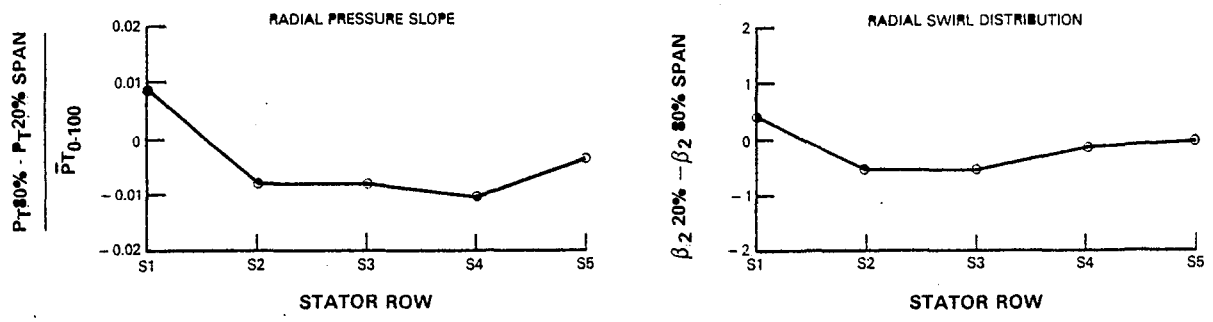

Figure 3.2-11 Low-Pressure Compressor Radial Pressure Slope and Radial Swirl Distribution

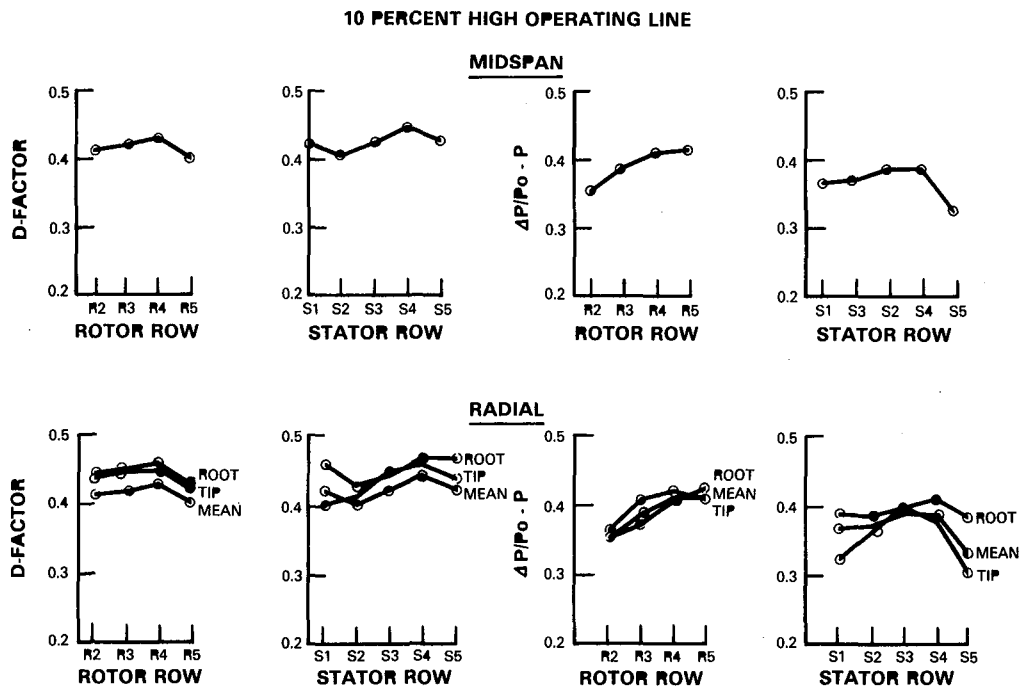

Figure 3.2-12 Low-Pressure Compressor Predicted Part Speed Midspan and Radial Loading

3.2.3 Blading Selection

3.2.3.1 General Airfoil Selection

Controlled diffusion airfoils are used throughout the low-pressure compressor. Figure 3.2-13 compares a conventional 65 series thickness distribution on a circular arc meanline airfoil to a controlled diffusion airfoil. Existing cascade data indicate that controlled diffusion airfoils offer potential

advantages over conventional series airfoils in terms of loss, critical Mach number and low loss range (References 1 and 2). The controlled diffusion airfoils were designed at the aerodynamic design point and their performance was evaluated at the following additional points:

1. Cruise operating line:
   63 percent of maximum cruise power (88.7 percent of low-pressure rotor speed, point of peak low-pressure compressor loadings).

2 10 percent high operating line at constant speed above the 63 percent maximum cruise point. (chosen for surge margin evaluation).

3. 15 percent high operating line at constant speed above the aerodynamic design point. (chosen for surge margin evaluation).

4. Cruise operating line maximum corrected flow (limiting for stator 1 only). (chosen for flow verification.)

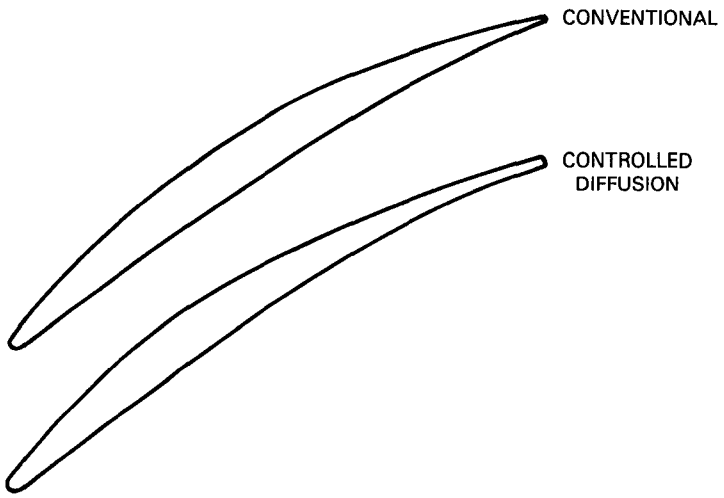

Figure 3.2-13 Airfoil Profile Comparison of a Controlled Diffusion Airfoil and a Conventional, 65 Series Thickness Distribution on a Circular Arc Meanline Airfoil

The controlled diffusion airfoils were designed to have sufficient area margin at the maximum flow condition and to be in the low loss range for the cruise operating line conditions. Some increase in loss was allowed for the high operating line conditions. Analysis of conventional airfoils indicated that some of the airfoil sections had insufficient low loss range to meet operating line conditions. Most were separated at the high operating line conditions, indicating the gain achievable with controlled diffusions airfoils.

A blade-to-blade calculation was performed for all airfoils at several span locations. Controlled diffusion airfoil incidence was established to best satisfy the off-design requirements listed above. Where a range of incidence would satisfy the requirements, aerodynamic design point loss was minimized. Controlled diffusion airfoil deviation was established to satisfy the aerodynamic design point exit angle requirement with the blade-to-blade solution.

The predicted loss and separation of the controlled diffusion airfoils is less than or equal to the corresponding conventional series airfoils. Figure 3.2-14 and Table 3.2-III compare the calculated two-dimensional loss on the operating line. At the design point, the controlled diffusion airfoils are more than 5 percent lower in two-dimensional loss than the conventional series airfoils, with an even greater advantage at the off-design points.

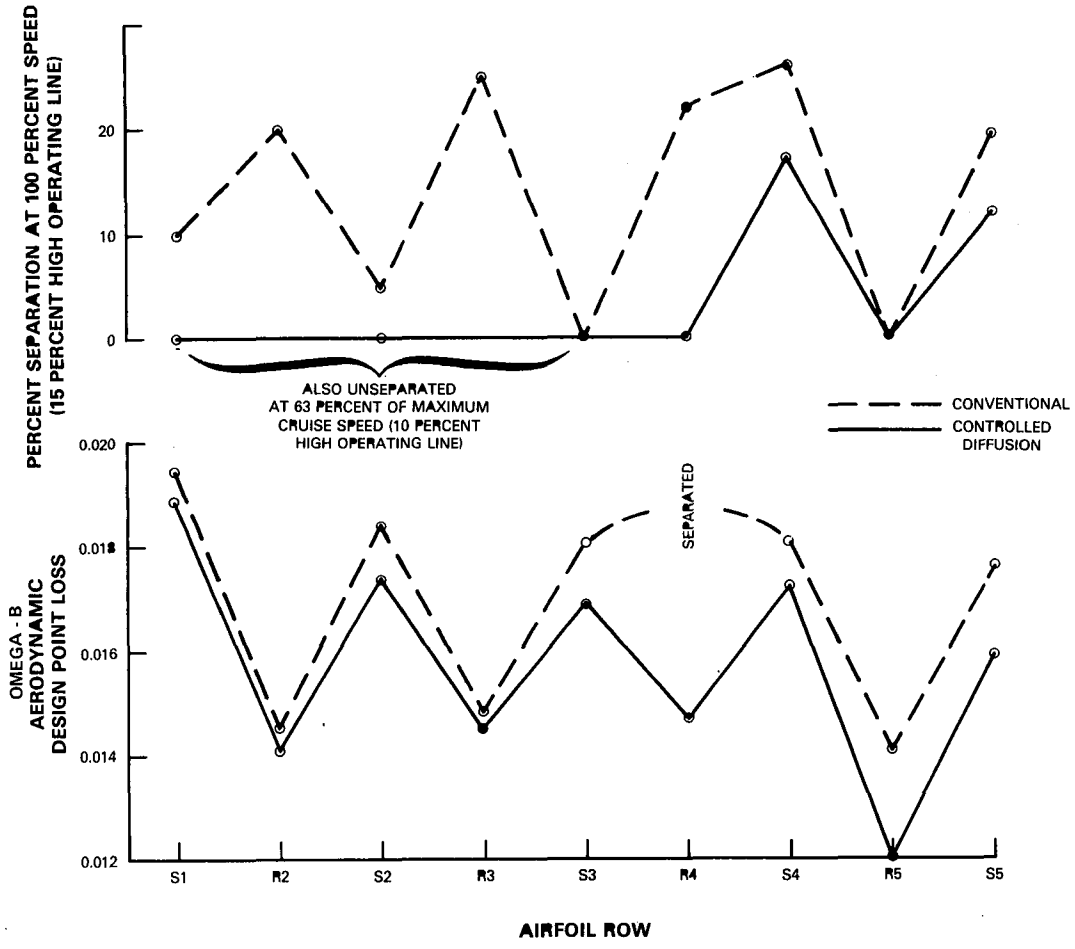

Figure 3.2-14 Comparison of Controlled Diffusion Airfoil and Conventional Airfoil Performance at 40 Percent Span

TABLE 3.2-III

CONTROLLED DIFFUSION AIRFOIL VS CONVENTIONAL AIRFOIL LOSS COMPARISON
(Cruise Operating Line)

Row	Conv. Series	Percent Span	Aerodynamic Design Point		63 percent of Maximum Cruise		Maximum Flow	
			CDA	Conv.	CDA	Conv.	CDA	Conv.
S1	DCA	20	0.0189	0.0200	*	Sep.	0.0190	**
S1		40	0.0188	0.0194	*	Sep.	0.0201	**
S1		60	0.0183	0.0189	*	0.0182	0.0194	Sep.
S1		80	0.0176	Sep.	*	0.0182	0.0189	Sep.
R2	65/CA	20	0.0153	Sep.	0.0151	Sep.	0.0160	Sep.
R2		40	0.0141	0.0146	0.0130	0.0150	0.0148	0.0149
R2		60	0.0135	0.0137	*	0.0125	0.0143	0.0139
R2		80	0.0136	0.0139	*	Sep.	0.0140	0.0130
S2	65/CA	20	0.0185	0.0192	0.0177	0.0191	0.0190	0.0199
S2		40	0.0147	0.0184	0.0156	0.0185	0.0182	0.0191
S2		60	0.0168	0.0174	0.0154	0.0182	0.0175	0.0184
S2		80	0.0161	0.0169	0.0142	Sep.	0.0166	Sep.
R3	65/CA	20	0.0157	Sep.	0.0134	Sep.	0.0160	Sep.
R3		40	0.0145	0.0149	0.0137	Sep.	0.0147	Sep.
R3		60	0.0138	0.0143	0.0134	Sep.	0.0139	Sep.
R3		80	0.0135	Sep.	0.0140	Sep.	0.0135	Sep.
S3	0400	20	0.0180	0.0189	0.0178	0.0187	0.0181	0.0184
S3		40	0.0169	0.0181	0.0163	0.0180	0.0170	0.0182
S3		60	0.0167	0.0173	0.0160	0.0175	0.0161	0.0172
S3		80	0.0162	0.0170	0.0167	0.0175	0.0162	0.0170
R4	65/CA	20	0.0157	Sep.	0.0158	Sep.	0.0160	Sep.
R4		40	0.0147	Sep.	0.0131	Sep.	0.0148	Sep.
R4		60	0.0140	Sep.	*	Sep.	0.0142	Sep.
R4		80	0.0136	Sep.	0.0123	Sep.	0.0137	0.0149
S4	0400	20	0.0183	0.0184	0.0178	0.0173	0.0179	0.0182
S4		40	0.0172	0.0181	0.0174	0.0182	0.0175	0.0180
S4		60	0.0166	0.0171	0.0170	0.0180	0.0170	0.0176
S4		80	0.0162	0.0169	0.0167	0.0174	0.0165	0.0168
R5	0400	20	0.0148	0.0149	0.0149	Sep.	0.0148	Sep.
R5		40	0.0120	0.0141	*	0.0144	*	0.0141
R5		60	0.0117	0.0137	*	0.0139	*	0.0137
R5		80	0.0116	0.0134	0.0118	*	0.0118	0.0138
S5	0400	20	0.0162	0.0188	0.0169	0.0190	0.0177	0.0184
S5		40	0.0159	0.0176	0.0148	0.0183	0.0155	0.0181
S5		60	0.0156	0.0174	0.0155	0.0181	0.0149	0.0172
S5		80	0.0149	0.0173	0.0155	Sep.	0.0148	Sep.

CA = Circular Arc
CDA = Controlled Diffusion Airfoil.
DCA = Double Circular Arc
Sep. = Suction surface separated - see Table 3.2-IV
* Pressure surface laminar, turbulent transition failed.
** Blade-to-blade calculation failed.

Table 3.2-IV compares the amount of suction surface separation on the cruise operating line. None of the controlled diffusion airfoils are separated but several of the conventional series airfoils sections are separated. The increased low loss range of the controlled diffusion airfoils is even more evident on the high operating line (Table 3.2-V) where almost all of the conventional series airfoil sections are separated and most of the controlled diffusion airfoil sections are not separated. In Table 3.2-V, the blade-to-blade calculations for the high operating line at 63 percent of maximum cruise power, where the front end is more critical, were only run through stator 3. The more critical condition for the back end is the high operating line at the aerodynamic design point speed. A low-pressure compressor airfoil final geometry summary is contained in Table 3.2-VI.

TABLE 3.2-IV

PERCENT SUCTION SURFACE SEPARATION
(Cruise Operating Line)

Airfoil Row	Percent Span	Aerodynamic Design Point		63% of Maximum Cruise		Maximum Flow	
		CDA	Conv.	CDA	Conv.	CDA	Conv.
S1	20	0	0	0	18	0	**
S1	40	0	0	0	1	0	**
S1	60	0	0	0	0	0	3
S1	80	0	2	0	0	0	6
R2	20	0	10	0	16	0	12
R2	40	0	0	0	0	0	0
R2	60	0	0	0	0	0	0
R2	80	0	0	0	8	0	0
S2	20	0	0	0	0	0	0
S2	40	0	0	0	0	0	0
S2	60	0	0	0	0	0	0
S2	80	0	0	0	2	0	1
R3	20	0	6	0	10	0	7
R3	40	0	0	0	3	0	3
R3	60	0	0	0	2	0	2
R3	80	0	1	0	9	0	3
S3	20	0	0	0	0	0	0
S3	40	0	0	0	0	0	0
S3	60	0	0	0	0	0	0
S3	80	0	0	0	0	0	0
R4	20	0	15	0	12	0	15
R4	40	0	5	0	4	0	5
R4	60	0	1	0	2	0	3
R4	80	0	1	0	11	0	0
S4	20	0	0	0	0	0	0
S4	40	0	0	0	0	0	0
S4	60	0	0	0	0	0	0
S4	80	0	0	0	0	0	0
R5	20	0	0	0	7	0	3
R5	40	0	0	0	0	0	0
R5	60	0	0	0	0	0	0
R5	80	0	0	0	6	0	0
S5	20	0	0	0	0	0	0
S5	40	0	0	0	0	0	0
S5	60	0	0	0	0	0	0
S5	80	0	0	0	2	0	2

CDA = Controlled Diffusion Airfoil.
** Blade-to-blade calculation failed.

3.2.3.2 Stator 1

The Energy Efficient Engine flight design requirements specify that stator 1 have anti-icing capability. To satisfy this requirement and to facilitate fabrication, the chord and thickness are sufficiently large to pass the anti-icing air and the locus of leading edge points is a straight line. In addition, because the first test of the low-pressure compressor will be in the Integrated Core/Low Spool, stator 1 has been made adjustable to facilitate adjusting the low-pressure compressor flow, if required.

TABLE 3.2-V

PERCENT SUCTION SURFACE SEPARATION

		100% Speed 15% High Operating Line		63% of Maximum cruise 10% High Operating Line	
Airfoil Row	Percent Span	CDA	Conv.	CDA	Conv.
S1	20	0	29	0	100*
S1	40	0	10	0	97*
S1	60	0	8	0	96*
S1	80	0	12	0	99*
R2	20	6	22	26	30
R2	40	0	20	0	98*
R2	60	0	23	0	**
R2	80	0	97*	0	**
S2	20	0	17	0	28
S2	40	0	5	0	18
S2	60	0	4	0	16
S2	80	0	12	0	20
R3	20	0	26	30	33
R3	40	0	25	0	25
R3	60	0	26	0	24
R3	80	11	31	15	27
S3	20	0	32	28	33
S3	40	0	0	0	17
S3	60	0	18	0	20
S3	80	0	26	0	26
R4	20	28	28		
R4	40	0	22		
R4	60	0	18		
R4	80	0	18		
S4	20	24	39		
S4	40	17	26		
S4	60	18	27		
S4	80	22	31		
R5	20	31	28		
R5	40	0	0		
R5	60	0	0		
R5	80	0	10		
S5	20	22	28		
S5	40	12	19		
S5	60	0	20		
S5	80	0	24		

CDA = Controlled Difusion Airfoil.
* Laminar separation, laminar-turbulent transition failed due to excessive leading edge spike.
** Blade-to-blade calculation failed.

TABLE 3.2-VI

FINAL AIRFOIL GEOMETRY SUMMARY

	Rotor			
	2	3	4	5
Airfoil Series	CDA	CDA	CDA	CDA
Number of Airfoils	82	88	90	74
Material	AMS 4928	AMS 4928	AMS 4928	AMS 4928
Root Radius, cm	49.58	49.50	46.91	42.16
(in)	(19.52)	(19.49)	(18.47)	(16.60)
Mean Radius, cm	54.51	53.84	51.16	46.79
(in)	(21.46)	(21.20)	(20.14)	(18.42)
Tip Radius, cm	59.08	58.24	55.42	51.10
(in)	(23.26)	(22.93)	(21.82)	(20.12)
Length, cm	9.49	8.79	8.71	9.27
(in)	(3.74)	(3.46)	(3.43)	(3.65)
Hub/tip Ratio	0.84	0.85	0.85	0.83
Root Chord, cm	4.17	3.84	3.63	4.14
(in)	(1.64)	(1.51)	(1.43)	(1.63)
Mean Chord, cm	4.19	3.84	3.61	4.11
(in)	(1.65)	(1.51)	(1.42)	(1.62)
Tip Chord, cm	4.50	3.84	3.61	4.06
(in)	(1.77)	(1.51)	(1.42)	(1.60)
Aspect Ratio	2.28	2.29	2.40	2.24
Root Thickness/Chord	0.085	0.083	0.085	0.064
Mean thickness/Chord	0.057	0.064	0.065	0.045
Tip Thickness/Chord	0.030	0.045	0.045	0.036
Root Camber, degrees	43.4	35.6	43.9	43.2
Mean Camber, degrees	18.4	20.3	22.2	18.0
Tip Camber, degrees	27.9	25.8	28.7	26.2
Root Chord, degrees	20.0	22.5	25.1	31.6
Mean Chord, degrees	31.3	34.4	35.7	39.1
Tip Chord, degrees	42.6	45.4	47.4	47.9
Root Solidity	1.096	1.086	1.108	1.184
Mean Solidity	1.002	0.999	1.011	1.034
Tip Solidity	0.993	0.923	0.930	0.938

CDA = Controlled Diffusion Airfoils

TABLE 3.2-VI (Continued)

	Stator				
	1	2	3	4	5
Airfoil Series	CDA	CDA	CDA	CDA	
Number of Airfoils	76	102	110	108	90
Material	(Steel)	AMS 4135	AMS 4135	AMS 4135	AMS 4135
Root Radius, cm	48.52	49.75	48.65	45.00	39.32
(in)	(19.10)	(19.59)	(19.15)	(17.72)	(15.48)
Mean Radius, cm	53.80	54.33	52.73	49.15	43.99
(in)	(21.18)	(21.39)	(20.76)	(19.35)	(17.32)
Tip Radius, cm	58.84	58.95	57.09	53.51	48.39
(in)	(23.17)	(23.21)	(22.48)	(21.07)	(19.05)
Length, cm	10.13	9.14	8.64	8.76	9.78
(in)	(3.99)	(3.60)	(3.40)	(3.45)	(3.85)
Hub/tip Ratio	0.83	0.84	0.85	0.84	0.81
Root Chord, cm	6.70	4.18	3.78	3.62	3.91
(in)	(2.64)	(1.65)	(1.49)	(1.43)	(1.54)
Mean Chord, cm	6.68	4.19	3.76	3.63	3.94
(in)	(2.63)	(1.65)	(1.48)	(1.43)	(1.55)
Tip Chord, cm	6.68	4.19	3.78	3.63	3.94
(in)	(2.63)	(1.65)	(1.49)	(1.43)	(1.55)
Aspect Ratio	1.54	2.20	2.29	2.44	2.50
Root Thickness/Chord	0.050	0.070	0.070	0.069	0.068
Mean Thickness/Chord	0.061	0.070	0.070	0.069	0.068
Tip Thickness/Chord	0.070	0.070	0.070	0.069	0.069
Root Camber, degrees	39.4	40.8	34.5	47.4	58.6
Mean Camber, degrees	22.7	22.9	27.0	36.3	42.9
Tip Camber, degrees	22.4	36.2	39.5	50.3	56.3
Root Chord, degrees	35.4	34.8	28.4	26.3	17.5
Mean Chord, degrees	30.5	27.5	25.6	23.1	12.1
Tip Chord, degrees (from axial)	30.2	32.7	31.2	29.2	15.9
Root Solidity	1.659	1.363	1.360	1.386	1.426
Mean Solidity	1.493	1.248	1.252	1.266	1.278
Tip Solidity	1.371	1.156	1.160	1.171	1.168

CDA = Controlled Diffusion Airfoil.

3.2.3.3 Rotor Tilts

Canting the rotor blades (negative axial tilt) to match the sloping flowpath caused a substantial centrifugal bending moment. To reduce rotor root bending stresses, the rotor blades were tilted towards the suction surface by the following amounts:

Rotor	Tangential Tilt, cm (in)	
1	0.254	(0.10)
2	0.762	(0.30)
3	1.143	(0.45)
4	1.270	(0.50)

3.2.4 Performance Predictions

3.2.4.1 Efficiency

The Energy Efficient Engine low-pressure compressor, a moderately conservative design with aerodynamics well within experience attained in high bypass turbofan engines, has a predicted efficiency of 90.0 percent in the fully developed flight propulsion system measured from the stator 1 exit to the stator 5 exit. If stator 1 is included with the low-pressure compressor, the fully developed flight propulsion system predicted efficiency is 85.9 percent. Table 3.2-VII shows a performance prediction based on test data from a Pratt & Whitney Aircraft commercial engine low-pressure compressor, including stator 1. The first Integrated Core/Low Spool test is debited 2.5 percent which consists of 2 percent for radial and streamwise mismatches, clearances, etc., and 0.5 percent for adjusting the flow to obtain the desired engine bypass ratio with the adjustable stator 1.

3.2.4.2 Surge Margin

In the preliminary design phase, the target surge margin at the aerodynamic design point was set at 20 percent. During the detailed design, it was realized that the critical surge margin requirement would occur at part speed, therefore, loadings were balanced on a 10 percent high operating line at 63 percent of maximum cruise thrust flight condition (88.7 percent of aerodynamic design point speed). The resulting calculated surge margin at aerodynamic design point speed is 18 percent and at the 63 percent of maximum cruise point is 16 percent.

Figure 3.2-15 shows that the static pressure loading of the low-pressure compressor at 18 percent surge margin at design speed and 16 percent surge margin at 63 percent of maximum cruise are at the limits defined by our experience. This indicates that the surge margin is aggressive, but attainable. Figure 3.2-16 shows that the average D-factor loading level of the low-pressure compressor at the above surge points is well below our peak loading experience.

TABLE 3.2-VII

LOW-PRESSURE COMPRESSOR PERFORMANCE PROJECTIONS

		Efficiency, percent	
		Adiabatic	Polytropic
Test		0.8799	0.8959
Predicted Change			
	Two-dimensional		-0.0027
	Leading Edge Radius		-0.0004
	Mach Number		-0.0001
	Endwall		-0.0003
	Cavity		-0.0010
	Rotor Clearance		-0.0005
	Stator 1 Loss		-0.0204
		0.8600	0.8705
	Tip Trenching	+0.0020	
Predicted		0.8620	0.8724
Goals:			
	Flight Propulsion System	0.859	0.869
	First Integrated Core/Low Spool Test	0.834	0.846

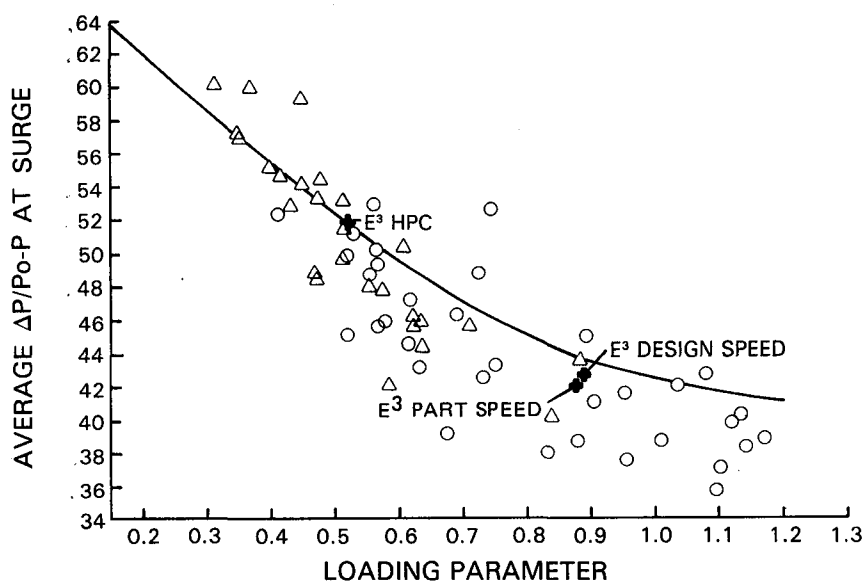

Figure 3.2-15 Low-Pressure Compressor Surge Correlation with Loading Level Shown With Points of Previous Experience

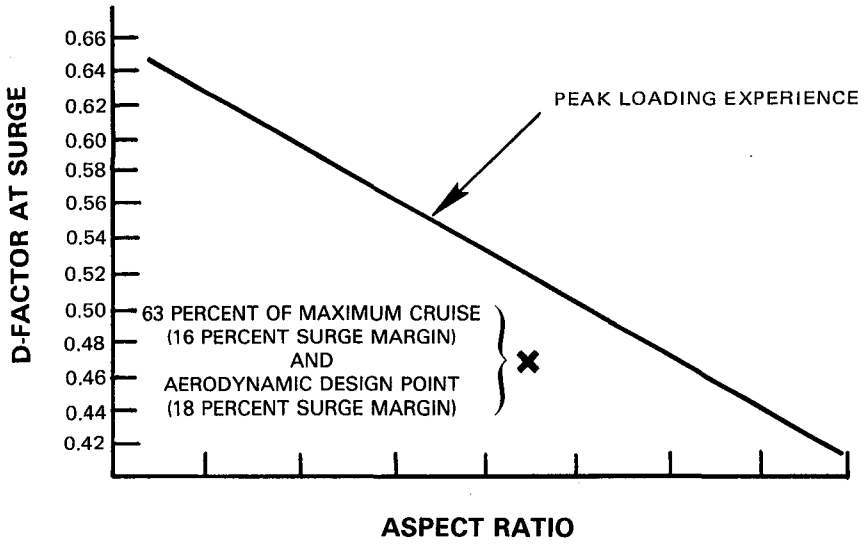

Figure 3.2-16 Low-Pressure Compressor Surge Correlation with D-Factor

A low-pressure compressor stability audit was conducted in the preliminary design phase and used to evaluate the final design. A typical stability audit is shown in Table 3.2-VIII for the takeoff point. The effect of both surge line and operating line change are accounted for as functions of the stability threats. The major destabilizing influences are power transients and engine deterioration. This audit shows the available surge margin substantially exceeds the required surge margin for the takeoff point (90.7 percent speed).

TABLE 3.2-VIII

TYPICAL SURE MARGINE AUDIT FOR
LOW-PRESSURE COMPRESSOR AT TAKEOFF

	Fixed Quantity, percent	Random Quantity, percent
Surge Line Degradation		
Engine Deterioration	1	±0.5
Distortion	2	0
Engine Production Clearance	0	±1.0
Operating Line Degradation		
Engine Power Transients	4	0
Control Production Tolerance	0	±1.1
Control Deterioration	0	±0.6
Engine Deterioration	2	±1.1
Engine Production Tolerance	0	±1.0
Sum of Fixed	9	
Sum of Random		±2.2
Required Margin	11.2	
Available Surge Margin	16.3	

The low-pressure compressor design includes a bleed between rotor 5 and stator 5 for surge protection. The bleed ports are sized for 15 percent bleed. It is anticipated the bleeds will be used only for starting and, in the flight propulsion system, for reverse operation where the expected requirement should not exceed 10 percent. There will be no need to open the bleeds above 63 percent of cruise power because the loadings were balanced on a high operating line at this point and ample surge margin is available.

3.3 LOW-PRESSURE COMPRESSOR MECHANICAL DESIGN

3.3.1 Overview

The primary concerns during the Energy Efficient Engine low-pressure compressor mechanical design were to minimize design and fabrication costs, while maintaining the aerodynamic flowpath of the Flight Propulsion System over the range of operating speeds encountered during testing. As a result, low cost designs were adopted in the rotor, vane and shroud, and case assemblies as well as in the bleed system.

A steel bolted rotor was selected to replace the Flight Propulsion System welded titanium configuration. Raw material savings were realized, and the need for a weld development program was avoided. Design costs were also reduced through the utilization of an existing design configuration.

Vane outer shroud and mating case designs were simplified to avoid intricate machining. Hence, the heavier than optimum designs that resulted did not require the normal in-depth iterative analysis normally needed in flight weight hardware.

The bleed system uses many existing design parts. The bleed actuator, translating links, and most fasteners are JT9D engine parts. The use of these parts saved substantial design effort and will result in considerable hardware savings.

A fan/low-pressure compressor temperature and pressure summary was developed early in the design phase for use in the detailed design and analyses of the individual pieces of hardware. These analyses were conducted using the aerodynamic definition presented in this report in conjunction with a preliminary mechanical definition of the low-pressure compressor. Stabilized data were generated at sea level takeoff on a 28.9°C (84°F) day, the aerodynamic design point (ADP), and sea level idle on a 28.9°C (84°F) day. The results of these analyses are shown on a crosssection of the fan/low-pressure compressor components in Figure 3.3-1.

3.3.2 Rotor Design

3.3.2.1 General Description

The Integrated Core/Low Spool low-pressure compressor rotor consists of four low alloy steel (AMS 6414) disks bolted together at two flange locations. The compressor stages are identified in Figure 3.3-2 by the designations of R2 for the first stage rotor, R3 for the second stage rotor, R4 for the third stage rotor, and R5 for the fourth stage. The R1 designation is used to identify the fan stage.

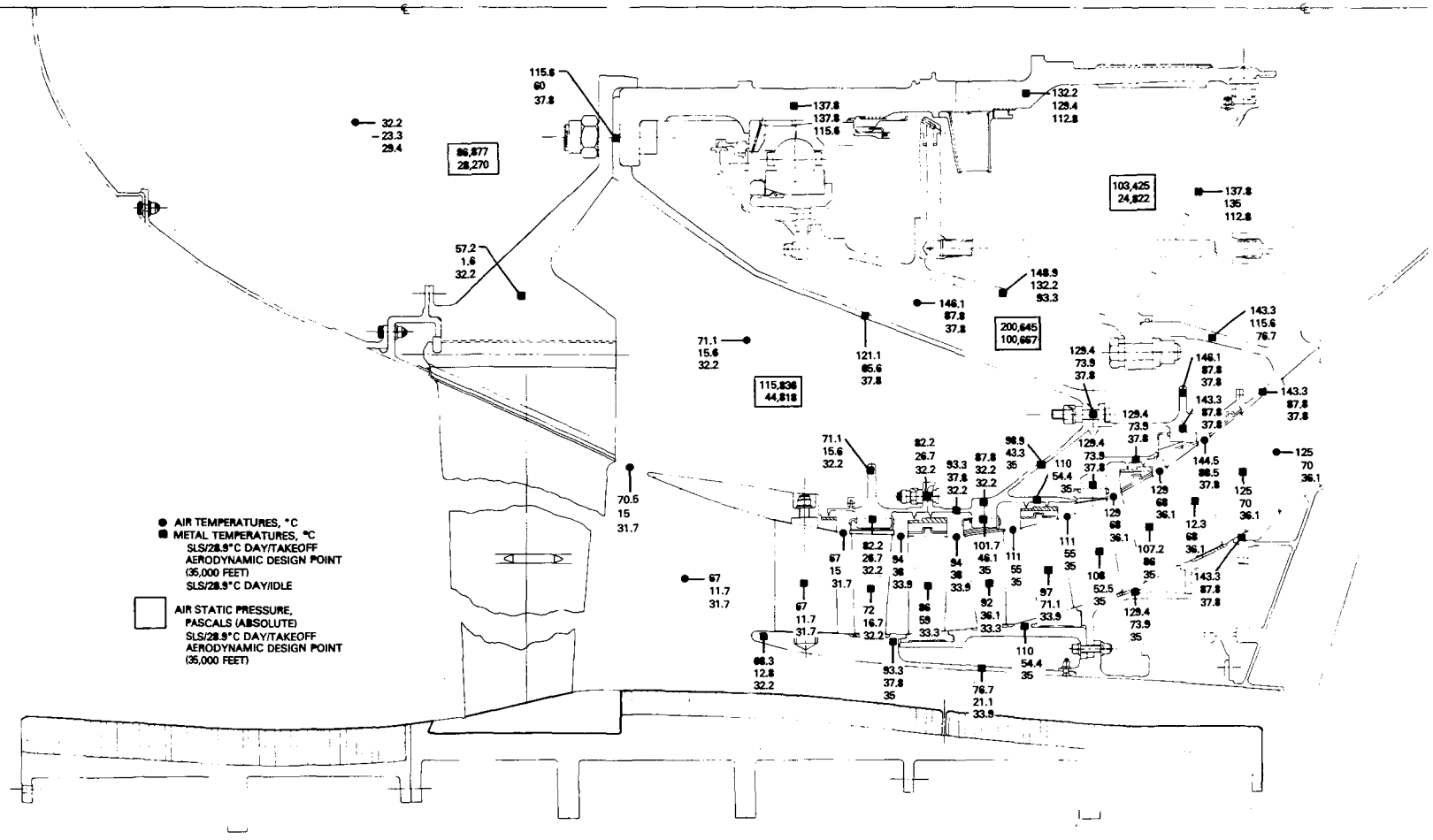

Figure 3.3-1A Low-Pressure Compressor Pressure and Temperature Analysis Results (^{o}C, Pascals)

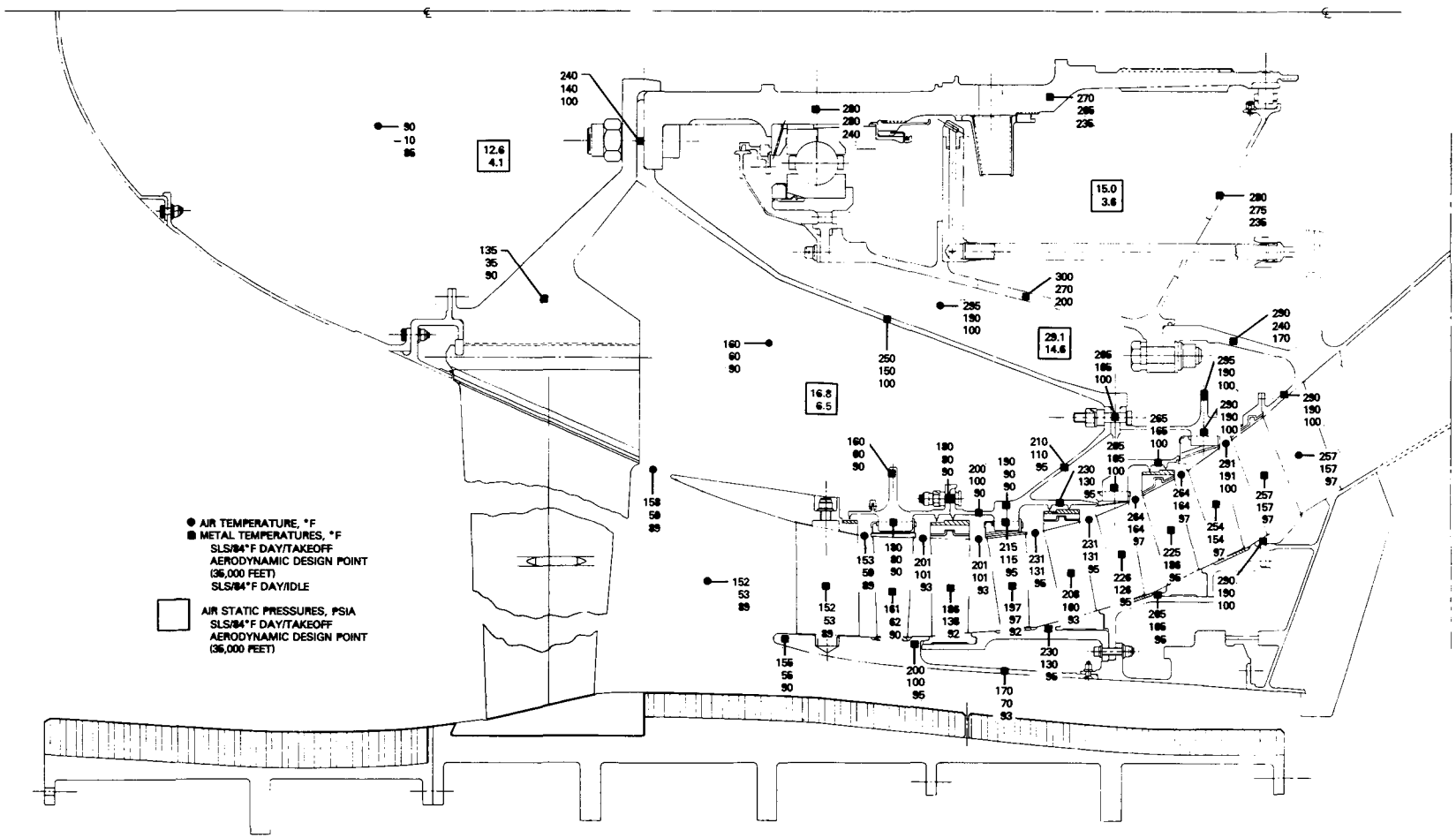

Figure 3.3-1B Low-Pressure Compressor Pressure and Temperature Analysis Results (^{O}F, psi)

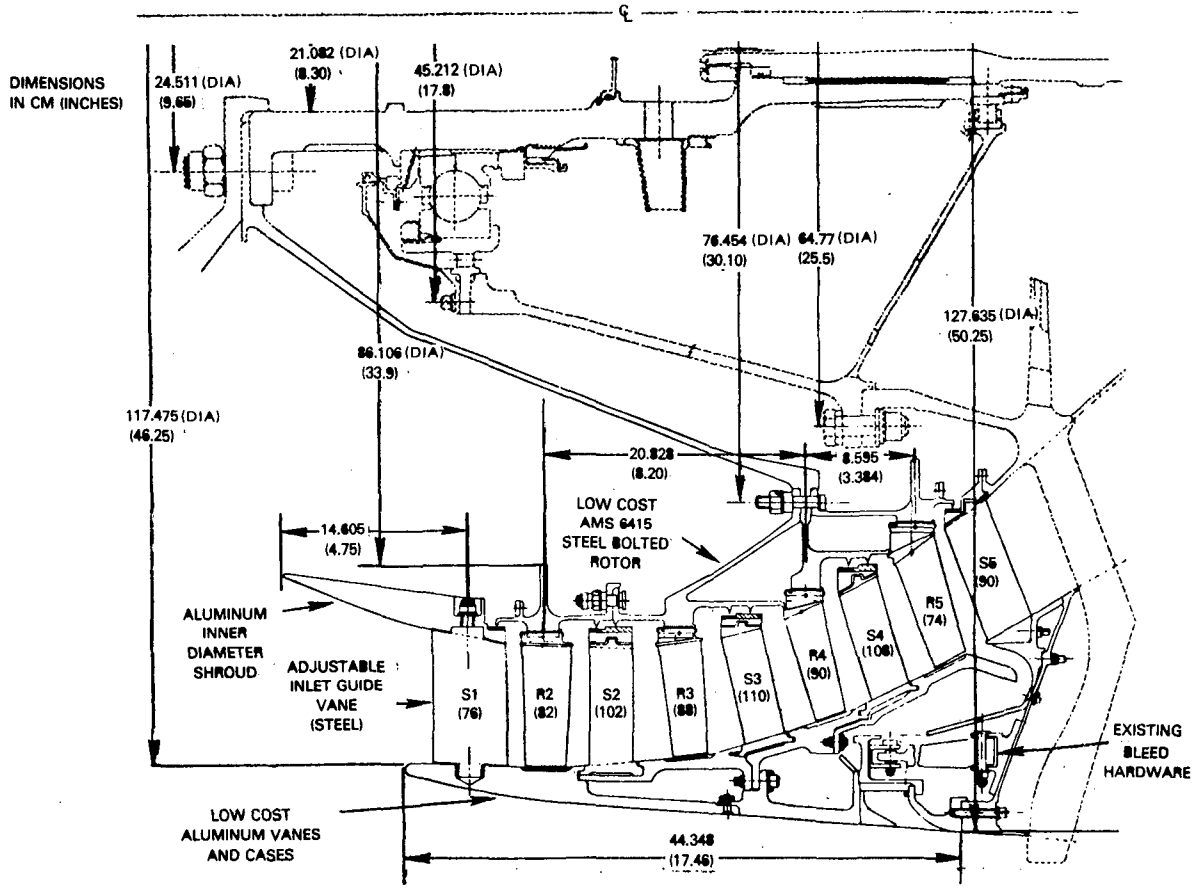

Figure 3.3-2 Low Cost Integrated Core/Low Spool Low-Pressure Compressor Component - Aerodynamics Remain the Same as for the Flight Propulsion System

Rotor 4 features integral hub and disk geometry. A bolt circle is provided in the disk portion which allows the coupling of rotors 3 and 5 to rotor 4. The forward section of the hub is flanged and attaches to the fan and low-pressure rotor system with the fan tie rods. To complete the rotor assembly, rotor 2 is bolted to rotor 3 at a flange located between the two stages.

The configuration of the Integrated Core/Low Spool low-pressure compressor rotor is very similar to a JT9D engine rotor with differences only in two areas. The size of the Energy Efficient Engine low-pressure compressor is slightly smaller than the JT9D low-pressure compressor. In addition, the Energy Efficient Engine utilizes integral knife edge seals for economic reasons in the experimental hardware, whereas the JT9D engine seals are separate parts.

3.3.2.2 Low Cost Factors

The main thrust of the bolted rotor design was to reduce program costs and risks without impacting the validity of component performance. This objective was accomplished in several ways.

A. Material substitution - changing the material specification from titanium (AMS 4928) to steel reduced program costs significantly. Moreover, it reduced the raw material delivery risks inherent in the current titanium market and thus ensured the availability of material consistent with the required fabrication schedules.

B. Bolted rotor design - The use of the bolted design eliminated the need for a weld development program that would be required to determine the weld parameters needed to join the large diameter titanium disks. Utilization of a known and tested design also reduced the risk associated with the fabrication and testing of new hardware.

C. Utilization of existing parts - The rotor bolts, nuts and washers used at the two flange locations are existing parts. As a result, design and procurement costs were significantly reduced.

D. Incorporation of integral seal design - The use of integral knife edge seals reduced the number of rotor parts, simplified the design, and saved raw material costs while preserving the use of small seal cavities on the inner flowpath.

3.3.2.3 Material Selection

The material originally selected for use in the rotor was titanium. This material has been retained for the Flight Propulsion System. However, the escalating cost of titanium and its long delivery time prompted a survey of alternative materials that could be substituted for the Integrated Core/Low Spool test program. The result of this survey was the selection of AMS 6414 wrought alloy steel, which is a low alloy steel with excellent low temperature properties. This material is readily available, comparatively less expensive and has a successful history of applications in the JT8D engine low-pressure compressor.

3.3.2.4 Critical Speed

The low-pressure rotor is supported by three bearings. The two front bearings, supported at the compressor intermediate case provide moment restraint for the overhung fan/low-pressure compressor assembly to minimize maneuver deflections. The low-pressure turbine is cantilevered off the rear bearing, which is held by the turbine intermediate case structure and is axially positioned to minimize maneuver deflections at the more efficiency sensitive front stages.

The entire engine rotor and case structure was modeled to allow for vibratory interaction between components. Separate models were analyzed for the Flight Propulsion System and the Integrated Core/Low Spool configurations with the appropriate materials and weight differences. As a result of the analyses performed, no high energy modes are anticipated in the running range.

Figure 3.3-3 graphically summarizes the three rotor modes of concern for both the Integrated Core/Low Spool and Flight Propulsion System. The fan and low-pressure turbine modes have low strain energy (less than 16 percent) and

occur below minimum cruise speed. The high strain energy (greater than 70 percent) low shaft mode is predicted to occur above maximum rotor speed with acceptable margin (greater than 70 percent). The critical speeds, mode shapes, and associated strain energies for the Integrated Core/Low Spool are presented in Figure 3.3-4.

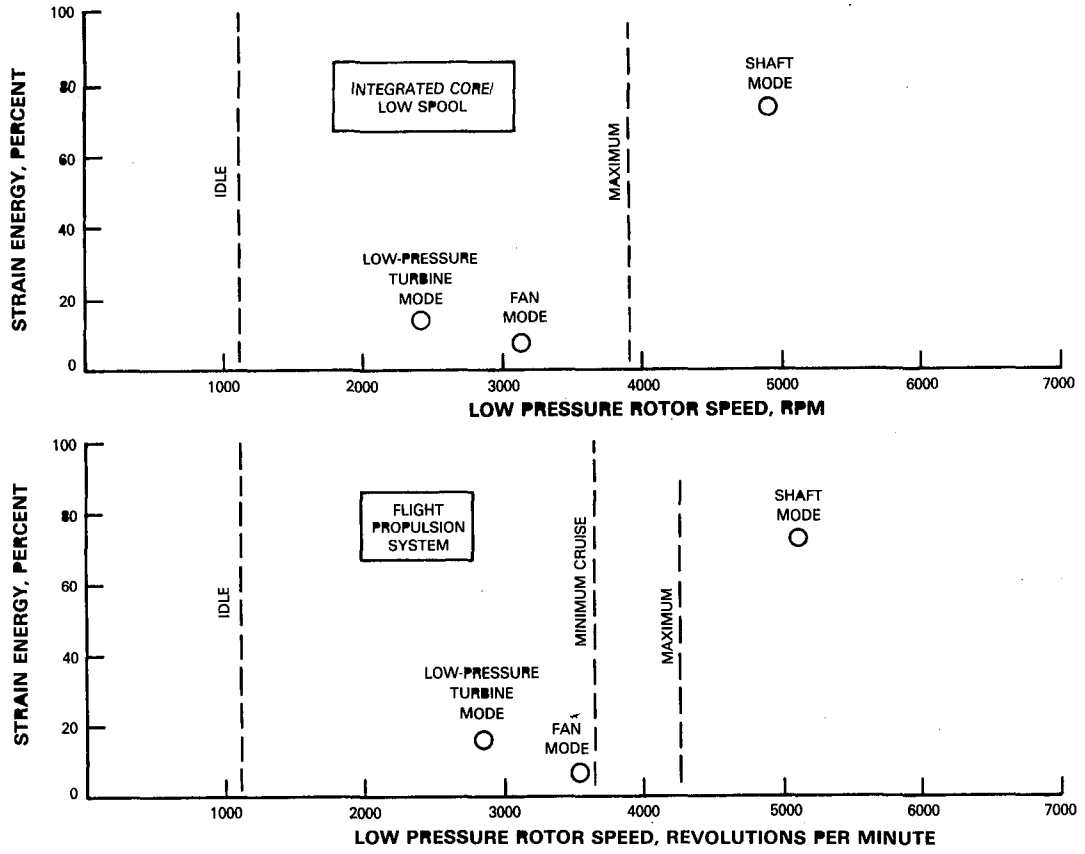

Figure 3.3-3 Low-Pressure Rotor Critical Speeds

The effect of the increased Integrated Core/Low Spool low-pressure compressor rotor weight resulting from the use of steel in place of titanium can be seen by comparing Figures 3.3-3 and 3.3-4. This shows that the increased weight will drop the Integrated Core/Low Spool fan mode down to 3130 rpm versus 3550 rpm for the Flight Propulsion System, but it remains acceptable.

As the low-pressure turbine design evolved and component weights and spring rates were defined, it became apparent that the low-pressure turbine mode was a problem due to its high (.20 percent) strain energy. In addition, forced response analysis indicated that the mode was very sensitive to rotor imbalance. A viscous oil-film damper was therefore incorporated into the number five bearing design to control the low-pressure turbine mode response. The damper design is a conventional piston ring type with .007 in radial clearance which was analytically shown to desensitize the mode and generate enough hydrodynamic force to insure lift off.

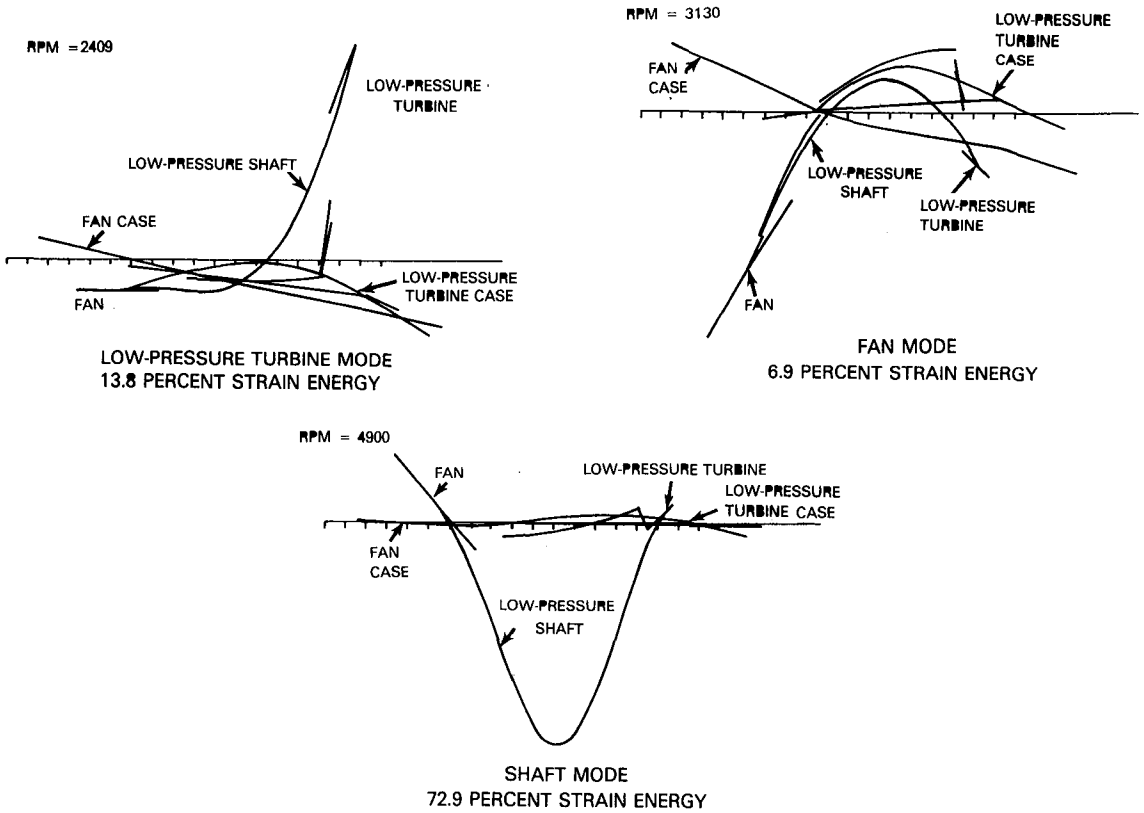

Figure 3.3-4 Low-Pressure Rotor Critical Speeds and Mode Shapes for Integrated Core/Low Spool Test

Figure 3.3-5 shows the rotor frame critical speed model. Figure 3.3-6 shows the rotor frame spring rates used in the model, and Figure 3.3-7 shows the effect of the number 5 bearing damper on rotor deflection.

3.3.2.5 Stress Analyses

Rotor stress analyses were accomplished by utilizing a computerized shell analysis program. The complete analysis included calculations at (1.) sea level takeoff on a 28.9°C (84°F) day, (2.) aerodynamic design point, (3.) single blade loss in rotor 2 at takeoff, and (4.) single blade loss in rotor 5 at takeoff.

The objectives of these analyses were to identify stress levels as well as deflection patterns, axial and radial growths of disk rims, snap diameter compatabilities, effects of blade loss on rotor stresses, and low cycle fatigue lives of the disks. Input data for the analyses included the definition of rotor rim loads due to centrifugal effects. A breakdown of these rim loads is presented in Table 3.3-I. In addition, temperature and pressure affects based on prior analyses results, shown in Figure 3.3-1, were input into the analyses.

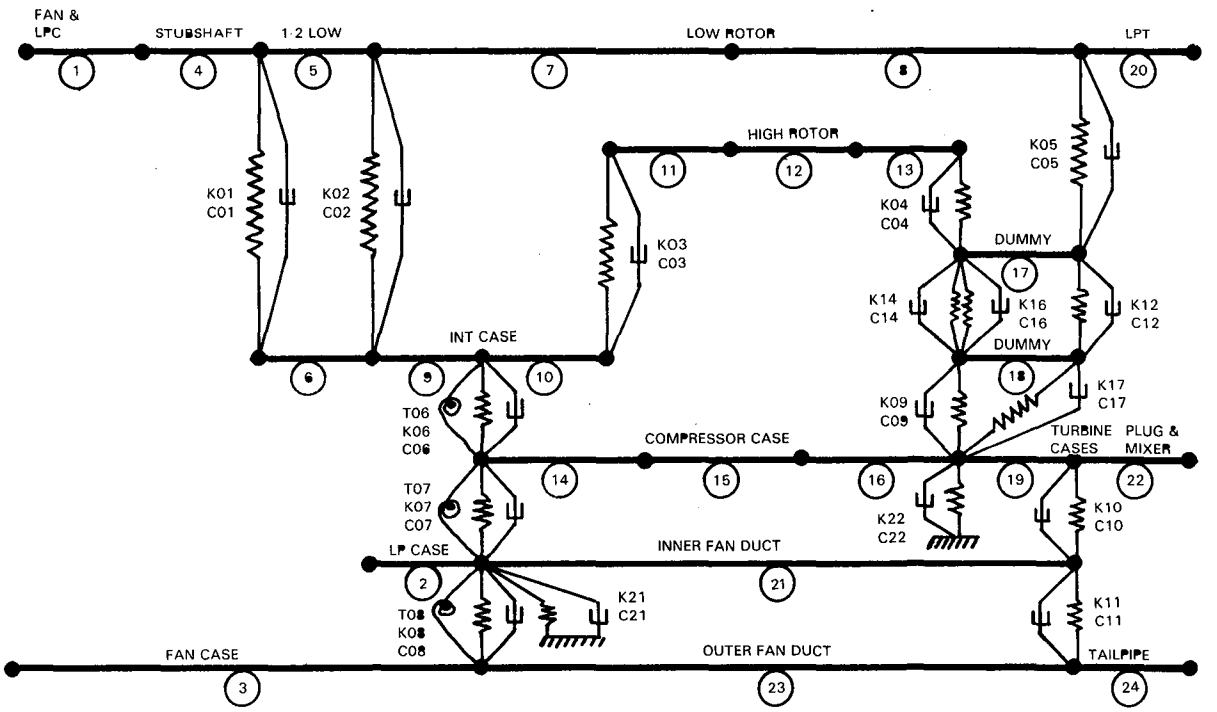

Figure 3.3-5 Low-Pressure Rotor Critical Speed Model

A summary of the stresses and lives calculated for the rotor disks is shown in Table 3.3-II. Shown in Figure 3.3-8 are some representative bending stresses, including the maximum level found in the rotor which is 1.98×10^8 Pascals (28,750 psi). All stresses and lives meet Integrated Core/Low Spool test requirements.

The blade loss analysis indicated little increase in rotor stress level. A maximum bending stress of 2.76×10^8 Pascals (40,000 psi) was identified when blade loss was applied at either rotor 2 or rotor 5. Analysis of the blade loss effects on the rotor tie bolts showed a maximum stress level of 1.38×10^7 Pascals (2000 psi) induced in the bolts.

Table 3.3-III summarizes the stress levels found in the disk lug attachments due to blade pull. The stresses are low and are consistent with the conservative nature of the rotor design.

SPAN IDENTIFICATION		ROTOR FRAME SPRINGRATES		
Span	Description	Spring Number	Value (lbs/in)	Description
1	Fan/LPC Rotor	K01*	$9.35X10^6$	#1 Bearing
2	LPC Case	K02*	$1.0X10^5$	#2 Bearing
3	Fan Case	K03*	$2.37X10^5$	#3 Bearing & Support (Equivalent)
4	Stubshaft	K04*	$1.0X10^6$	#4 Bearing
5	1-2 Low Shaft	K05*	$.40X10^6$ (IC/LS)	#5 Bearing
6	#1 Bearing Support Cone		$.60X10^6$ (FPS)	#5 Bearing
7	Low Shaft Forward	K06	$5.0X10^6$	Fan Intermediate Case-Linear
8	Low Shaft Aft	T06	$1.0X10^9$	Fan Intermediate Case-Trunnion
9	#2 Bearing Support	K07	$3.9X10^7$	Fan I/C Struts Linear
10	#3 Bearing Support	T07	$4.8X10^8$	Fan I/C Struts Trunnion
11	High Rotor	K08	$2.2X10^7$	Fan Exhaust Case-Linear
12	High Rotor	T08	$4.5X10^8$	Fan Exhaust Case-Trunnion
13	High Rotor	K09	$1.68X10^6$	Turbine Intermediate Case
14	High Compressor Case	K10	$5.0X10^5$	Fan Duct/Turbine Case Connector
15	High Compressor Case	K11	$1.0X10^9$	Fan Duct Bifurcation Beam
16	Diffusion/HPT Case	K12*	$1.33X10^6$	#5 Bearing Viscous Damper
17	Dummy	K14*	$5.16X10^5$	#4 Bearing Viscous Damper
18	Dummy	K16	$2.0X10^5$	#4 Bearing Centering Spring
19	Low Turb & Exhaust Case	K17	$5.8X10^5$	Turbine Intermediate Case
20	Low Pressure Turbine Rotor	K21	$1.0X10^5$	Front Mount
21	Inner Fan Duct	K22	$1.0X10^5$	Rear Mount
22	Plug Mixer			
23	Outer Fan Duct			
24	Tail Pipe			

* Springrates are a function of the type of load.

Figure 3.3-6 Low-Pressure Compressor Rotor Frame Spring Rates

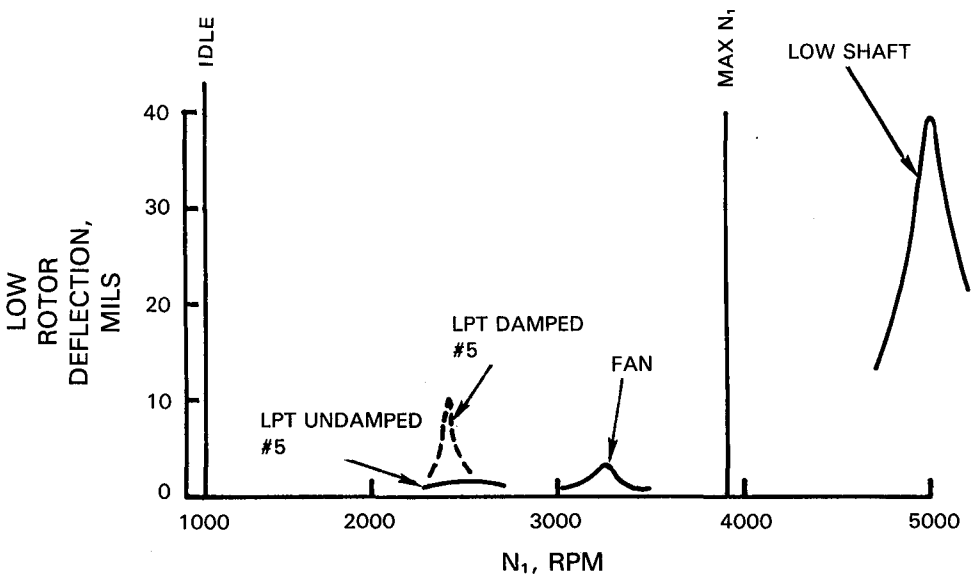

Figure 3.3-7 Low-Pressure Rotor Imbalance Response

TABLE 3.3-I

SUMMARY OF ROTOR RIM LOADS
(Total Newtons (Pounds) Pull Per Stage)

Location	Rotor 2	3	4	5
Blades	217,529 (48,905)	185,846 (41,782)	172,138 (38,700)	137,488 (30,910)
Attachment Platform and Blade Retention	163,402 (36,736)	194,929 (43,824)	228,583 (51,390)	286,362 (64,380)
Platform Seal	5471 (1230)	5871 (1320)	6005 (1350)	4937 (1110)
Disk Dead Rim	339,049 (76,225)	308,286 (69,309)	275,678 (61,978)	239,169 (53,770)
Total Rim Pull	725,451 (163,096)	694,933 (156,235)	682,403 (153,418)	667,956 (150,170)

Notes:

- Pulls are calculated at 3902 rpm.
- Integrated Core/Low Spool Redline Speed is 3902 rpm.
- $\text{Pull} = MRW^2 = \frac{W}{386.4} \times R \times \left(\frac{3902\ 2\pi}{60}\right)^2$

TABLE 3.3-II

SUMMARY OF DISK STRESSES AND LIVES

Rotor	Average Tangential Stress	Burst Margin	Radial Stress, Pascals (psi) Bolt Bore	Circle	Rim	Low Cycle Fatigue (Cycles) Bolt Bore	Circle	Rim
2	3.44×10^8 (49,856)	1.63	4.09×10^7 (5933)	-----	9.41×10^6 (1365)	Greater than 100,000	-----	10,000
3	3.38×10^8 (48,988)	1.64	1.91×10^7 (2772)	-----	1.02×10^7 (1458)	Greater than 100,000	-----	10,000
4	2.67×10^8 (38,675)	1.83	1.45×10^7 (2097)	4150	1.01×10^7 (1627)	Greater than 100,000	80,000	Greater than 100,000
5	2.96×10^8 (42,861)	1.72	8.75×10^6 (1270)	-----	1.05×10^7 (1520)	Greater than 100,000	-----	Greater than 100,000
2-3	3.91×10^8 (56,806)	1.53	-----	$\frac{3.77}{2.44} \times 10^7$ $\frac{(5472)}{(3535)}$	-----	-----	8000	-----

Notes:

- o Stress levels are based on takeoff condition.
- o At bolt circle locations, the most limiting design stresses are accounted.

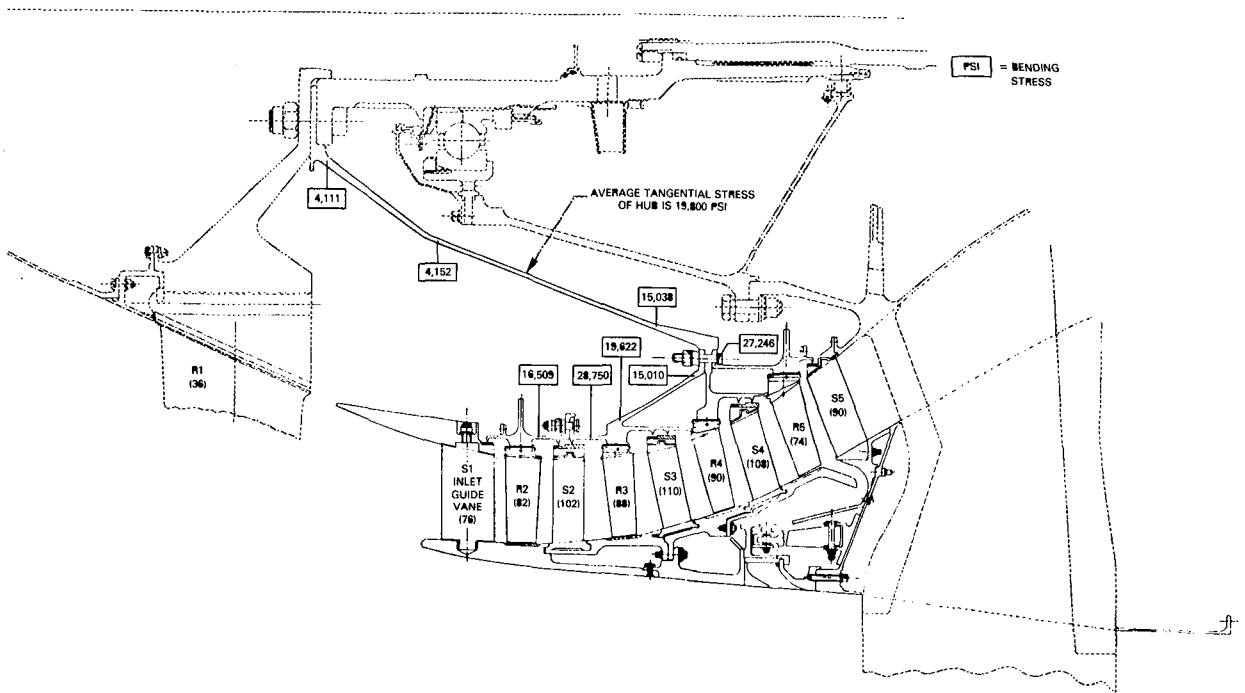

Figure 3.3-8 Low-Pressure Rotor Bending Stresses

TABLE 3.3-III

DISK LUG STRESSES
(Pascals (Pounds) per Square Inch)

Stress Location	Rotor 2	3	4	5
Disk Lug Tooth Bearing	8.21×10^7 (11,905)	6.98×10^7 (10,128)	6.79×10^7 (9847)	7.86×10^7 (11,400)
Disk Lug Tooth Shear	1.65×10^7 (2400)	1.79×10^7 (2594)	1.84×10^7 (2668)	1.76×10^7 (2553)
Disk Lug Tooth Bending	2.36×10^7 (3420)	2.79×10^7 (4027)	2.85×10^7 (4135)	2.5×10^7 (3663)
Disk Lug Neck Tensile	1.40×10^7 (2033)	1.59×10^7 (2303)	2.07×10^7 (2997)	1.69×10^7 (2448)
Disk Lug Torsional	8.45×10^6 (1226)	1.05×10^7 (1527)	1.20×10^7 (1744)	1.35×10^7 (1962)
Combined Bending and Tensile	5.30×10^7 (7689)	5.92×10^7 (8584)	6.05×10^7 (8770)	4.97×10^7 (7216)

3.3.2.6 Rotor Deflections and Radial Growths

The prime objective during this phase of the design was to maintain minimal slopes at the disk rims along with minimal radial growths since both factors influence blade tip clearance. Several iterations, which included varying the thickness and the location of disk appendages, preceeded the final design. The design objective was achieved and a summary is provided in Table 3.3-IV for reference.

TABLE 3.3-IV

RADIAL GROWTH AND RIM SLOPE

Rotor	Radial Growth, cm (in)	Rim Slope (Radians)
2	0.0980 (0.0386)	0.0002
3	0.1003 (0.0395)	0.0032
4	0.0800 (0.0315)	0.0004
5	0.0914 (0.0360)	0.0006

3.3.2.7 Integral Seals

As mentioned above, the low cost approach involved the use of an integral seal design to minimize the number of forgings required. These seals were designed to be thicker in cross section than those normally found on separate seals to minimize the chance of handling damage. The seal is tapered radially which increases durability and decreases the growth rate of any cracking that might occur. Fracture mechanics analysis indicates that the tapered design has greater life to rupture than the constant thickness design.

The airseals were reviewed for vibration characteristics and were found to have frequency margins (fm) in excess of 200 percent. Figure 3.3-9 summarizes the frequency status of these seals.

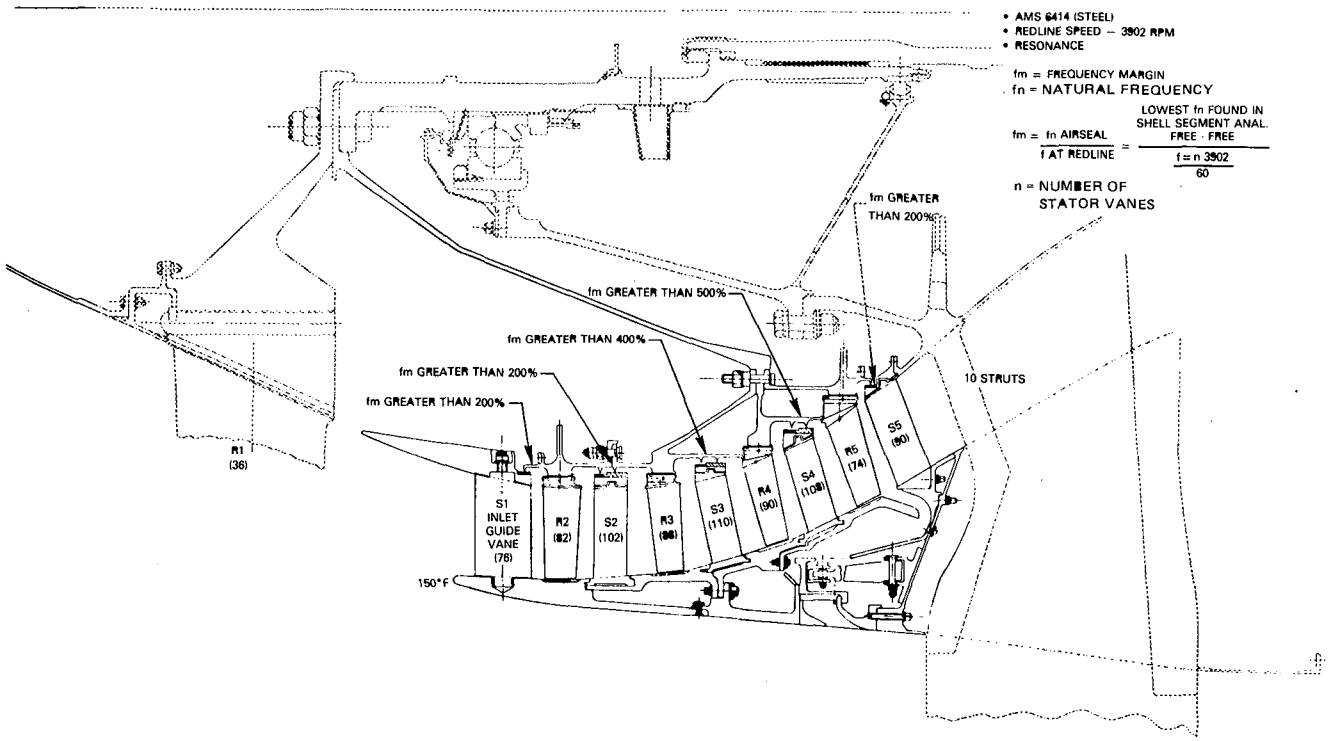

Figure 3.3-9 Low-Pressure Compressor Airseal Resonance Summary

3.3.2.8 Oil Drain Holes

The chance for oil leakage from the number 1 bearing area has been recognized as a potential problem during the Integrated Core/Low Spool test program. To avoid the possibility of oil retention in the rotor, six 0.157cm (0.062 inch) diameter oil drain holes have been placed in the cylindrical front disk support of rotor 5 (see Figure 3.1-1). These holes will prevent oil from being retained in this cavity and thus eliminate the possibility of rotor imbalance. The drain holes allow the oil to drain into the flowpath and eliminate the necessity of disassembling the rotor to eliminate any collection of oil.

These drain holes would not be used in the Flight Propulsion System since oil in the flowpath would contaminate the cabin air supply. They are only being used as a means to avoid a test problem in the Integrated Core/Low Spool.

The low cycle fatigue life of the rotor with drain holes was calculated to be greater than 10,000 cycles.

3.3.3 Blade Designs

3.3.3.1 General Description

The mechanical design of the four stages of low-pressure compressor blades is similar to the blades used in the JT9D engine. All four blades are fabricated from titanium (AMS 4928).

To minimize design and fabrication costs, existing design blade root profiles were utilized. This allows the use of available broach tooling for the rotor blade attachment slots and eliminates the requirement to design new tooling. Available blade locks were also incorporated.

A summary of general blade information is presented in Table 3.3-V.

TABLE 3.3-V

GENERAL BLADE INFORMATION

	Rotor			
Characteristic	2	3	4	5
Blade Material	AMS 4928	AMS 4928	AMS 4928	AMS 4928
Number of Blades	82	88	90	74
Airfoil Series*	CDA	CDA	CDA	CDA
Aspect Ratio	2.28	2.29	2.40	2.24
Thickness/Chord at Midspan	0.057	0.064	0.065	0.045
Average Chord, cm (in)	4.17 (1.64)	3.86 (1.52)	3.63 (1.43)	4.14 (1.63)
Foil Length at Stacking Line, cm (in)	9.50 (3.74)	8.79 (3.46)	8.76 (3.43)	9.32 (3.65)
Z Plane Radius, Cold, cm (in)	48.78 (19.201)	48.54 (19.112)	45.64 (17.970)	40.31 (15.870)

TABLE 3.3-V (Continued)

Characteristic	Rotor 2	3	4	5
Cant Angle	0	5.7	13.57	17.0
Broach Angle, degrees	18	19	19	24
Tangential Tilt at Tip, cm (in)	0.100	0.300	0.450	0.750
Disk Rim Width, cm (in)	2.54 (1.00)	2.29 (0.90)	2.29 (0.90)	2.82 (1.11)
Flight Propulsion System Redline Speed, rpm	4267	---	---	---
Max Blade Temperature, ^{o}C (^{o}F)	93.3 (200)	98.9 (210)	104.4 (220))	121.1 (250)
Aerodynamic Design Point Blade Temperature, ^{o}C (^{o}F)	16.7 (62)	36.1 (97)	52.2 (126)	67.8 (154)
Airfoil Stress at SLTO, KSI, P/A	3.8	3.9	3.4	3.1
Bending	.8	4.6	12.9	15.2

*Controlled Diffusion Airfoils

3.3.3.2 Airfoil Balancing

The blade and flowpath aerodynamic designs described in Section 3.2 were used as a basis for the mechanical design. During the mechanical design phase, the airfoils were balanced to minimize the airfoil bending stress at the root for the low cycle fatigue limiting condition of sea level takeoff. Tangential tilt was used to minimize this stress. The maximum stress on the airfoils after this balancing occurred on the trailing edge of the fifth stage blade. This stress was 1.24×10^{8} Pascals (18,000 psi) (pressure/area plus bending).

Along with airfoil balancing accomplished by tangential tilt, the blades were balanced about the attachment. This not only accounts for the centrifugal load of the blade and gas loads, but also for platform, dovetail, and blade lock pulls yielding zero moment at the intersection of the Z-plane and disk center line.

3.3.3.3 Broach Design

Available broach tooling was reviewed for suitability in the Energy Efficient Engine. A common broach for rotors 2 and 5 was selected, and one for rotors 3 and 4 was identified. Analyses of the selected dovetail and disk lug designs with final calculated loads (Table 3.3-VI) and geometry verified that the attachment stresses, shown in Table 3.3-VII are all acceptable. Broach angles were set to further balance the airfoil to root per established criteria.

TABLE 3.3-VI

BLADE PULLS
(Newtons (Pounds) Pull Per Blade at 3902 rpm)

	Rotor			
	2	3	4	5
Dovetail, Neck, Platform, Lock and Retainer	1992.7 (448)	2215.1 (498)	2539.8 (571)	3869.8 (870)
Rubber Seal (approximate)	66.7 (15)	66.7 (15)	66.7 (15)	66.7 (15)
Airfoil	2652.8 (596.4)	2111.9 (474.8)	1912.6 (430.0)	1857.9 (417.7)
Total	4712.2 (1059.4)	4393.7 (987.8)	4519.1 (1016)	5794.4 (1302.7)

TABLE 3.3-VII

ATTACHMENT STRESSES
(Pascals x 10^7 (psi))

	Rotor			
Stress	2	3	4	5
Blade Neck Tensile	2.41 (3500)	2.48 (3600)	2.55 (3700)	2.34 (3400)
Lug Neck Tensile	1.38 (2000)	1.59 (2300)	2.07 (2300)	1.65 (2400)
Blade Bending	4.27 (6200)	2.62 (3800)	2.69 (3900)	4.14 (6000)
Lug Bending	2.34 (3400)	2.76 (4000)	2.83 (4100)	2.55 (3700
Blade Combined	6.76 (9800)	5.10 (7400)	5.24 (7600)	6.41 (9300)
Lug Combined	5.24 (7600)	5.93 (8600)	6.07 (8800)	4.96 (7200)
Blade-Lug Bearing	8.21 (11,900)	6.76 (9800)	6.96 (10,100)	7.86 (11,400)
Blade Shear	2.55 (3700)	1.86 (2700)	1.93 (2800)	2.41 (3500)
Lug Shear	1.59 (2300)	1.79 (2600)	1.86 (2700)	1.79 (2600)

3.3.3.4 Blade Locks

The utilization of existing dovetail designs made it possible to use existing blade lock designs as well. These locks are a two piece design consisting of a retainer and a lock as shown in Figure 3.3-10. Blade lock slot geometry and side play of the lock was made similar to that in the JT9D engine. Lock retainers for the blades are also the same as in the JT9D engine except that the length of each was modified for the Energy Efficient Engine.

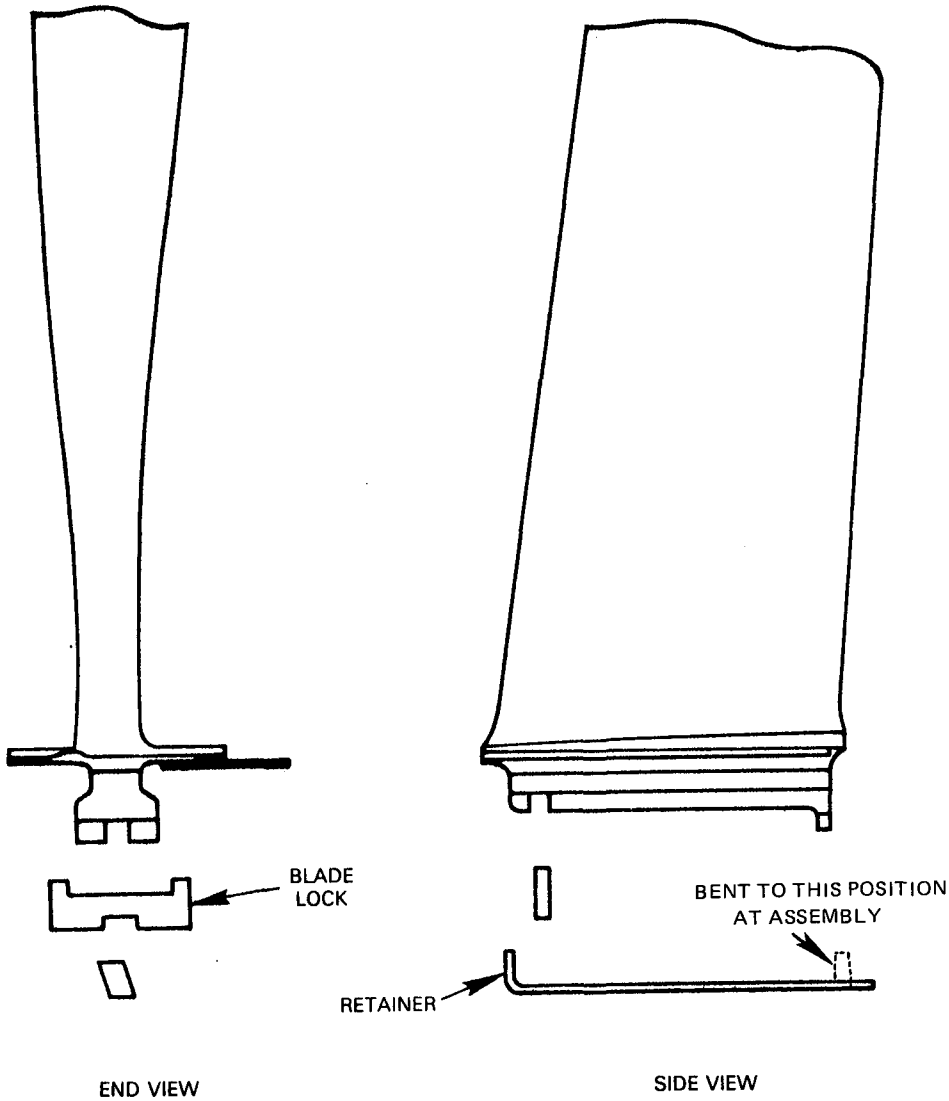

Figure 3.3-10 Low-Pressure Compressor Blade Lock Design (Typical of all Stages)

3.3.3.5 Blade Root Sealing

Blade root sealing was incorporated to minimize leakage through the attachment based on two schemes that are currently in use in other engine models. To minimize leakage between platforms, a rubber strip is bonded on the underside

of the platform and seals the gap between adjacent blades. To seal between the disk lugs and platforms and to seal around the dovetails, silicone rubber is used. This rubber is applied as the blades are being installed.

3.3.3.6 Hot to Cold Conversion

Airfoil section data, as well as Z-plane and platform dimensions, were converted from their hot design point positions to cold manufacturing positions. These conversions take into account blade and disk centrifugal and thermal growths. In addition to radial changes, the flowpath angles of the blade platforms were tilted slightly to ensure a smooth or 'dam' free flowpath when hardware tolerances are considered.

Axial and tangential deflections were not included due to their small magnitude. Untwist and uncamber effects were analyzed using a NASTRAN computer analysis. The canted blade position and elliptical leading edges on the controlled diffusion airfoils made other forms of analysis difficult. The airfoil designs were modified as a result of the untwist portion of the analysis. Figures 3.3-11 through 3.3-14 show the magnitude of the untwist for each blade. Uncamber was found to be minimal and was not accounted for.

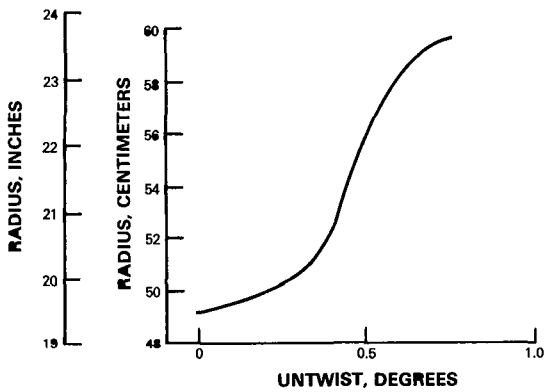

Figure 3.3-11 Rotor 2 Untwist vs. Radius

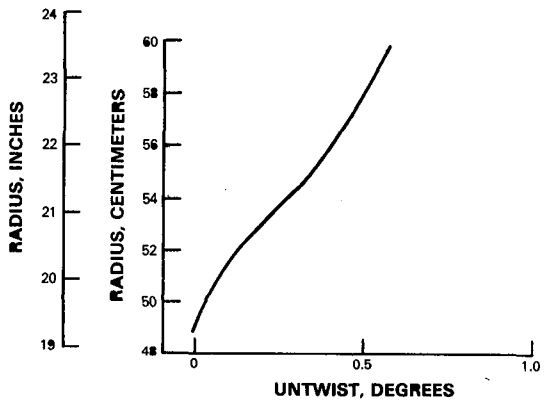

Figure 3.3-12 Rotor 3 Untwist vs. Radius

3.3.3.7 Blade Structural Analysis

The four stages of blades were analyzed for flutter and resonance margins using beam vibration analysis and tip mode frequency analysis. Critical engine order resonances were avoided. These include the low orders (2E, 3E, and 4E) and vane passing order in each stage, and the 10th (10E) and 20th

* Untwist is the measurement, in degrees, of airfoil rotation due to centrifugal and gas load effects in the direction to remove the as designed root to tip airfoil section twist.

(20E) in the fifth stage for the intermediate case strut order. Any critical resonance must have adequate margin at both redline and minimum cruise speeds and be out of the idle regime.

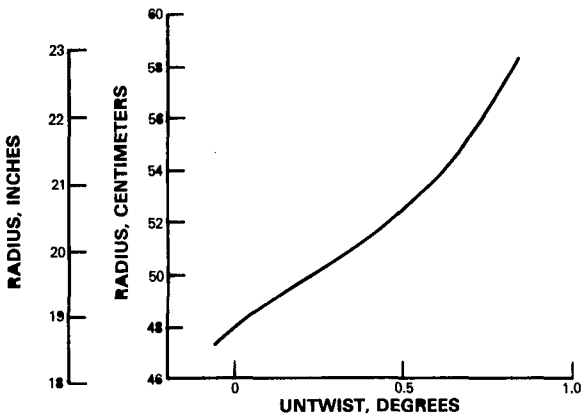

Figure 3.3-13 Rotor 4 Untwist vs. Radius

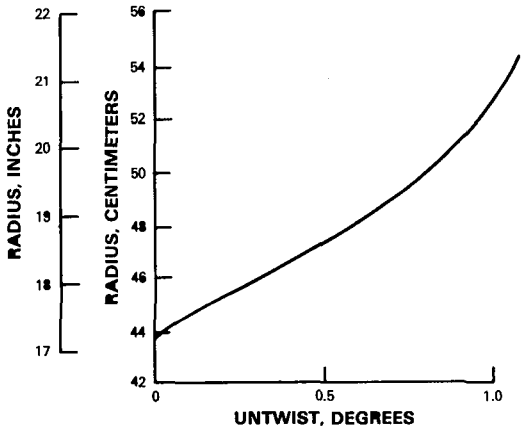

Figure 3.3-14 Rotor 5 Untwist vs. Radius

Figures 3.3-15 through 3.3-18 show the final resonance diagrams for the four rotors. Numerous iterations of the airfoil designs with the aerodynamic design group were required before all requirements were met. The final designs now meet all requirements.

Flutter was checked after the final designs were set and no flutter is predicted. Figures 3.3-19 and 3.3-20 show this status.

3.3.4 Stator Case Design

3.3.4.1 General Description

The static case structure of the low-pressure compressor consists of six separate full ring (360 degrees), aluminum cases consisting of:

1. Splitter (Inlet Guide Vane Case)
2. Second Stage Vane Case
3. Third Stage Vane Case
4. Fourth Stage Vane Case
5. Fifth Stage Vane Case
6. Bleed Case

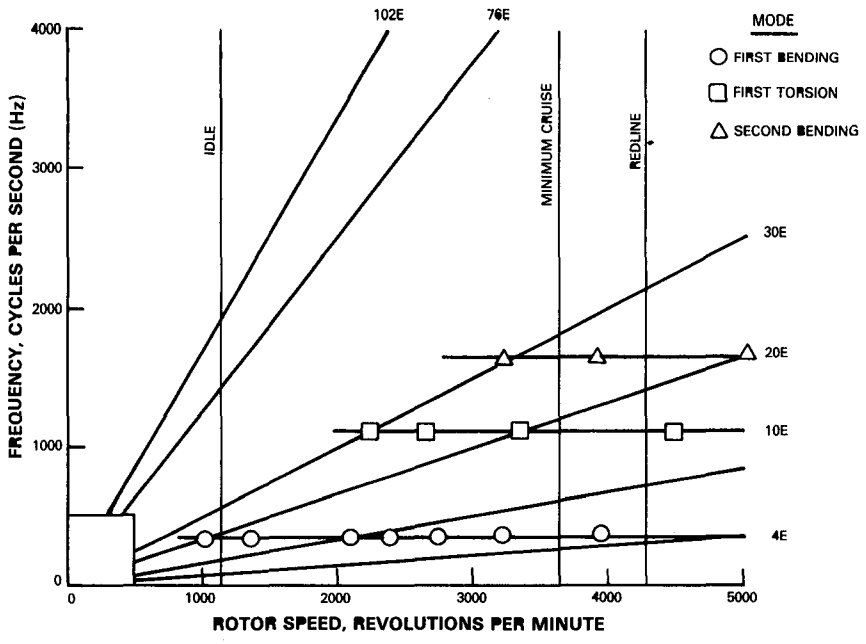

Figure 3.3-15 Rotor 2 Blade Resonance Diagram

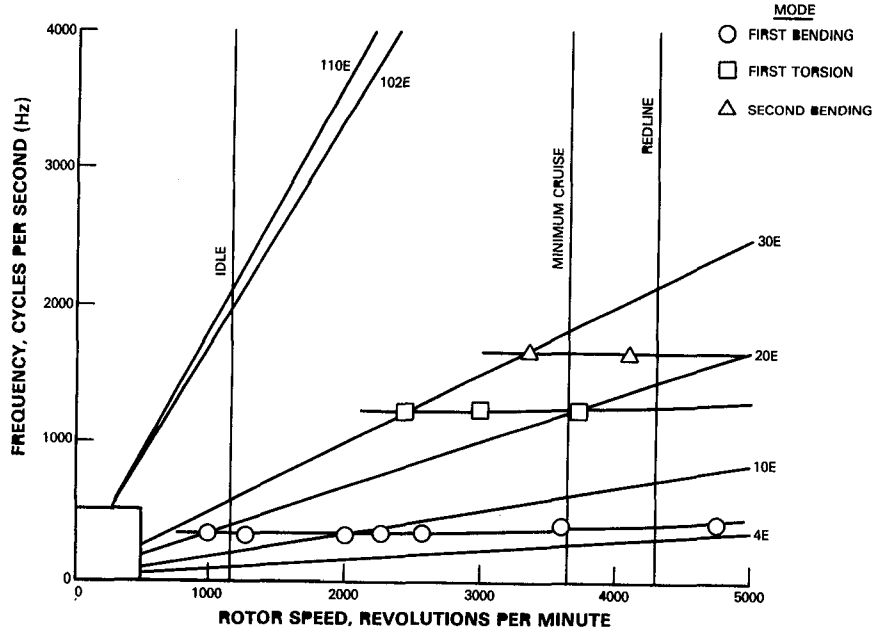

Figure 3.3-16 Rotor 3 Blade Resonance Diagram

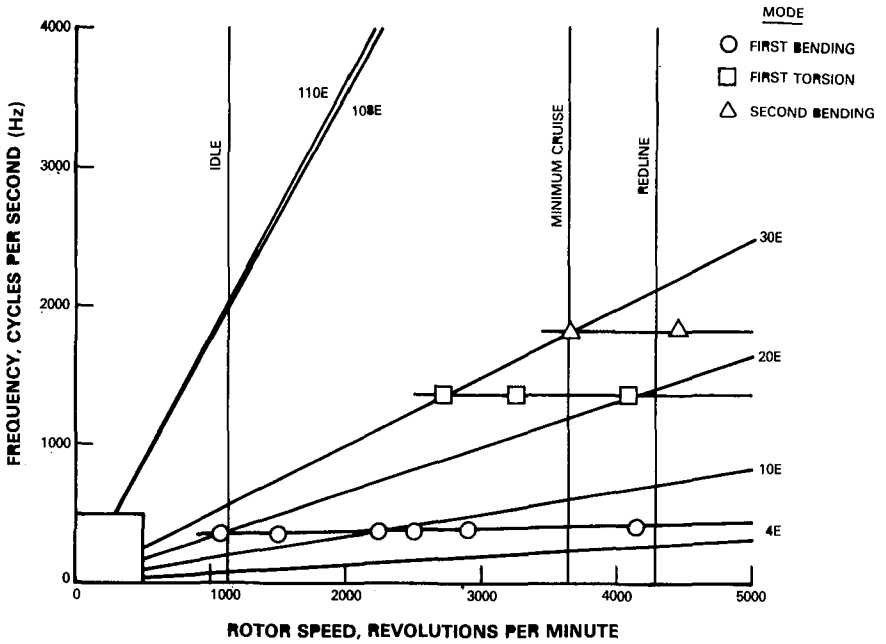

Figure 3.3-17 Rotor 4 Blade Resonance Diagram

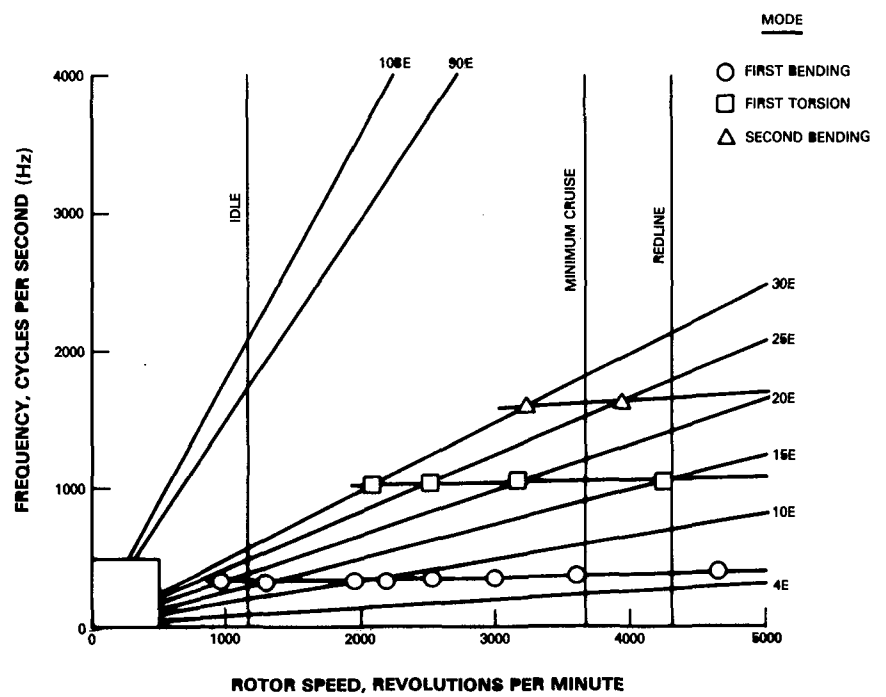

Figure 3.3-18 Rotor 5 Blade Resonance Diagram

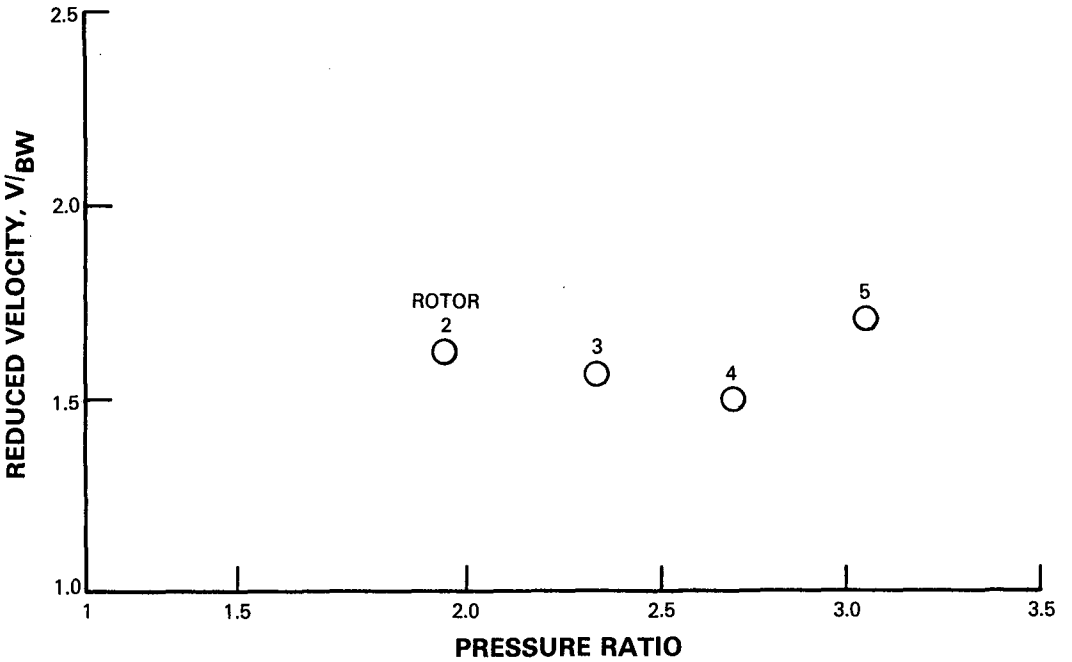

Figure 3.3-19 Low-Pressure Compressor Blade Torsional Flutter

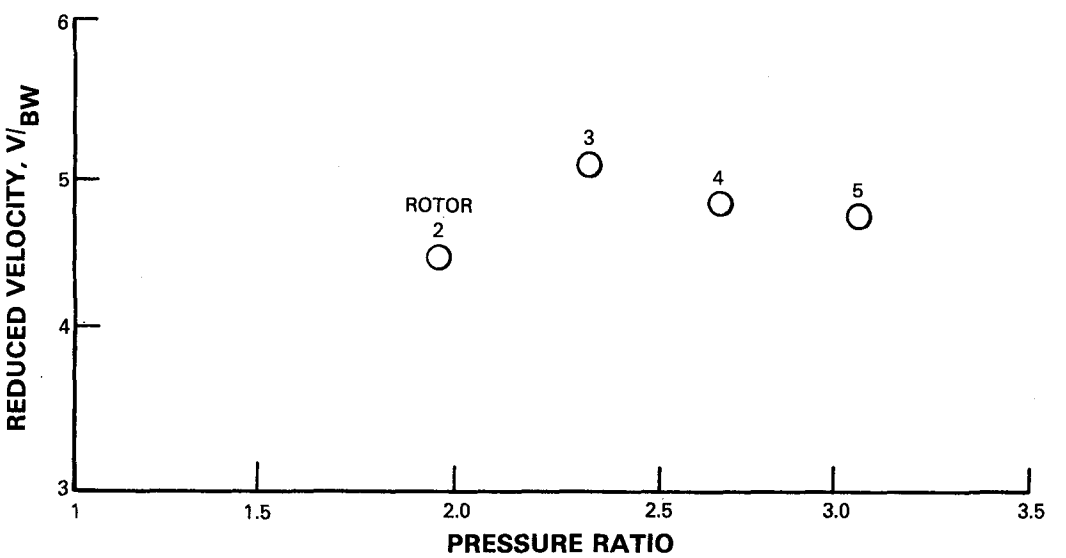

Figure 3.3-20 Low-Pressure Compressor Blade Bending Flutter

Figure 3.3-21 shows the location of these cases. The vane cases retain and form the outer shrouds of the vanes.

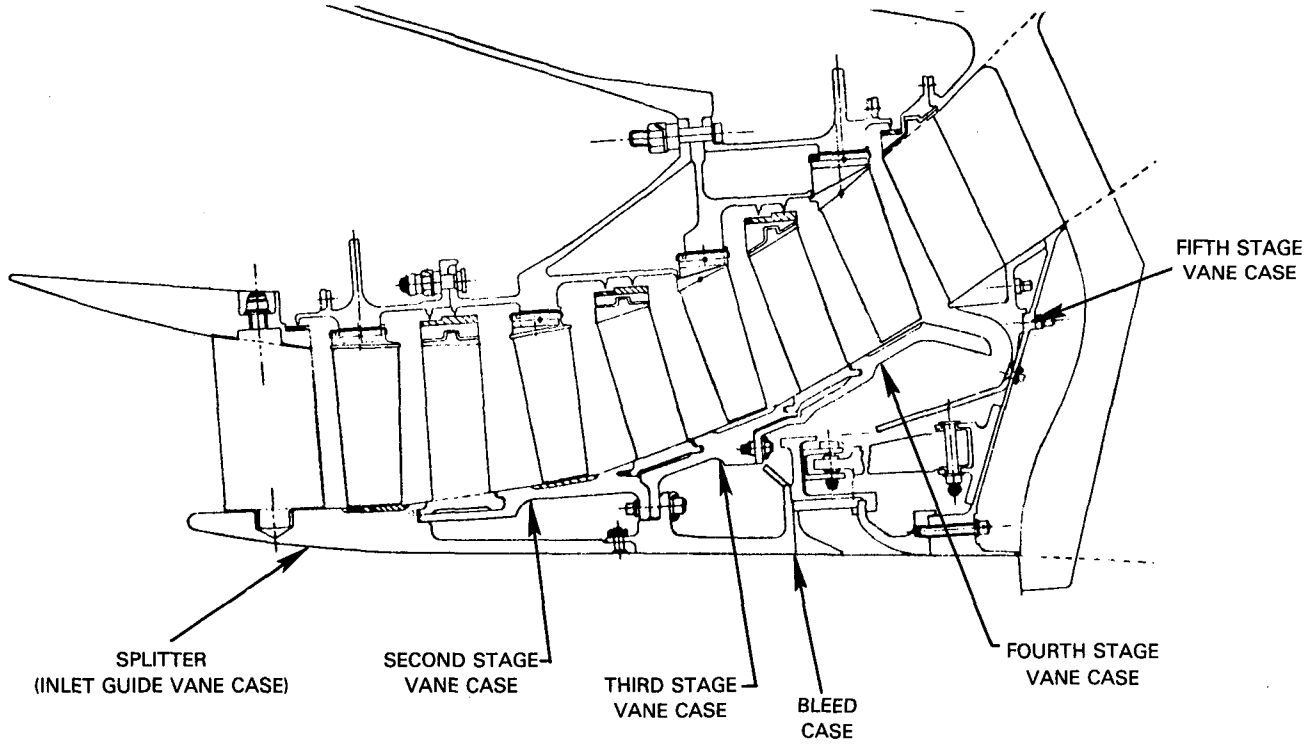

Figure 3.3-21 Low-Pressure Compressor Stator Case Locations

3.3.4.2 Case Design and Analysis

Aluminum was chosen as the material for all six cases because of its inherent cost, weight, and machineability advantages. Specifically, AMS 4312 was selected. This is an AMS 6061 alloy which is cold worked to improve corrosion resistance and machining properties. Silicon rubber (PWA 407) was specified as the blade tip abradable for its proven abradability characteristics in low-pressure compressors.

To minimize design and fabrication costs, the thicknesses of these cases were not optimized for flight weight. This approach not only reduces design time, but it minimizes the number of machining steps necessary during fabrication. It results, however, in a heavier, 'over designed' configuration.

After the initial case configurations were established, a computer aided shell analysis was performed from which the stress conditions were determined. The maximum bending stress found in any one of the cases was 6.89×10^7 Pascals

(10,000 psi). Maximum hoop stress was 1.65×10^8 Pascals (24,000 psi). These are well within design allowables. Stresses at the vane retention hooks due to reaction loads were very low and well within allowable limits also.

An analysis of second stage blade loss effects was also performed. Stresses were found to increase at the bleed case/intermediate case junction, but were still considered low and well within design allowables for a flight engine. Containment during blade loss was also analyzed for all four vane cases and was found to be acceptable.

Vane anti-rotation capability is provided by vane hook pins at each vane hook location on the second, third and fourth stage cases. These pins are pressed into the case and engage each vane on the forward hook. The fifth stage vanes are secured individually by bolts that thread into the base of each part through holes in the vane case.

Jack screws are provided for disassembly of the tight fitting flanges on the splitter case/number 2 vane case and the bleed case/intermediate case flanges.

The rear edge of the fourth stage vane case and the forward edge of the fifth stage vane case form the annulus contour for the bleed air discharge from the flowpath. It is predicted that a nominal 15 percent bleed flow will be provided by the 374 cm^2 (58 square inches) of bleed area.

The temperature/pressure analysis results presented previously in Figure 3.3-1 were used in the design and analyses of the compressor cases.

3.3.5 Adjustable Inlet Guide Vane

3.3.5.1 General Description

The ability to adjust the incidence angle of the inlet guide vane (Stator 1) has been included in the Integrated Core/Low Spool test low-pressure compressor design. This feature provides the capability to compensate for incidence angle and surge margin problems that are possible in the first run of a new compressor design. A plus or minus ten degree range of adjustability has been provided. The Flight Propulsion System design would use a fixed stator.

3.3.5.2 Guide Vane Design

The inlet vanes were designed to be individually resetable. A redundant locking scheme, which consists of a trunnion lock nut and split flange with interference fit, was adopted to provide secure vane retention. The locking features are located on the inner vane trunnion. Included in the design of the vane were the leading edge instrumentation provisions required for the Integrated Core/Low Spool test. The vane with locking provisions and instrumentation is shown in Figure 3.3-22.

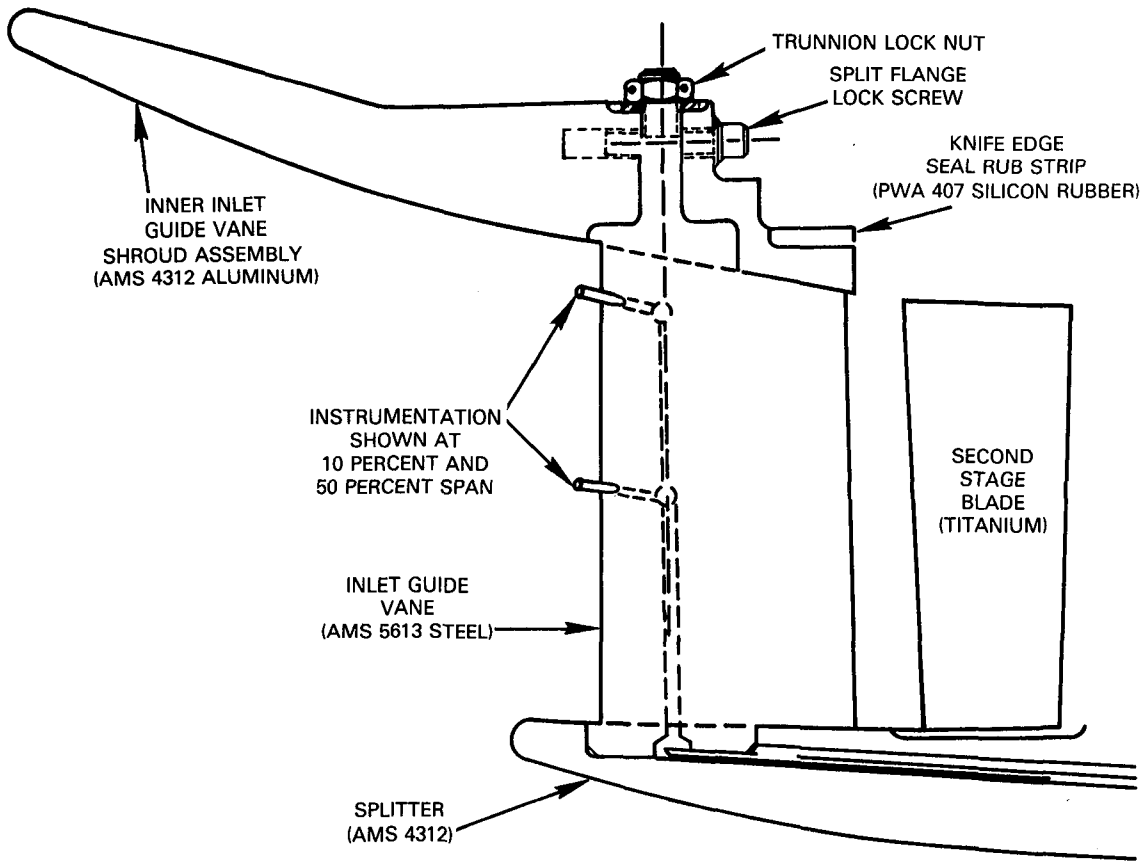

Figure 3.3-22 Adjustable Low-Pressure Compressor Inlet Guide Vane

The adjustable inlet guide vane is equipped with a larger-than-normal airfoil thickness to provide sufficient cross section for the passage of anti-ice air. However, this option was not included in the Flight Propulsion System design, but could be specified if required, without having to modify the low-pressure compressor aerodynamics.

Vane gas loads were calculated and were used to size the inlet guide vane inner and outer trunnion diameters for minimum stress. The vane was analyzed for resonance using beam vibration analysis to ensure that any fan blade passing order (36E) would be out of the Integrated Core/Low Spool test operating range. The resonance diagram in Figure 3.3-23 shows that an adequate 7 percent margin exists on the first coupled mode at redline with 20 percent margin on first bending at idle. The first torsion and bending mode resonance occurs between idle and minimum cruise and the first coupled mode has sufficient margin above redline speed. The maximum stress calculated for this vane is 1.43×10^7 Pascals (2070 psi) at the leading edge at sea level takeoff, well within allowables.

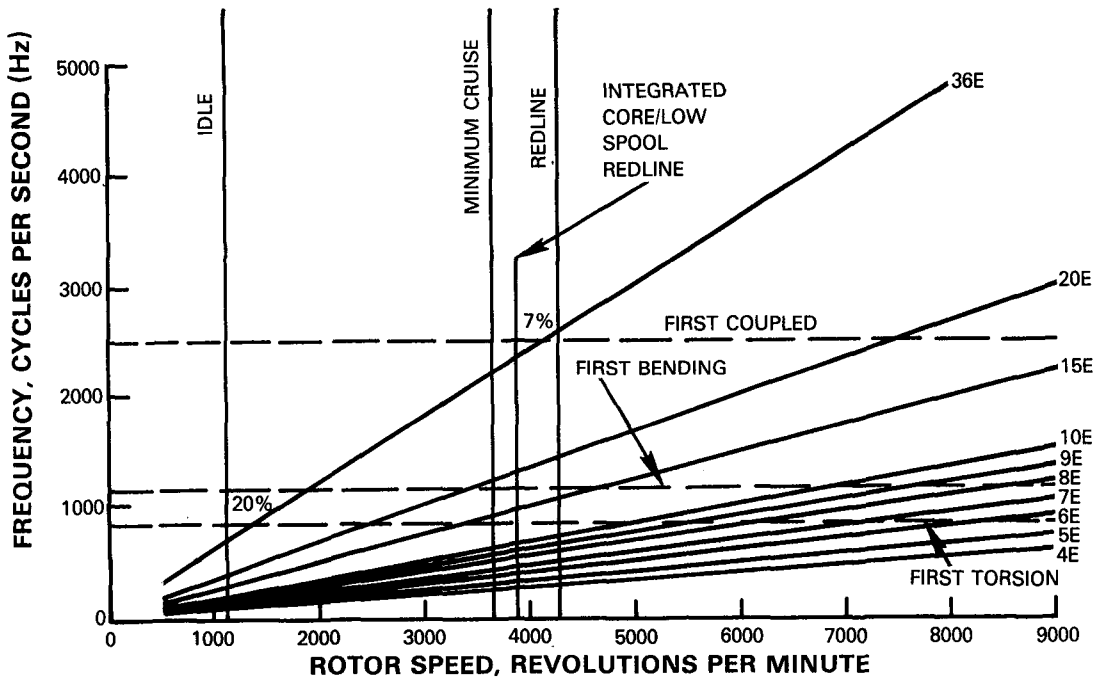

Figure 3.3-23 Low-Pressure Compressor Inlet Guide Vane Resonance Diagram

Bending and torsional flutter parameters were calculated according to the flutter design system. Comparison of the results to previous experience shows that neither type of flutter is expected to occur. (These results are shown in Figures 3.3-25 and 3.3-26).

AMS 5613 (A-410) steel alloy was selected for use in the Integrated Core/Low Spool test since it is compatible with the instrumentation requirements of the experimental hardware. AMS 4312 aluminum remains specified for the Flight Propulsion System.

3.3.5.3 Inlet Guide Vane Inner Shroud

The inlet guide vane inner shroud provides the inner flowpath contour between the fan and the low-pressure compressor inlet. It also serves as the means to lock the adjustable vanes in position.

The shroud is designed as a two piece assembly which is bolted together with a tight fit to trap the inner vane trunnion in position. The shroud material is aluminum (AMS 4312). PWA 407 silicon rubber is used as the abradable material for the rotor knife edge seal on the rear shroud piece. The shroud assembly

was designed as an experimental configuration and is, therefore, heavier in cross section than flight requirements would dictate. Analyses results indicate that minimum stress and vibration requirements will be met.

3.3.5.4 Vane Instrumentation

Provisions for leading edge pressure and temperature instrumentation have been designed into 8 of the 76 adjustable vanes. Kielhead probe location and lead work routing locations were specified. The Kielhead probes are brazed to the leading edge of the airfoil at the correct incidence angle. The lead work from each is cemented into channels machined into the concave airfoil to make a smooth surface. The lead work is fed through the outer vane trunnion where sufficient flexibility is provided to allow vane adjustment. The lead work is then let through channels cut in the inner fan flowpath to the intermediate case inner cavity. It will then be fed out of the engine through the upper bifurcation.

3.3.6 Stator Assemblies

3.3.6.1 General Description

The second, third, fourth and fifth stage stator assemblies were designed using the airfoil descriptions presented in Section 3.2 with low-cost-of-fabrication features incorporated at the inner and outer shrouds. The stator assemblies use individual footed vanes that are bonded in rubber to the inner shroud ring. The second, third and fourth stage assemblies are split into 180 degree segments to facilitate assembly. The fifth stage is a full 360 degree stator. A summary of stator vane geometry is presented in Table 3.3-VIII. Typical stator construction is shown in Figure 3.3-24.

3.3.6.2 Stator Design

The individual vanes for each stage are machined from AMS 4312 aluminum. The airfoil surfaces are machined to the contours described in Section 3.2. Each vane has inner and outer platforms with conical flowpath surfaces. The outer vane platform on each vane has two vane "feet" that engage the hooks on the mating cases that were described earlier. The forward foot on each vane has an anti-rotation slot that engages the anti-rotation pin in the case vane hook. The vane platforms were designed to be significantly heavier than required for a flight configuration to reduce analysis requirements and to minimize the number of machining steps during fabrications.

Stress analysis was performed on each vane. The maximum bending stress occurs on the trailing edge of the second stage and on the leading edge of all other stages. Vane axial deflections due to gas loading were also determined. Both the stress levels and deflections are well within allowable limits. The values resulting from these analyses are shown in Table 3.3-IX.

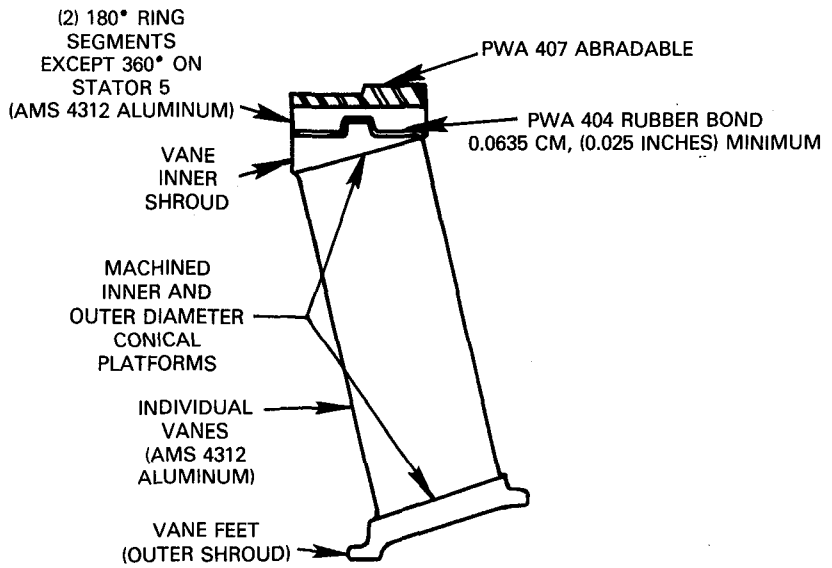

Figure 3.3-24 Typical Low-Pressure Compressor Stator Construction

TABLE 3.3-VIII

LOW-PRESSURE COMPRESSOR STATOR GEOMETRY

	Stator				
	(Inlet Guide Vane) 1	2	3	4	5
Root Radius, cm (in)	48.52 (19.10)	49.75 (19.59)	48.65 (19.15)	45.00 (17.72)	39.32 (15.48)
Tip Radius, cm (in)	58.84 (23.17)	58.95 (23.21)	57.09 (22.48)	53.51 (21.07)	48.39 (19.05)
Root Thickness/Chord	0.050	0.070	0.070	0.069	0.068
Tip Thickness/Chord	0.070	0.070	0.070	0.069	0.069
Root Stagger Angle, degrees	54.64	55.18	61.61	63.68	72.51
Tip Stagger Angle, degrees (from tangential)	59.81	57.31	58.76	60.77	74.06
Root Chord, cm (in)	6.70 (2.636)	4.18 (1.645)	3.78 (1.49)	3.62 (1.425)	3.91 (1.537)
Hub/Tip	0.825	0.844	0.852	0.841	0.813
Aspect Ratio	1.54	2.20	2.29	2.44	2.50
Cant Angle, degrees	-	-	11.90	15.33	21.33

TABLE 3.3-IX

LOW-PRESSURE COMPRESSOR STATOR STRESSES AND DEFLECTIONS

Stator	Maximum Stress		Edge	Axial Deflection	
	Pascals	psi		cm	In
2	1.08×10^8	15,700	Trailing	0.086	0.034
3	5.4×10^7	7900	Leading	0.028	0.011
4	3.1×10^7	4500	Leading	0.003	0.001
5	3.2×10^7	4700	Leading	0.005	0.002

Flutter analysis was performed on each stage of the low-pressure compressor and the results are shown on Figures 3.3-25 and 3.3-26. The values of both the bending and torsional flutter parameters are within design and experience limits. Flutter is not expected to occur at any operating condition.

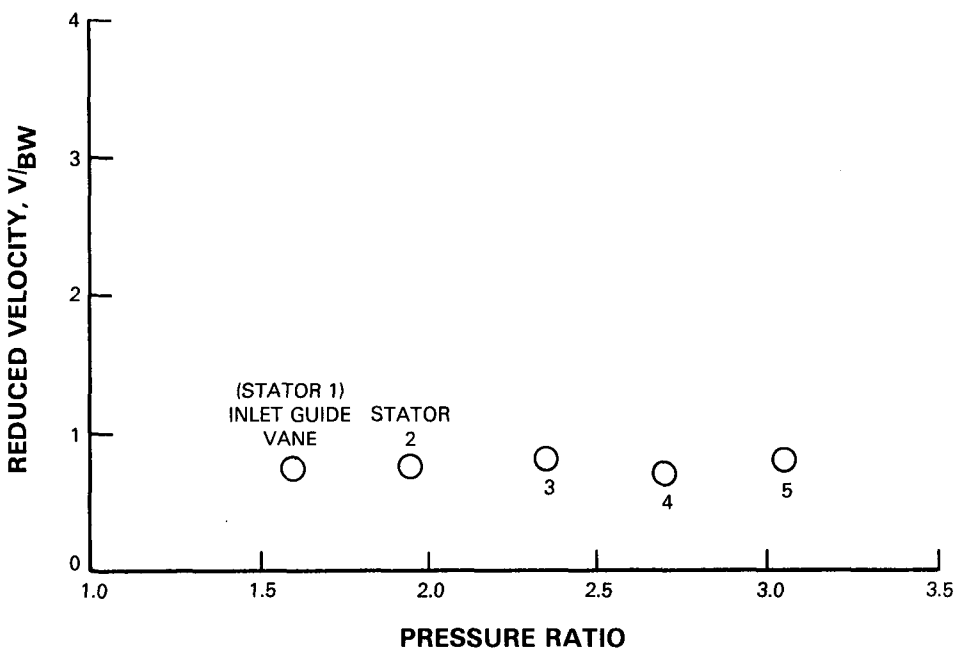

Figure 3.3-25 Low-Pressure Compressor Stator Bending Flutter

The individual vanes are bonded to the inner stator shroud with PWA 404 rubber. The shrouds are machined AMS 4312 aluminum rings. PWA 407 silicon rubber is used on the inner stator surface as an abradable for the mating rotor knife edge seals.

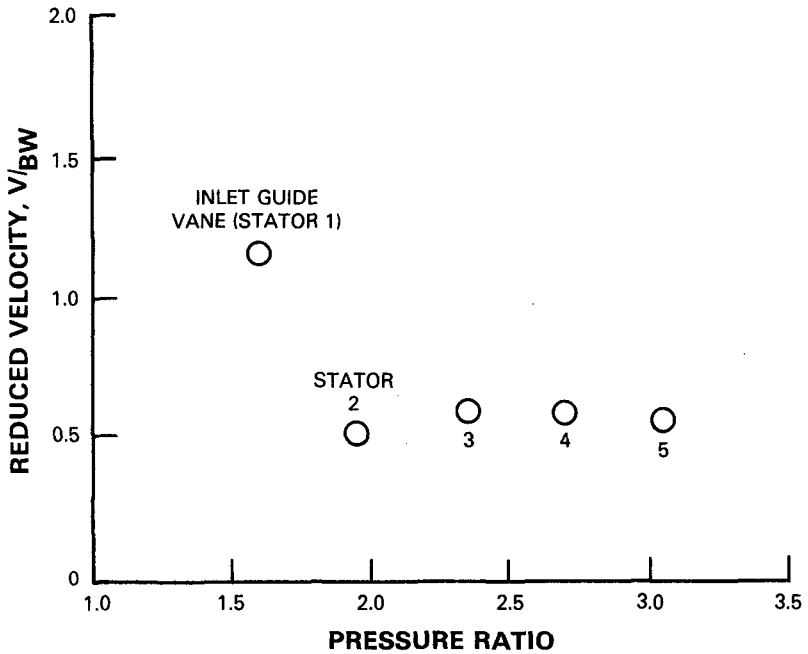

Figure 3.3-26 Low-Pressure Compressor Stator Torsional Flutter

3.3.7 Bleed System Design

A full annular bleed system, shown in Figure 3.3-27, has been provided at the exit of the low-pressure compressor to ensure compressor stability at low power and thrust reverse conditions. A low cost design has been adopted that makes use of existing JT9D engine hardware, thereby saving considerable design and manufacturing cost.

The design is based on the mature JT9D-7 engine station 3.0 bleed system and uses the actuator, bearings, links, bushing, pins, seals, and valve brackets from that engine. The relationship between the links and actuator was changed to fit the available space without modifying valve movement. The bleed valve is a newly designed 360 degree aluminum ring.

The linear movement of the hydraulic bleed actuator controls the forward and aft movement of the bleed valve ring. The bleed is in the closed position when forward and open when moved rearward. The Integrated Core/Low Spool design will be unmodulated (either open or closed), but the Flight Propulsion System bleed could be fully modulated, if required.

With the bleed ring in the aft position, bleed air is allowed to flow from the compressor flowpath ahead of the fifth stator, out through turning vanes in the low-pressure compressor case into the fan duct. The turning vanes, which are made of cast aluminum, direct the air at the fan exit guide vanes at the proper incidence angle.

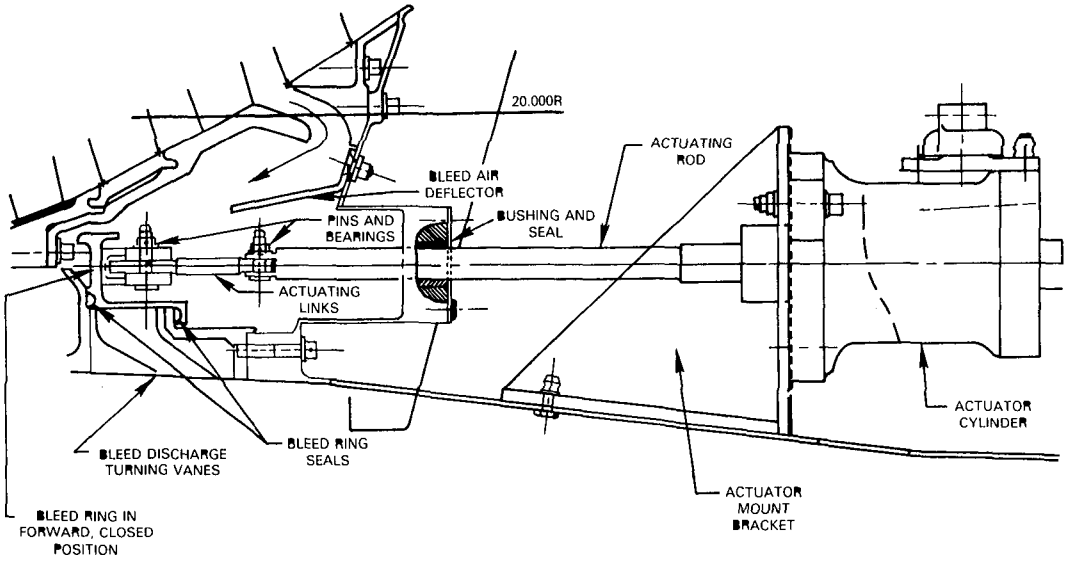

Figure 3.3-27 Energy Efficient Engine Bleed Valve and Actuator

The design goal was to provide a minimum 15 percent bleed flow up to the 40 percent of maximum cruise power. A flow of 14.1 percent was achieved at this condition. The various bleed flows predicted to be provided by this system are presented in Table 3.3-X.

TABLE 3.3-X

LOW-PRESSURE COMPRESSOR BLEED FLOW

Condition	Flow		
	Kg/sec	lb/sec	Percent Wcore
Flight Propulsion System			
Flight Idle	1.12	5.42	21.0
40 percent of maximum cruise	2.99	6.60	14.1
Integrated Core/Low Speed			
30 percent of takeoff	5.67	12.5	14.4
Ground Idle			20.0

3.3.8 Compressor Axial Spacing

The initial flowpath axial gaps in the low-pressure compressor were selected based on experience with similar compressor designs. Following completion of the compressor design, the actual gaps were compared to the estimated gaps.

Tables 3.3-XI and 3.3-XII summarize the factors considered when gapping the compressor in addition to the actual values calculated. Both inner and outer flowpath gaps are shown. The inner gap clearance is the controlling clearance

since it is smaller. For the Flight Propulsion System design, a new flow path iteration would be performed to reduce this clearance to zero. The negative clearance at R5-S5 indicates that the design clearance is smaller than required for Flight Propulsion System. This would be corrected upon redesign.

TABLE 3.3-XI

FLOWPATH INNER DIAMETER GAPS

	Required Gap Locations, cm (in)							
	S1-R2	R2-S2	S2-R3	R3-S3	S3-R4	R4-S4	S4-R5	R5-S5
Stator Tolerance	0.056 (0.022)	0.056 (0.022)	0.056 (0.022)	0.056 (0.022)	0.056 (0.022)	0.066 (0.026)	0.066 (0.026)	0.046 (0.018)
Rotor Tolerance	0.081 (0.032)	0.081 (0.032)	0.076 (0.030)	0.076 (0.030)	0.071 (0.028)	0.074 (0.029)	0.076 (0.030)	0.076 (0.030)
Bearing Play	0.145 (0.057)	- -	0.145 (0.057)	- -	0.145 (0.057)	- -	0.145 (0.057)	- -
Blade Lock	- -	- -	- -	- -	- -	0.102 (0.040)	- -	0.102 (0.040)
Rotor Deflection	0.015 (0.006)	0.015 (0.006)	0.020 (0.008)	0.020 (0.008)	0.023 (0.009)	0.023 (0.009)	0.013 (0.005)	0.013 (0.005)
Case Deflection	- -	0.109 (0.043)	- -	0.107 (0.042)	- -	0.046 (0.018)	- -	0.074 (0.029)
Disk Rim Deflection at Surge	0.051 (0.020)	0.051 (0.020)	0.051 (0.020)	0.051 (0.020)	0.117 (0.046)	0.117 (0.046)	0.051 (0.020)	0.051 (0.020)
Stator Deflection at Surge	0.328 (0.129	0.309 (0.1215)	0.309 (0.1215)	0.147 (0.058)	0.147 (0.058)	0.169 (0.0665)	0.169 (0.0665)	- -
Rotor Surge	0.046 (0.018)	0.046 (0.018)	0.006 (0.0025)	0.006 (0.0025)	0.033 (0.013)	0.033 (0.013)	0.025 (0.010)	0.025 (0.010)
Gyro Deflection	0.457 (0.180)	0.399 (0.157)	0.436 (0.1715)	0.387 (0.1525)	0.439 (0.173)	0.371 (0.146)	0.409 (0.161)	0.348 (0.137)
Total	1.179 (0.464)	1.066 (0.4195)	1.099 (0.432)	0.85 (0.335)	1.031 (0.406)	1.001 (0.394)	0.954 (0.376)	0.735 (0.289)
Actual	1.316 (0.518)	1.115 (0.439)	1.59 (0.626)	1.425 (0.561)	1.501 (0.591)	1.118 (0.440)	1.052 (0.414)	0.630 (0.248)
Clearance	0.137 (0.054)	0.049 (0.0195)	0.491 (0.194)	0.575 (0.226)	0.470 (0.185)	0.117 (0.046)	0.098 (0.038)	-0.105 (-0.041)

TABLE 3.3 - XII

FLOWPATH OUTER DIAMETER GAPS

	Required Gap Locations, cm (in)							
	S1-R2	R2-S2	S2-R3	R3-S3	S3-R4	R4-S4	S4-R5	R5-S5
Stator Tolerance	0.056 (0.022)	0.056 (0.022)	0.061 (0.024)	0.061 (0.024)	0.056 (0.022)	0.056 (0.022)	0.066 (0.026)	0.066 (0.026)
Rotor Tolerance	0.081 (0.032)	0.081 (0.032)	0.076 (0.030)	0.076 (0.030)	0.071 (0.028)	0.071 (0.028)	0.076 (0.030)	0.076 (0.030)
Bearing Play	0.145 (0.057)	- -	0.145 (0.057)	- -	0.145 (0.057)	- -	0.145 (0.057)	- -
Rotor Deflection	0.015 (0.006)	0.015 (0.006)	0.020 (0.008)	0.020 (0.008)	0.023 (0.009)	0.023 (0.009)	0.013 (0.005)	0.013 (0.005)
Case Deflection	- -	0.109 (0.043)	- -	0.107 (0.042)	- -	0.046 (0.018)	- -	0.074 (0.029)
Blade Gyro	0.559 (0.220)	0.500 (0.197)	0.538 (0.212)	0.478 (0.188)	0.521 (0.205)	0.452 (0.178)	0.488 (0.192)	0.427 (0.168)
Blade Surge	0.607 (0.239)	0.607 (0.239)	0.551 (0.217)	0.551 (0.217)	0.665 (0.262)	0.665 (0.262)	0.312 (0.123)	0.312 (0.123)
Total	1.463 (0.576)	1.368 (0.539)	1.391 (0.548)	1.293 (0.509)	1.481 (0.583)	1.313 (0.517)	1.100 (0.433)	0.968 (0.381)
Actual	1.803 (0.710)	1.765 (0.695)	4.521 (1.780)	3.073 (1.210)	2.616 (1.030)	2.096 (0.825)	2.235 (0.880)	2.311 (0.910)
Clearance	0.340 (0.134)	0.397 (0.156)	3.130 (1.232)	1.780 (0.701)	1.135 (0.447)	0.783 (0.308)	1.135 (0.447)	1.343 (0.529)

3.3.9 Blade Tip and Knife Edge Seal Clearances

Blade tip-to-case and knife edge seal-to-stator clearances were established after the completion of the mechanical design of the related hardware. Analysis revealed final clearances that are considerably lower than those predicted during the preliminary design of the low-pressure compressor due to the increased stiffness in the compressor intermediate case structure.

The low-pressure compressor was designed to allow the blade tips to run on line with the flowpath wall at the aerodynamic design point. The rubstrips have shallow trenches to allow for normal operating excursions of rotor whirl,

maneuver, and cowl loading. Rub-in from hardware tolerances and case ovalization will be permitted. To minimize the effect of tolerances on tip gap, the blade tips will be machined after installation in the rotor assembly. This will eliminate the 'long' blade and will allow for more accurate mating of the rotor with the cases during assembly of the compressor since the actual parts will be measured and the blade tip diameters adjusted accordingly. The blade tip diameter has been left oversize to account for this operation.

The blade tip radial clearances and the factors affecting them are shown in Table 3.3-XIII.

Knife edge to inner shroud rubstrip analysis was also performed. The factors affecting these clearances are the same as for the blade tip clearances shown in Table 3.3-XIII. Table 3.3-XIV shows the aerodynamic design point and cold knife edge seal clearance values.

TABLE 3.3-XIII

LOW-PRESSURE COMPRESSOR BLADE TIP CLEARANCES AND SIGNIFICANT FACTORS AFFECTING CLEARANCES

	Blade Tip Clearances, cm (in)				
	R2	R3	R4	R5	Average
Trench Depth	0.033 (0.013)	0.033 (0.013)	0.053 (0.021)	0.079 (0.031)	0.048 (0.019)
Sea Level Takeoff Transient	0.033 (0.013)	0.025 (0.010)	0.023 (0.009)	0.023 (0.009)	0.025 (0.010)
Steady State	0.097 (0.038)	0.086 (0.034)	0.094 (0.037)	0.089 (0.035)	0.091 (0.036)
Cold	0.124 (0.049)	0.117 (0.046)	0.089 (0.035)	0.102 (0.040)	0.107 (0.042)
	Factors Affecting				
Rotor Whirl	0.0013 (0.0005)	0.0013 (0.0005)	0.0025 (0.0001)	0.0025 (0.001)	
Maneuver, Sea Level Takeoff	0.010 (0.004)	0.010 (0.004)	0.010 (0.004)	0.010 (0.004)	
Pinch	0.010 (0.004)	0.008 (0.003)	0.030 (0.012)	0.056 (0.022)	

TABLE 3.3-XIII (Continued)

	R2	R3	R4	R5	Average
Cowl Load	0.010 (0.004)	0.010 (0.004)	0.010 (0.004)	0.010 (0.004)	
Total	0.0313 (0.0125)	0.0293 (0.0115)	0.0525 (0.021)	0.0785 (0.031)	
	Rub-in Allowables				
Tolerances	0.020 (0.008)	0.020 (0.008)	0.020 (0.008)	0.020 (0.008)	
Case Ovalization	0.020 (0.008)	0.020 (0.008)	0.010 (0.004)	0 (0.0)	
Total	0.040 (0.016)	0.040 (0.016)	0.030 (0.012)	0.020 (0.008)	

TABLE 3.3-XIV

KNIFE-EDGE SEAL CLEARANCES

	Cold Gap		Aerodynamic Design Point Gap	
Seal Location	cm	in	cm	in
Inlet Guide Vane (Stator 1)	0.094	0.037	0.005	0.002
S2 Front	0.099	0.039	0.033	0.013
S2 Rear	0.091	0.036	0.020	0.008
S3 Front	0.084	0.033	0.020	0.008
S3 Rear	0.076	0.030	0.018	0.007
S4 Front	0.053	0.021	0.041	0.016
S4 Rear	0.051	0.020	0.020	0.008
S5	0.064	0.025	0.043	0.017

This Page Intentionally Left Blank

4.0 CONCLUSIONS

The major design goals for the low-pressure compressor are defined in Section 1.0 of this report. Analysis and design efforts have been aimed at achieving these goals. Table 4-I compares the as-designed status of the present low-pressure compressor with these goals at the aerodynamic design point.

TABLE 4-I

STATUS OF LOW-PRESSURE COMPONENT MAJOR DESIGN GOALS

Parameter	Goal	Status
Pressure Ratio	1.77	1.77
Flight Propulsion System Adiabatic Efficiency, percent	89.9	90.0
Integrated Core/Low Spool Adiabatic Efficiency, percent	87.5	87.5
Inlet Corrected Flow, kg/sec (in)	56.97 (125.6)	56.97 (125.6)
Surge Margin, percent	20	18
Integrated Core/Low Spool Low Cycle Fatigue Life, Cycles	1000	8000

The goal of reducing design and fabrication costs in the Integrated Core/Low Spool test compressor was achieved through the use of a steel bolted rotor, low cost stator designs, and existing hardware in the bleed system.

This Page Intentionally Left Blank

References

1. Stephens, H. E.: "Application of Supercritical Airfoil Technology to Compressor Cascades: Comparison of Theoretical and Experimental Results", AIAA Paper 78-1138, AIAA 11th Fluid and Plasma Dynamics Conference, Seattle, Washington, July 1978.

2. Stephens, H. E. and Hobbs, D. E.: "Design and Performance Evaluation of Supercritical Airfoils for Axial Flow Compressors", Naval Air Systems Command, FR11455, Contract N00019-C-0546, February 1979.

This Page Intentionally Left Blank

APPENDIX A

LOW-PRESSURE COMPRESSOR AERODYNAMIC SUMMARY

The following nine pages contain the aerodynamic summaries of each stage of the low-pressure compressor component design. Explanations of column headings can be found in Appendix B, Nomenclature.

STATOR 1 AERODYNAMIC SUMMARY

RUN NO 0 SPEED CODE 0 POINT NO 0

SL	V-1 M/SEC	V-2 M/SEC	VM-1 M/SEC	VM-2 M/SEC	V0-1 M/SEC	V0-2 M/SEC	RHOVM-1 KG/M2_SEC	RHOVM-2 KG/M2_SEC	PO/PO INLET_	TO/TO INLET	%EFF-A IDI-INLET	%EFF-P IDI-INLET	EPSI-1 RADIAN	EPSI-2 RADIAN
1	292.7	214.1	194.2	191.5	217.2	95.9	238.82	261.50	1.5474	1.1632	81.43	82.54	0.2252	0.0948
2	278.0	214.5	194.9	195.5	198.3	88.4	243.79	273.59	1.5775	1.1551	89.70	90.34	0.1756	0.0767
3	268.3	210.0	192.9	191.3	186.4	86.4	246.74	271.25	1.5817	1.1519	92.15	92.64	0.1302	0.0608
4	261.8	206.7	191.2	188.5	178.8	84.8	249.04	269.69	1.5875	1.1517	93.06	93.50	0.0917	0.0472
5	258.5	198.0	190.5	177.3	174.7	88.1	251.68	254.36	1.5721	1.1540	89.60	90.24	0.0627	0.0367

SL	B-1 DEGREE	B-2 DEGREE	M-1	M-2	INCS DEGREE	INCM DEGREE	DEV DEGREE	TURN DEGREE	D-EQC	OMEGA-B IDIAL	LOSS-P IDIAL	P02/ P01	PO/PO STAGE	TO/TO STAGE	%EFF-A IDI-STG	%EFF-P IDI-STG
1	48.2	26.3	0.8536	0.6045	-11.93	-4.61	6.57	21.84	0.3920	0.1249	0.0342	0.9526	1.5474	1.1632	81.43	82.54
2	45.6	24.2	0.8082	0.6079	-8.58	-1.46	3.29	21.47	0.3502	0.0465	0.0135	0.9838	1.5775	1.1551	89.70	90.34
3	44.1	24.2	0.7774	0.5950	-7.09	-0.18	3.05	19.87	0.3372	0.0355	0.0108	0.9884	1.5817	1.1519	92.15	92.64
4	43.1	24.2	0.7568	0.5851	-6.91	0.26	3.34	18.92	0.3320	0.0375	0.0118	0.9882	1.5875	1.1517	93.06	93.50
5	42.5	26.4	0.7454	0.5583	-7.74	0.32	4.30	16.14	0.3533	0.0973	0.0312	0.9700	1.5721	1.1540	89.60	90.24

SL	V-1 FT/SEC	V-2 FT/SEC	VM-1 FT/SEC	VM-2 FT/SEC	V0-1 FT/SEC	V0-2 FT/SEC	RHOVM-1 LBM/FT2SEC	RHOVM-2 LBM/FT2SEC	PCT TE _SPAN_	TO/TO INLET	%EFF-A IDI-INLET	%EFF-P IDI-INLET	EPSI-1 DEGREE	EPSI-2 DEGREE
1	960.3	702.6	643.7	628.2	712.7	314.7	48.91	53.56	0.1000	1.1632	81.43	82.54	12.903	5.430
2	912.2	703.8	639.3	641.3	650.6	290.0	49.93	56.03	0.3000	1.1551	89.70	90.34	10.061	4.397
3	880.2	688.9	632.9	627.8	611.6	283.6	50.53	55.55	0.5000	1.1519	92.15	92.64	7.458	3.485
4	858.9	678.1	627.5	618.4	586.6	278.2	51.01	55.24	0.7000	1.1517	93.06	93.50	5.257	2.705
5	848.0	649.6	625.0	581.7	573.2	289.0	51.55	52.09	0.9000	1.1540	89.60	90.24	3.590	2.105

NCORR INLET _RPM___	WCORR INLET LBM/SEC	WCORR INLET KG/SEC	TO/TO INLEI_	PO/PO INLEI_	EFF-AD INLET ___%__	EFF-P INLET __%___	TO/TO STAGE	P02/P01	PO/PO STAGE_	EFF-AD STAGE ___%__	EFF-P STAGE __%___
4215.00	122.62	55.62	1.1552	1.5734	89.08	89.75	1.1960	0.9763	1.7137	89.08	89.75

ROTOR 2 AERODYNAMIC SUMMARY

RUN NO 0 SPEED CODE 0 POINT NO 0

SL	V-1 M/SEC	V-2 M/SEC	VM-1 M/SEC	VM-2 M/SEC	V0-1 M/SEC	V0-2 M/SEC	U-1 M/SEC	U-2 M/SEC	V'-1 M/SEC	V'-2 M/SEC	V0'-1 M/SEC	V0'-2 M/SEC	RHOVM-1 KG/M2_SEC	RHOVM-2 KG/M2_SEC	EPSI-1 RADIAN	EPSI-2 RADIAN	PO/PO INLEI
1	214.7	242.6	192.2	173.7	95.7	169.3	222.8	223.3	230.4	181.9	-127.0	-54.0	262.22	252.68	0.0665	0.0272	1.8022
2	215.8	244.6	196.9	188.1	88.2	156.4	231.2	231.6	243.3	202.6	-142.9	-75.3	275.05	280.98	0.0572	0.0164	1.8448
3	211.5	235.4	193.1	183.0	86.3	148.0	239.5	240.0	246.5	204.8	-153.2	-91.9	273.03	278.05	0.0425	0.0036	1.8358
4	208.0	227.0	190.0	177.3	84.7	141.8	247.9	248.3	250.5	206.8	-163.3	-106.5	271.28	272.59	0.0282	-0.0041	1.8271
5	199.1	210.2	178.6	156.0	88.0	140.9	256.3	256.6	245.4	194.2	-168.3	-115.7	255.74	240.25	0.0183	-0.0032	1.7801

SL	B-1 DEGREE	B-2 DEGREE	B'-1 DEGREE	B'-2 DEGREE	M-1	M-2	M'-1	M'-2	INCS DEGREE	INCM DEGREE	DEV DEGREE	TURN DEGREE	D-EQC	OMEGA-B IDIAL	LOSS-P IDIAL	P02/ P01	%EFF-A IDIAL	%EFF-P IDIAL
1	26.5	44.3	33.51	17.27	0.6062	0.6744	0.6504	0.5058	-17.15	-7.73	10.10	16.24	0.3560	0.0533	0.0237	1.1652	91.96	92.12
2	24.2	39.7	36.00	21.80	0.6118	0.6835	0.6899	0.5661	-12.34	-3.42	4.88	14.20	0.3024	0.0198	0.0089	1.1696	96.60	96.64
3	24.1	39.0	38.45	26.66	0.5997	0.6576	0.6990	0.5721	-10.63	-2.89	3.92	11.79	0.2941	0.0127	0.0057	1.1607	97.62	97.68
4	24.0	38.6	40.67	30.98	0.5892	0.6330	0.7096	0.5767	-8.34	-3.16	3.89	9.69	0.2890	0.0193	0.0082	1.1508	96.13	96.21
5	26.2	42.1	43.31	36.56	0.5617	0.5828	0.6924	0.5383	-7.92	-5.00	7.56	6.75	0.3125	0.0441	0.0176	1.1340	91.15	91.31

SL	V-1 FT/SEC	V-2 FT/SEC	VM-1 FT/SEC	VM-2 FT/SEC	V0-1 FT/SEC	V0-2 FT/SEC	U-1 FT/SEC	U-2 FT/SEC	V'-1 FT/SEC	V'-2 FT/SEC	V0'-1 FT/SEC	V0'-2 FT/SEC	RHOVM-1 LBM/FT2SEC	RHOVM-2 LBM/FT2SEC	EPSI-1 DEGREE	EPSI-2 DEGREE	PCT TE _SPAN
1	704.4	795.9	630.5	570.0	314.1	555.5	730.9	732.7	755.8	596.9	-416.8	-177.2	53.70	51.75	3.810	1.557	0.1000
2	708.0	802.5	646.2	617.1	289.5	513.0	758.4	760.0	798.4	664.7	-468.9	-247.0	56.33	57.55	3.276	0.941	0.3000
3	694.0	772.4	633.6	600.6	283.2	485.7	786.0	787.3	808.8	672.0	-502.8	-301.6	55.92	56.95	2.436	0.208	0.5000
4	682.6	744.9	623.5	581.8	277.8	465.2	813.5	814.6	822.0	678.7	-535.7	-349.4	55.56	55.83	1.617	-0.350	0.7000
5	653.2	689.6	586.0	511.7	288.7	462.4	841.1	841.9	805.2	637.0	-552.3	-379.5	52.38	49.21	1.050	-0.181	0.9000

WC1/A1 LBM/SEC _SQFI__	WC1/A1 KG/SEC __SQM_	TO/TO _INLEI	PO/PO _INLEI	EFF-AD INLET ___%__	EFF-P INLET __%___	I02/I01	P02/P01	EFF-AD ROTOR __%___	EFF-P ROTOR __%___
35.85	175.02	1.2047	1.8184	90.09	90.89	1.0446	1.1558	94.52	94.63

STATOR 2 AERODYNAMIC SUMMARY

RUN NO 0 SPEED CODE 0 POINT NO 0

SL	V-1 M/SEC	V-2 M/SEC	VM-1 M/SEC	VM-2 M/SEC	V0-1 M/SEC	V0-2 M/SEC	RHOVM-1 KG/M2_SEC	RHOVM-2 KG/M2_SEC	P0/P0 INLEI	T0/T0 INLEI_	%EFF-A IDI-INLEI	%EFF-P IDI-INLEI	EPSI-1 RADIAN	EPSI-2 RADIAN
1	245.4	190.4	177.9	182.2	169.1	78.5	257.53	282.65	1.7838	1.2197	81.80	83.20	0.0212	-0.0391
2	246.6	203.5	190.8	190.6	156.2	71.4	283.96	303.81	1.8329	1.2091	90.35	91.13	-0.0041	-0.0586
3	236.9	196.2	185.0	183.3	147.9	70.1	280.25	295.90	1.8276	1.2027	92.70	93.29	-0.0212	-0.0743
4	227.6	188.7	178.1	175.8	141.8	68.7	273.41	285.66	1.8171	1.2008	92.63	93.22	-0.0328	-0.0886
5	208.4	168.6	153.4	154.0	141.1	68.7	236.75	249.44	1.7632	1.2005	87.71	88.64	-0.0408	-0.1078

SL	B-1 DEGREE	B-2 DEGREE	__M-1_	__M-2_	INCS DEGREE	INCM DEGREE	DEV DEGREE	TURN DEGREE	Q-E0C_	OMEGA-B _IDI0L_	LOSS-P _IDI0L	P02/ _P01__	P0/P0 SI0GE_	T0/T0 SI0GE_	%EFF-A IDI-SIG	%EFF-P IDI-SIG
1	43.5	23.3	0.6830	0.5435	-11.40	-4.11	7.91	20.22	0.3306	0.0455	0.0156	0.9878	1.1528	1.0486	85.02	85.32
2	39.3	20.6	0.6876	0.5610	-9.98	-2.55	4.11	18.73	0.3061	0.0229	0.0083	0.9938	1.1615	1.0470	92.76	92.92
3	38.6	21.0	0.6620	0.5412	-9.22	-1.75	3.56	17.66	0.3018	0.0161	0.0060	0.9959	1.1555	1.0443	94.88	94.99
4	38.5	21.4	0.6347	0.5178	-9.16	-1.68	3.56	17.11	0.3039	0.0226	0.0087	0.9946	1.1447	1.0426	92.28	92.42
5	42.5	24.1	0.5775	0.4620	-10.64	-3.33	6.88	18.43	0.3406	0.0437	0.0170	0.9912	1.1237	1.0400	84.43	84.69

SL	V-1 EI/SEC	V-2 EI/SEC	VM-1 EI/SEC	VM-2 EI/SEC	V0-1 EI/SEC	V0-2 EI/SEC	RHOVM-1 LBM/EI2SEC	RHOVM-2 LBM/EI2SEC	PCT TE _SE0N_	T0/T0 INLEI	%EFF-A IDI-INLEI	%EFF-P IDI-INLEI	EPSI-1 DEGREE	EPSI-2 DEGREE
1	805.2	650.9	583.7	597.8	554.7	257.5	52.74	57.89	0.1000	1.2197	81.80	83.20	1.216	-2.239
2	809.0	667.8	626.0	625.4	512.4	234.3	58.16	62.22	0.3000	1.2091	90.35	91.13	-0.236	-3.355
3	777.1	643.9	607.0	601.4	485.3	230.1	57.40	60.60	0.5000	1.2027	92.70	93.29	-1.215	-4.259
4	746.9	619.2	584.2	576.8	465.3	225.3	56.00	58.51	0.7000	1.2008	92.63	93.22	-1.881	-5.074
5	683.7	553.2	503.2	505.2	462.9	225.5	48.49	51.09	0.9000	1.2005	87.71	88.64	-2.335	-6.178

NCORR INLET _RPM___	WCORR INLET LBM/SEC	WCORR INLET KG/SEC	TO/TO INLEI_	PO/PO INLEI	EFF-AD INLET ___%___	EFF-P INLET __%___	T0/T0 SI0GE	P02/P01	P0/P0 SI0GE_	EFF-AD STAGE ___%__	EFF-P STAGE __%___
4215.00	122.62	55.62	1.2067	1.8052	88.90	89.78	1.0446	0.9927	1.1474	89.66	89.86

ROTOR 3 AERODYNAMIC SUMMARY

RUN NO 0 SPEED CODE 0 POINT NO 0

SL	V-1 M/SEC	V-2 M/SEC	VM-1 M/SEC	VM-2 M/SEC	V0-1 M/SEC	V0-2 M/SEC	U-1 M/SEC	U-2 M/SEC	V'-1 M/SEC	V'-2 M/SEC	V0'-1 M/SEC	V0'-2 M/SEC	RHOVM-1 KG/M2_SEC	RHOVM-2 KG/M2_SEC	EPSI-1 RADIAN	EPSI-2 RADIAN	P0/P0 INLEI
1	202.0	232.5	186.0	172.4	78.7	156.1	223.3	221.5	235.6	184.4	-144.6	-65.4	287.00	284.16	-0.0817	-0.1619	2.0813
2	206.9	235.5	194.1	185.1	71.6	145.6	230.9	229.3	251.1	203.1	-159.3	-83.6	307.73	315.90	-0.0912	-0.1612	2.1497
3	199.4	223.2	186.5	174.2	70.4	139.5	238.6	237.1	251.2	199.7	-168.2	-97.5	299.72	303.43	-0.1023	-0.1647	2.1367
4	191.7	213.7	178.8	163.5	69.0	137.7	246.2	244.8	251.8	195.4	-177.2	-107.2	289.41	288.14	-0.1100	-0.1668	2.1299
5	172.2	194.2	157.8	133.4	69.0	141.2	253.9	252.6	243.0	173.8	-184.8	-111.5	254.54	235.45	-0.1040	-0.1591	2.0796

SL	B-1 DEGREE	B-2 DEGREE	B'-1 DEGREE	B'-2 DEGREE	__M-1_	__M-2_	_M'-1_	_M'-2_	INCS DEGREE	INCM DEGREE	DEV DEGREE	TURN DEGREE	Q-E0C_	OMEGA-B _IDI0L_	LOSS-P _IDI0L	P02/ _P01_	%EFF-A _IDI0L	%EFF-P _IDI0L
1	22.9	42.3	37.77	20.91	0.5538	0.6281	0.6461	0.4981	-14.82	-5.27	6.29	16.86	0.3689	0.0382	0.0147	1.1677	94.18	94.32
2	20.2	38.4	39.31	24.46	0.5708	0.6397	0.6927	0.5517	-12.83	-3.91	3.43	14.85	0.3327	0.0189	0.0083	1.1728	96.75	96.83
3	20.7	38.9	42.01	29.42	0.5504	0.6060	0.6933	0.5421	-11.88	-3.69	3.84	12.59	0.3416	0.0127	0.0055	1.1694	97.74	97.80
4	21.1	40.3	44.75	33.46	0.5284	0.5785	0.6940	0.5290	-10.50	-3.47	4.46	11.28	0.3641	0.0194	0.0083	1.1725	96.67	96.74
5	23.6	46.8	49.52	40.09	0.4723	0.5218	0.6665	0.4671	-8.45	-2.96	9.09	9.43	0.4385	0.0379	0.0154	1.1821	94.40	94.54

SL	V-1 EI/SEC	V-2 EI/SEC	VM-1 EI/SEC	VM-2 EI/SEC	V0-1 EI/SEC	V0-2 EI/SEC	U-1 EI/SEC	U-2 EI/SEC	V'-1 EI/SEC	V'-2 EI/SEC	V0'-1 EI/SEC	V0'-2 EI/SEC	RHOVM-1 LBM/EI2SEC	RHOVM-2 LBM/EI2SEC	EPSI-1 DEGREE	EPSI-2 DEGREE	PCT TE _SE0N_
1	662.6	762.9	610.2	565.6	258.2	512.0	732.6	726.7	773.0	605.0	-474.4	-214.7	58.78	58.20	-4.681	-9.279	0.1000
2	678.7	772.6	636.7	607.2	235.1	477.8	757.7	752.2	823.7	666.3	-522.6	-274.4	63.02	64.70	-5.225	-9.238	0.3000
3	654.2	732.4	612.0	571.7	230.9	457.8	782.7	777.8	824.1	655.1	-551.8	-320.0	61.39	62.15	-5.864	-9.435	0.5000
4	628.9	701.2	586.8	536.3	226.3	451.7	807.8	803.3	826.1	641.3	-581.5	-351.6	59.27	59.01	-6.304	-9.558	0.7000
5	565.1	637.2	517.7	437.6	224.4	463.1	832.9	828.8	797.4	570.3	-606.5	-345.7	52.13	48.22	-6.071	-9.118	0.9000

WC1/A1 LBM/SEC _SQEI__	WC1/A1 KG/SEC __SQM_	TO/TO _INLEI	PO/PO _INLEI	EFF-AD INLET ___%___	EFF-P INLET __%___	I02/I01	P02/P01	EFF-AD ROTOR __%____	EFF-P ROTOR __%__
34.79	169.88	1.2650	2.1171	90.06	91.05	1.0483	1.1727	96.00	96.10

STATOR 3 AERODYNAMIC SUMMARY

RUN NO 0 SPEED CODE 0 POINT NO 0

SL	V-1 M/SEC	V-2 M/SEC	VM-1 M/SEC	VM-2 M/SEC	V0-1 M/SEC	V0-2 M/SEC	RHOVM-1 KG/M2_SEC	RHOVM-2 KG/M2_SEC	PO/P0 INLEI_	TO/TO INLEI	%EFF-A IOI=INLEI	%EFF-P IOI=INLEI	EPSI-1 RADIAN	EPSI-2 RADIAN
1	235.2	181.2	174.9	170.6	157.2	61.0	286.78	300.17	2.0585	1.2781	82.24	83.93	-0.2117	-0.2965
2	238.3	193.1	187.6	184.6	146.9	56.5	318.65	334.66	2.1372	1.2672	90.58	91.53	-0.2151	-0.2932
3	226.5	183.1	177.4	174.7	140.8	54.7	307.32	321.65	2.1288	1.2587	93.03	93.73	-0.2182	-0.2892
4	217.8	174.0	167.6	165.6	139.0	53.3	293.60	307.30	2.1200	1.2583	92.60	93.33	-0.2241	-0.2861
5	200.1	152.2	140.4	142.0	142.5	54.8	246.05	262.58	2.0664	1.2624	87.74	88.92	-0.2380	-0.2862

SL	B-1 DEGREE	B-2 DEGREE	__M=1_	__M=2_	INCS DEGREE_	INCM DEGREE	DEV DEGREE	TURN DEGREE	D=EQ_	OMEGA-B _IOI@L_	LOSS-P _IOI@L	P02/ _P01__	PO/PO SI@GE_	TO/TO SI@GE	%EFF-A IOI=SIG	%EFF-P IOI=SIG
1	41.7	19.9	0.6358	0.4821	-9.12	-1.32	6.95	21.77	0.3860	0.0440	0.0155	0.9896	1.1555	1.0479	87.67	87.94
2	37.8	17.2	0.6478	0.5175	-10.20	-2.32	4.08	20.60	0.3395	0.0240	0.0089	0.9941	1.1660	1.0480	93.05	93.20
3	38.1	17.5	0.6156	0.4912	-10.05	-2.17	4.18	20.61	0.3468	0.0169	0.0064	0.9962	1.1649	1.0466	95.32	95.43
4	39.4	17.9	0.5902	0.4658	-10.01	-2.16	4.41	21.43	0.3666	0.0223	0.0087	0.9953	1.1668	1.0479	93.82	93.96
5	45.1	21.2	0.5385	0.4049	-8.69	-0.97	8.21	23.96	0.4299	0.0419	0.0166	0.9925	1.1728	1.0515	90.12	90.35

SL	V-1 EI/SEC	V-2 EI/SEC	VM-1 EI/SEC	VM-2 EI/SEC	V0-1 EI/SEC	V0-2 EI/SEC	RHOVM-1 LBM/EI2SEC	RHOVM-2 LBM/EI2SEC	PCT TE _SE@N_	TO/TO INLEI	%EFF-A IOI=INLEI	%EFF-P IOI=INLEI	EPSI-1 DEGREE	EPSI-2 DEGREE
1	771.6	594.5	573.9	559.7	515.8	200.2	58.78	61.48	0.1000	1.2781	82.24	83.93	-12.129	-16.989
2	781.8	633.4	615.5	605.6	482.0	185.5	65.24	68.54	0.3000	1.2672	90.58	91.53	-12.326	-16.800
3	743.2	600.6	582.1	573.1	462.0	179.6	62.94	65.88	0.5000	1.2587	93.03	93.73	-12.502	-16.570
4	714.4	570.8	549.9	543.3	456.1	174.8	60.13	62.94	0.7000	1.2583	92.60	93.33	-12.840	-16.394
5	656.4	499.5	460.7	466.0	467.5	179.9	50.39	53.78	0.9000	1.2624	87.74	88.92	-13.637	-16.397

NCORR INLET _RPM___	WCORR INLET LBM/SEC	WCORR INLET KG/SEC	TO/TO INLEI_	PO/PO INLEI_	EFF-AD INLET ___%___	EFF-P INLET __%___	TO/TO STAGE_	P02/P01	PO/PO STAGE_	EFF-AD STAGE ___%___	EFF-P STAGE __%___
4215.00	122.62	55.62	1.2650	2.1035	89.21	90.27	1.0483	0.9936	1.1652	92.05	92.23

ROTOR 4 AERODYNAMIC SUMMARY

RUN NO 0 SPEED CODE 0 POINT NO 0

SL	V-1 M/SEC	V-2 M/SEC	VM-1 M/SEC	VM-2 M/SEC	V0-1 M/SEC	V0-2 M/SEC	U-1 M/SEC	U-2 M/SEC	V'-1 M/SEC	V'-2 M/SEC	V0'-1 M/SEC	V0'-2 M/SEC	RHOVM-1 KG/M2_SEC	RHOVM-2 KG/M2_SEC	EPSI-1 RADIAN	EPSI-2 RADIAN	PO/PO INLEI
1	183.2	217.4	172.4	155.0	61.8	152.4	213.6	208.2	229.8	164.8	-151.9	-55.8	302.64	291.02	-0.3434	-0.4174	2.4099
2	195.1	225.4	186.6	177.3	57.2	139.2	220.9	215.9	248.2	193.2	-163.7	-76.8	337.24	344.49	-0.3360	-0.3988	2.4997
3	185.5	212.7	177.0	167.5	55.4	131.1	228.2	223.7	247.4	191.4	-172.8	-92.5	324.93	331.92	-0.3354	-0.3900	2.4818
4	176.5	203.2	168.0	158.1	54.0	127.6	235.4	231.4	247.3	189.1	-181.5	-103.7	310.85	316.08	-0.3361	-0.3858	2.4700
5	154.7	184.3	144.4	129.4	55.5	131.3	242.7	239.1	236.4	168.4	-187.2	-107.8	266.25	257.63	-0.3321	-0.3782	2.4134

SL	B-1 DEGREE	B-2 DEGREE	B'-1 DEGREE	B'-2 DEGREE	__M=1_	__M=2_	_M'=1_	_M'=2_	INCS DEGREE	INCM DEGREE	DEV DEGREE	TURN DEGREE	D=EQ_	OMEGA-B _IOI@L_	LOSS-P _IOI@L	P02/ _P01__	%EFF-A _IOI@L	%EFF-P _IOI@L
1	19.3	44.8	40.81	19.98	0.4876	0.5697	0.6117	0.4318	-12.61	-4.28	9.61	20.82	0.4590	0.0462	0.0200	1.1743	93.94	94.09
2	16.8	38.3	40.75	23.54	0.5234	0.5952	0.6457	0.5101	-11.82	-4.17	3.76	17.21	0.3753	0.0212	0.0093	1.1697	96.52	96.61
3	17.2	38.2	43.91	29.09	0.4981	0.5622	0.6641	0.5058	-10.97	-3.94	3.30	14.82	0.3742	0.0129	0.0056	1.1657	97.80	97.87
4	17.7	39.2	46.96	33.54	0.4728	0.5355	0.6626	0.4983	-9.89	-3.70	3.56	13.42	0.3848	0.0203	0.0086	1.1651	96.60	96.69
5	21.0	45.8	52.25	40.17	0.4116	0.4820	0.6292	0.4403	-8.78	-3.53	8.12	12.08	0.4517	0.0434	0.0176	1.1692	93.77	93.92

SL	V-1 EI/SEC	V-2 EI/SEC	VM-1 EI/SEC	VM-2 EI/SEC	V0-1 EI/SEC	V0-2 EI/SEC	U-1 EI/SEC	U-2 EI/SEC	V'-1 EI/SEC	V'-2 EI/SEC	V0'-1 EI/SEC	V0'-2 EI/SEC	RHOVM-1 LBM/EI2SEC	RHOVM-2 LBM/EI2SEC	EPSI-1 DEGREE	EPSI-2 DEGREE	PCT TE _SE@N
1	600.9	713.3	565.8	508.6	202.6	500.0	700.9	683.2	753.9	540.6	-498.3	-183.2	61.98	59.60	-19.675	-23.916	0.1000
2	640.2	739.5	612.1	581.4	187.8	456.7	724.7	708.5	814.3	633.8	-537.0	-251.8	69.07	70.55	-19.250	-22.850	0.3000
3	608.7	697.9	580.9	549.6	181.8	430.2	748.6	733.8	811.6	627.9	-566.8	-303.6	66.55	67.98	-19.219	-22.345	0.5000
4	579.1	666.7	551.3	518.7	177.0	418.8	772.5	759.1	811.5	620.4	-595.4	-340.3	63.66	64.74	-19.259	-22.104	0.7000
5	507.5	604.7	473.7	424.4	182.1	430.8	796.4	784.4	775.7	552.4	-614.2	-353.6	54.53	52.76	-19.030	-21.667	0.9000

WC1/A1 LBM/SEC _SQEI__	WC1/A1 KG/SEC __SQM_	TO/TO _INLEI	PO/PO _INLEI	EFF-AD INLET ___%___	EFF-P INLET __%__	I02/I01	P02/P01	EFF-AD ROTOR __%____	EFF-P ROTOR __%___
32.70	159.67	1.3249	2.4584	90.01	91.19	1.0473	1.1687	95.75	95.85

STATOR 4 AERODYNAMIC SUMMARY

RUN NO 0 SPEED CODE 0 POINT NO 0

SL	V-1 M/SEC	V-2 M/SEC	VM-1 M/SEC	VM-2 M/SEC	V0-1 M/SEC	V0-2 M/SEC	RHOVM-1 KG/M2_SEC	RHOVM-2 KG/M2_SEC	PO/PO INLEI	TO/TO INLEI_	%EFF-A IDI=INLEI	%EFF-P IDI=INLEI	EPSI-1 RADIAN	EPSI-2 RADIAN
1	220.1	161.7	156.6	156.9	154.6	39.3	292.84	312.93	2.3841	1.3417	82.26	84.26	-0.4477	-0.5108
2	228.2	181.5	179.1	178.2	141.3	34.4	346.56	366.24	2.4859	1.3279	90.45	91.59	-0.4381	-0.4928
3	216.0	173.0	170.1	169.8	133.2	33.1	335.36	353.65	2.4741	1.3164	93.19	94.00	-0.4269	-0.4789
4	206.8	165.3	161.1	162.0	129.7	32.6	320.45	338.57	2.4597	1.3159	92.66	93.53	-0.4193	-0.4674
5	198.3	144.6	133.0	139.9	133.4	36.4	263.59	289.74	2.3985	1.3233	87.68	89.09	-0.4195	-0.4619

SL	B-1 DEGREE	B-2 DEGREE	M=1	M=2	INCS DEGREE	INCM DEGREE	DEV DEGREE	TURN DEGREE	D-FAC	OMEGA-B IDIAL	LOSS-P IDIAL	P02/ P01	PO/PO STAGE	TO/TO STAGE	%EFF-A IDI=STG	%EFF-P IDI=STG
1	44.3	14.3	0.5772	0.4179	-7.45	-0.68	10.18	29.93	0.4653	0.0542	0.0190	0.9893	1.1617	1.0497	87.52	87.79
2	37.8	11.0	0.6030	0.4736	-9.77	-2.83	6.58	26.78	0.3876	0.0256	0.0094	0.9944	1.1632	1.0472	92.97	93.13
3	37.5	11.1	0.5715	0.4525	-10.06	-3.09	6.82	26.42	0.3868	0.0168	0.0064	0.9967	1.1619	1.0456	95.61	95.72
4	38.2	11.4	0.5456	0.4316	-10.62	-3.68	7.25	26.82	0.3970	0.0229	0.0091	0.9958	1.1602	1.0459	93.99	94.13
5	44.5	14.6	0.4931	0.3749	-8.72	-1.83	10.95	29.90	0.4564	0.0484	0.0195	0.9926	1.1602	1.0483	89.31	89.55

SL	V-1 EI/SEC	V-2 EI/SEC	VM-1 EI/SEC	VM-2 EI/SEC	V0-1 EI/SEC	V0-2 EI/SEC	RHOVM-1 LBM/EI2SEC	RHOVM-2 LBM/EI2SEC	PCT TE SPAN	TO/TO INLEI	%EFF-A IDI=INLEI	%EFF-P IDI=INLEI	EPSI-1 DEGREE	EPSI-2 DEGREE
1	722.1	530.6	513.8	514.7	507.4	128.9	59.98	64.09	0.1000	1.3417	82.26	84.26	-25.653	-27.269
2	748.6	595.6	587.7	584.8	463.7	112.8	70.98	75.01	0.3000	1.3279	90.45	91.59	-25.099	-28.234
3	708.8	567.7	558.0	557.2	437.0	108.6	68.68	72.43	0.5000	1.3164	93.19	94.00	-24.457	-27.436
4	678.5	542.2	528.6	531.6	425.5	107.0	65.63	69.34	0.7000	1.3159	92.66	93.53	-24.023	-26.782
5	617.9	474.3	436.4	459.0	437.6	119.4	53.99	59.34	0.9000	1.3233	87.68	89.09	-24.033	-26.466

NCORR INLET RPM	WCORR INLET LBM/SEC	WCORR INLET KG/SEC	TO/TO INLEI	PO/PO INLEI	EFF-AD INLET %	EFF-P INLET %
4215.00	122.62	55.62	1.3249	2.4431	89.31	90.56

TO/TO STAGE	P02/P01	PO/PO STAGE	EFF-AD STAGE %	EFF-P STAGE %
1.0473	0.9938	1.1614	91.83	92.01

ROTOR 5 AERODYNAMIC SUMMARY

RUN NO 0 SPEED CODE 0 POINT NO 0

SL	V-1 M/SEC	V-2 M/SEC	VM-1 M/SEC	VM-2 M/SEC	V0-1 M/SEC	V0-2 M/SEC	U-1 M/SEC	U-2 M/SEC	V'-1 M/SEC	V'-2 M/SEC	V0'-1 M/SEC	V0'-2 M/SEC	RHOVM-1 KG/M2_SEC	RHOVM-2 KG/M2_SEC	EPSI-1 RADIAN	EPSI-2 RADIAN	PO/PO INLEI
1	160.2	179.6	155.1	125.9	40.1	128.1	194.9	185.9	219.0	138.6	-154.7	-57.8	309.46	267.81	-0.5534	-0.4022	2.6955
2	182.5	198.6	179.1	165.9	35.0	109.1	202.3	194.2	245.0	186.5	-167.3	-85.1	367.44	364.22	-0.5196	-0.5603	2.8049
3	174.7	190.1	171.4	159.7	33.7	103.2	209.7	202.5	245.7	188.0	-176.0	-99.3	356.24	356.55	-0.5015	-0.5377	2.7969
4	167.1	184.8	163.8	153.3	33.2	103.2	217.1	210.8	246.3	187.2	-183.9	-107.5	341.52	343.93	-0.4892	-0.5232	2.7944
5	146.9	166.9	142.2	126.0	36.9	109.4	224.5	219.1	235.4	167.0	-187.6	-109.6	293.90	279.97	-0.4747	-0.5066	2.7327

SL	B-1 DEGREE	B-2 DEGREE	B'-1 DEGREE	B'-2 DEGREE	M=1	M=2	M'=1	M'=2	INCS DEGREE	INCM DEGREE	DEV DEGREE	TURN DEGREE	D-FAC	OMEGA-B IDIAL	LOSS-P IDIAL	P02/ P01	%EFF-A IDIAL	%EFF-P IDIAL
1	13.9	45.1	43.67	24.39	0.4138	0.4569	0.5659	0.3525	-7.70	-2.31	10.85	19.28	0.5405	0.0549	0.0219	1.1390	92.86	92.99
2	10.6	32.8	41.78	26.69	0.4741	0.5103	0.6393	0.4792	-8.01	-3.70	2.64	15.10	0.3727	0.0212	0.0087	1.1283	95.84	95.92
3	10.8	32.5	44.80	31.55	0.4570	0.4901	0.6427	0.4848	-7.03	-3.26	1.57	13.25	0.3660	0.0103	0.0042	1.1299	97.93	97.97
4	11.3	34.0	47.81	35.08	0.4365	0.4756	0.6433	0.4818	-6.49	-2.99	2.04	12.73	0.3784	0.0153	0.0063	1.1360	97.06	97.13
5	14.5	41.4	52.79	41.46	0.3811	0.4260	0.6107	0.4264	-5.82	-2.59	7.38	11.34	0.4458	0.0373	0.0146	1.1401	93.95	94.06

SL	V-1 EI/SEC	V-2 EI/SEC	VM-1 EI/SEC	VM-2 EI/SEC	V0-1 EI/SEC	V0-2 EI/SEC	U-1 EI/SEC	U-2 EI/SEC	V'-1 EI/SEC	V'-2 EI/SEC	V0'-1 EI/SEC	V0'-2 EI/SEC	RHOVM-1 LBM/EI2SEC	RHOVM-2 LBM/EI2SEC	EPSI-1 DEGREE	EPSI-2 DEGREE	PCT TE SPAN
1	525.5	589.3	508.8	413.2	131.7	420.2	639.3	609.9	718.7	454.7	-507.6	-189.7	63.38	54.85	-31.708	-34.501	0.1000
2	598.4	651.5	587.5	544.4	114.9	357.9	663.7	637.1	803.9	611.8	-548.8	-279.1	75.25	74.60	-29.770	-32.105	0.3000
3	573.2	623.7	562.4	523.9	110.6	338.5	688.0	664.3	806.0	616.9	-577.4	-325.8	72.96	73.03	-28.735	-30.808	0.5000
4	548.2	606.3	537.3	502.8	108.9	338.8	712.4	691.5	808.0	614.2	-603.4	-352.8	69.95	70.44	-28.026	-29.977	0.7000
5	482.0	547.5	466.5	413.4	121.1	359.0	736.7	718.7	772.4	548.0	-615.6	-359.7	60.19	57.34	-27.198	-29.025	0.9000

WC1/A1 LBM/SEC SQEI	WC1/A1 KG/SEC SQM	TO/TO INLEI	PO/PO INLEI	EFF-AD INLET %	EFF-P INLET %
30.60	149.42	1.3754	2.7711	89.81	91.16

I02/I01	P02/P01	EFF-AD ROTOR %	EFF-P ROTOR %
1.0381	1.1342	95.56	95.64

STATOR 5 AERODYNAMIC SUMMARY

RUN NO 0 SPEED CODE 0 POINT NO 0

SL	V-1 M/SEC	V-2 M/SEC	VM-1 M/SEC	VM-2 M/SEC	V0-1 M/SEC	V0-2 M/SEC	RHOVM-1 KG/M2_SEC	RHOVM-2 KG/M2_SEC	PO/P0 INLET	TO/TO INLET	%EFF-A IDI=INLET	%EFF-P IDI=INLET	EPSI-1 RADIAN	EPSI-2 RADIAN
1	181.1	130.0	125.3	129.8	130.8	7.2	265.87	287.19	2.6679	1.3960	81.49	83.82	-0.6124	-0.6394
2	200.2	144.1	144.3	144.0	111.5	-1.8	364.27	373.59	2.7932	1.3787	89.85	91.20	-0.5854	-0.6061
3	192.6	140.3	141.1	140.3	105.5	-1.7	358.64	369.58	2.7901	1.3647	93.18	94.09	-0.5560	-0.5839
4	187.9	137.2	135.4	137.2	105.7	-1.6	347.36	362.83	2.7852	1.3653	92.84	93.79	-0.5337	-0.5647
5	170.3	137.5	128.2	137.4	112.1	4.1	283.86	313.04	2.7194	1.3760	87.76	89.35	-0.5212	-0.5573

SL	B-1 DEGREE	B-2 DEGREE	M-1	M-2	INCS DEGREE	INCM DEGREE	DEV DEGREE	TURN DEGREE	D-FAC	OMEGA-B IDIAL	LOSS-P IDIAL	P02/ P01	P0/P0 STAGE	TO/TO STAGE	%EFF-A IDI=SIG	%EFF-P IDI=SIG
1	46.0	3.2	0.4608	0.3273	-4.57	0.28	8.55	42.82	0.5478	0.0876	0.0303	0.9889	1.1260	1.0404	85.03	85.28
2	33.5	-0.6	0.5148	0.4182	-9.88	-4.75	3.99	34.13	0.3966	0.0252	0.0092	0.9958	1.1236	1.0364	92.46	92.59
3	32.7	-0.6	0.4969	0.4105	-10.38	-5.24	4.22	33.29	0.3892	0.0160	0.0061	0.9975	1.1269	1.0360	95.87	95.95
4	33.6	-0.6	0.4840	0.4023	-11.02	-5.93	4.62	34.20	0.3993	0.0223	0.0089	0.9967	1.1319	1.0379	94.58	94.69
5	40.6	2.5	0.4352	0.3492	-8.19	-3.21	8.29	38.07	0.4630	0.0519	0.0216	0.9937	1.1324	1.0402	89.45	89.65

SL	V-1 FT/SEC	V-2 FT/SEC	VM-1 FT/SEC	VM-2 FT/SEC	V0-1 FT/SEC	V0-2 FT/SEC	RHOVM-1 LBM/FT2SEC	RHOVM-2 LBM/FT2SEC	PCT TE SPAN	TO/TO INLET	%EFF-A IDI=INLET	%EFF-P IDI=INLET	EPSI-1 DEGREE	EPSI-2 DEGREE
1	594.2	426.4	411.0	425.7	429.1	23.5	54.45	58.82	0.1000	1.3960	81.49	83.82	-35.089	-36.636
2	657.0	538.3	545.7	538.2	365.9	-6.0	74.61	76.52	0.3000	1.3787	89.85	91.20	-33.540	-34.724
3	631.9	526.0	528.6	526.0	346.2	-5.5	73.45	75.69	0.5000	1.3647	93.18	94.09	-31.859	-33.452
4	616.5	515.9	509.8	515.9	346.8	-5.3	71.14	74.31	0.7000	1.3653	92.84	93.79	-30.577	-32.470
5	558.9	451.2	420.7	450.7	367.8	19.9	58.14	64.11	0.9000	1.3760	87.76	89.35	-29.861	-31.933

NCORR INLET RPM	WCORR INLET LBM/SEC	WCORR INLET KG/SEC	TO/TO INLET	PO/PO INLET	EFF-AD INLET %%	EFF-P INLET %%
4215.00	122.62	55.62	1.3754	2.7561	89.26	90.67

TO/TO STAGE	P02/P01	PO/PO STAGE	EFF-AD STAGE %%	EFF-P STAGE %%
1.0381	0.9946	1.1281	91.37	91.51

APPENDIX B

NOMENCLATURE

Defined below are the terms used in the main body of this report in addition to those used in Appendix A.

Term	Definition
W_E CS1	Engine airflow corrected to stator 1 inlet conditions
N_1 Corrected to S1	Low-pressure rotor speed corrected to stator inlet conditions
U-Tip	Rotor 2 tip speed, corrected to stator 1 inlet conditions
W_E S1/A	Engine airflow corrected to stator 1 inlet conditions and divided by stator 1 inlet area
Cx/U	Average axial wheel speed divided by mean wheel speed
E	Two times the enthalpy rise, divided by the mean wheel speed squared times the number of stages (4)
D-Factor	Measure of diffusion along airfoil suction surface (Peak static pressure rise on suction surface divided by peak inlet velocity head
θ	Temperature correction factor, $\frac{\text{Tamb } (^\circ R)}{519}$ (standard day)
$Cm\sqrt{\theta_T}s1$	Thru flow velocity parameter where Cm is meridional velocity, $\sqrt{\theta_T}s1$ is the total temperature correction to stator 1 (ft/sec)
Reduced Velocity, V/BW	Airfoil flutter parameter where V is the relative air inlet velocity to the airfoil at 75 percent span in feet per second, B is half the airfoil chord at 75 percent span in feet, and W is flutter frequency in radians per second

Term	Definition
S1	Stator 1 or Low-Pressure Compressor inlet vane
$\Delta P/Po-P$	Measure of loading on blade end walls (Static pressure rise divided by inlet velocity head)
Root, Mean, Tip γ chord	Blade chord angle, angle between chord and axial direction
Z Plane and Z Plane Radius	Plane at which blade attachment and disk attachment make contact

Terms from Aerodynamic Summary - Appendix A

B-1	Absolute air angle at row inlet
B-2	Absolute air angle at row exit
B'-1	Relative air angle at row inlet
B'-2	Relative air angle at row exit
ESPI	Angle between tangent to streamline projected on meridional plane and axial direction
DEV	Deviation angle (Exit air angle minus the metal angle at trailing edge
D-FAC	Diffusion factor (see above)
EFF-A or -AD	Adiabatic efficiency
EFF-P	Polytropic efficiency
EPSI-1	Slope of meridional streamline at row inlet
EPSI-2	Slope of meridional streamline at row exit

Term	Definition
INCS	Incidence angle between inlet air direction and line tangent to blade suction surface at leading edge, degrees
INCM	Incidence angle between inlet air direction and line tangent to blade mean camber line at leading edge, degrees
LOSS-P	Loss parameter
M-1	Mach number at row inlet
M-2	Mach number at row exit
M'-1	Relative Mach number at row inlet
M'-2	Relative Mach number at row exit
NCORR	Low-pressure rotor speed, corrected
OMEGA-B	Total pressure loss coefficient (Mass average defect in relative total pressure divided by difference between inlet stagnation and static pressures)
PCT TE SPAN	Percent trailing edge span
PO/PO	Pressure ratio
PO2/PO1	Static pressure ratio
RHOVM-1	Density times meridional velocity at row inlet
RHOVM-2	Density times meridional velocity at row exit
TURN	Relative air turning from inlet to exit, degrees
TO/TO	Temperature ratio
U-1	Rotor tangential speed at row inlet

Term	Definition
U-2	Rotor tangential speed at row exit
V-1	Air velocity at row inlet
V-2	Air velocity at row exit
VM-1	Meridional velocity at row inlet
VM-2	Meridional velocity at row exit
V'-1	Relative air velocity at row inlet
V'-2	Relative air velocity at row exit
$V\theta$-1	Tangential velocity at row inlet
$V\theta$-2	Tangential velocity at row exit
$V\theta'$-1	Relative tangential velocity at row inlet
$V\theta'$-2	Relative tangential velocity at row exit
WCORR	Airflow, corrected
WC1/A1	Stage inlet corrected airflow divided by stage inlet area

DISTRIBUTION LIST

GOVERNMENT AGENCIES

NASA Headquarters
600 Independence Ave., SW
Washington, D.C. 20546
Attention: RTP-6/R.S. Colladay
RTM-6/L. Harris
RRP-6/J. Facey
Library

NASA-Lewis Research Center
21000 Brookpark Road
Cleveland, OH 44135

Attention:	D. L. Nored	MS 301-2
	C. C. Ciepluch	MS 301-4 (20 copies)
	J. W. Schaefer	MS 301-4
	G. K. Sievers	MS 301-2
	Library	MS 60-3 (2 copies)
	Report Control Office	MS 5-5
	Tech Utilization Office	MS 3-19
	M. A. Beheim	MS 3-5
	M. J. Hartmann	MS 5-3
	R. A. Rudey	MS 60-4
	R. A. Weber	MS 500-127
	W. C. Strack	MS 501-10
	T. P. Moffitt	MS 77-2
	R.E. Jones	MS 86-6
	L.P. Ludwig	MS 23-2
	D.C. Mikkelson	Ms 86-1
	R. Purgert	MS 500-305
	J.F. Groeneweg	MS 54-3
	W. M. Braithwaite	MS 500-208
	R.L. Davies	MS 106-1
	R.H. Johns	MS 49-6
	L.J. Kaszubinski	MS 86-2
	L. Reid	MS 5-9
	R.J. Rulis	MS 86-2
	R.W. Niedzwiecki	MS 86-6
	AFSC Liaison Office	MS 501-3
	Army R&T Propulsion Lab	MS 302-2

NASA Ames Research Center
Moffett Field, CA 94035
Attention: 202-7/M. H. Waters
202-7/L. J. Williams
Library

NASA Langley Research Center
Langley Field, VA 23365
Attention: R. Leonard
D. Maiden
Library

NASA Dryden Flight Research Center
P.O. Box 273
Edwards, CA 93523
Attention: J. A. Albers
Library

NASA Scientific and Technical Information Facility
Linthicum Heights, MD 21090
Attention: Accessioning Dept. (10 copies)

Department of Defense
Washington, D.C. 20301
Attention: R. Standahar 3D1089 Pentagon

Wright-Patterson Air Force Base
Dayton, Ohio 45433
Attention: APL Chief Scientist AFWAL/PS

Wright-Patterson Air Force Base
Dayton, Ohio 45433
Attention: E.E. Abell ASD/YZE

Wright-Patterson Air Force Base
Dayton, Ohio 45433
Attention: H.I. Bush AFWAL/POT

Wright-Patterson Air Force Base
Dayton, Ohio 45433
Attention: E.E. Bailey (NASA Liaison)
AFWAL/NASA

Wright-Patterson Air Force Base
Dayton, Ohio 45433
Attention: R.P. Carmichael ASD/XRHI

Wright-Patterson Air Force Base
Dayton, Ohio 45433
Attention: R. Ellis ASD/YZN

Wright-Patterson Air Force Base
Dayton, Ohio 45433
Attention: W.H. Austin, Jr. ASD/ENF

Eustis Directorate
U.S. Army Air Mobility
R&D Laboratory
Fort Eustis, VA 23604
Attention: J. Lane, SAVDL-EU-Tapp

Navy Department
Naval Air Systems Command
Washington, D. C. 20361
Attention: W. Koven AIR-03E

Navy Department
Naval Air Systems Command
Washington, D. C. 20361
Attention: J.L. Byers AIR-53602

Navy Department
Naval Air Systems Command
Washington, D. C. 20361
Attention: E.A. Lichtman AIR-330E

Navy Department
Naval Air Systems Command
Washington, D. C. 20361
Attention: G. Derderian AIR-5362C

NAVAL AIR Propulsion Test Center
Trenton, NJ 08628
Attention: J. J. Curry
A. A. Martino

U.S. Naval Air Test Center
Code SY-53
Patuxent River, MD 20670
Attention: E. A. Lynch

USAVRAD Command
PO Box 209
St. Louis, MO 63166
Attention: Ropbert M. Titus (ASTIO)

Department of Transportation
NASA/DOT Joint Office of Noise Abatement
Washington, D.C. 20590
Attention: C. Foster

Federal Aviation Administration
Noise Abatement Division
Washington, D.C. 20590
Attention: E. Sellman AEE-120

Environmental Protection Agency
1835 K Street, NW
Washington, D.C. 20460
Attention: J. Schettino
J. Tyler

Environmental Protection Agency
2565 Plymouth Road
Ann Arbor, MI 48105
Attention: R. Munt

Federal Aviation Administration
12 New England Executive Park
Burlington, MA 18083
Attention: Jack A. Sain, ANE-200

ENGINE MANUFACTURERS

Curtiss Wright Corporation
Woodridge, NJ 07075
Attention: S. Lombardo
S. Moskowitz

Detroit Diesel Allison Div. G.M.C.
P.O. Box 894
Indianapolis, IN 46206
Attention: W. L. McIntire

Cummins Engine Co.
Technical Center
500 S. Poplar
Columbus, IN 47201
Attention: J. R. Drake

AVCO/Lycoming
550 S. Main Street
Stratford, CT 06497
Attention: H. Moellmann

Detroit Diesel Allison Div. G.M.C.
333 West First Street
Dayton, Ohio 45402
Attention: F. H. Walters

The Garrett Corporation
AIResearch Manufacturing Co.
Torrance, CA 90509
Attention: F. E. Faulkner

The Garrettt Corportion
AIResearch Manufacturing Co.
402 S. 36 Street
Phoenix, AZ 85034
Attention: Library

General Electric Co./AEG
One Jimson Road
Evendale, Ohio 45215
Attention: R. W. Bucy (3 copies)
T. F. Donohue

Pratt & Whitney Aircraft Group/UTC
Government Products Division
P.O. Box 2691
West Palm Beach, Fl 33402
Attention: B. A. Jones

The Garrettt Corportion
AIResearch Aviation Co.
19201 Susana Road
Compton, CA 90221
Attention: N. J. Palmer

AIResearch Manufacturing Co.
111 South 34th Street
P.O. Box 5217
Phoenix, AZ 85010
Attention: C. E. Corrigan
(93-120/503-4F)

Williams Research Co.
2280 W. Maple Road
Walled Lake, MI 48088
Attention: R. VanNimwegen
R. Horn

Teledyne CAE, Turbine Engines
1330 Laskey Road
Tolendo, Ohio 43612
Attention: W. Q. Wagner

General Electric Co./AEG
1000 Western Ave.
Lynn, MA 01910
Attention: R. E. Neitzel

Pratt & Whitney Aircraft Group/UTC
Commercial Products Division
East Hartford, CT 06108
Attention: W. Gardner (1 copy)
M. E. Brazier

AIRFRAME MANUFACTURERS

Boeing Commercial Airplane Co.
P.O. Box 3707
Seattle, WA 98124
Attention: P. E. Johnson MS 9H-46
D. C. Nordstrom MS 73-01

Boeing Aerospace Co.
P.O. Box 3999
Seattle, Wa 98124
Attention: D. S. Miller MS 40-26
H. Higgins

The Boeing Co., Wichita Division
Wichita, KS 67210
Attention: D. Tarkelson

Douglas Aircraft Company
McDonnell Douglas Corp.
3855 Lakewood Boulevard
Long Beach, CA 90846
Attention: R. T. Kawai Code 36-41
M. Klotzsche

Lockheed California Co.
Burbank, CA 91502
Attention: J. F. Stroud, Dept. 75-42
R. Tullis, Dept. 75-21
J. I. Benson

General Dynamics Convair
P. O. Box 80847
San Diego, CA 92138
Attention: S. Campbell, MZ 632-00

Rockwell International
International Airport
Los Angeles Division
Los Angeles, CA 90009
Attention: A. W. Martin

Gates Learjet Corp.
P. O. Box 7707
Wichita, KS 67277
Attention: E. Schiller

McDonnell Aircraft Co.
McDonnell Douglas Corp.
P. O. Box 516
St. Louis, MO 63166
Attention: F. C. Claser Dept. 243

Lockheed Georgia Co.
Marietta, GA 30060
Attention: H. S. Sweet

Grumman Aerospace Corp.
South Oyster Bay Road
Bethpage, New York 11714
Attention: C. Hoeltzer

Airlines

American Airlines
Maint. & Engr. Center
Tulsa, OK 74151
Attention: W. R. Neeley

Eastern Airlines
International Airport
Miami, FL 33148
Attention: A. E. Fishbein

Delta Airlines, Inc.
Hartsfield-Atlanta International Airport
Atlanta, GA 30320
Attention: C. C. Davis

TransWorld Airlines
605 Third Avenue
New York, NY 10016
Attention: A. E. Carrol

Pan American World Airways, Inc.
JFK International Airport
Jamica, NY 11430
Attention: J. G. Borger
A. MacLarty

United Airlines
San Francisco International Airport
Maint. Operations Center
San Francisco, CA 94128
Attention: J. J. Overton

Others

Hamilton Standard
Bradley Field
Windsor Locks, CT 06096
Attention: P. J. Dumais, MS 1A-3-1
A. T. Reiff, MS 1-2-2

FluiDyne Engineering Corp.
5900 Olson Memorial Highway
Minneapolis, MN 55422
Attention: J. S. Holdhusen

Rohr Corporation
P.O. Box 878
Foot & H Street
Chula Vista, CA 92012
Attention: Library

Solar Division
International Harvester
2200 Pacific Highway
San Diego, CA 92112
Attention: Library

Gas Dynamics Laboratories
Aerospace Engineering Building
University of Michigan
Ann Arbor, MI 48109
Attention: Dr. C. W. Kaufmann

Massachusetts Inst. of Technology
Dept. of Astronautics & Aeronautics
Cambridge, MA 02139

Massachusetts Inst. of Technology
Dept. of Structural Mechanics
Cambridege, MA 02139
Attention: James Mar

Westinghouse Electric Corp.
P.O. Box 5837
Beulah Road
Pittsburgh, PA 15236
Attention: Library

University of Tennessee
Space Institute
Tullahoma, TN 37388
Attention: Dr. V. Smith

TRW Equipment Group
TRW Inc.
23555 Euclid Ave.
Cleveland, OH 44117
Attention: I. Toth

Aerospace Corporation
R & D Center
Los Angeles, CA 90045
Attention: Library

George Shevlin
P.O. Box 1925
Washington, D.C. 20013

Brunswick Corporation
2000 Brunswick Lane
Deland, Fl 32720
Attention: A. Erickson